MAIN-SHOCK CHARACTERISTICS

ELEVATION CHANGES ASSOCIATED WITH THE EARTHQUAKE AND THEIR USE TO INFER FAULT-SLIP GEOMETRY

By Grant A. Marshall and Ross S. Stein,
U.S. Geological Survey

CONTENTS

	Page
Abstract	A105
Introduction	105
Data	106
Leveling network	106
Leveling errors	106
Observed coseismic elevation change	109
Modeling elevation changes	110
Elastic-half-space models	110
Planar one-rake model	110
Nonplanar one-rake model	111
Two-rake model	111
Elastic-half-space results	111
Sensitivity of results to data distribution	116
Nonhomogeneous elastic models	117
Layered model	118
Wedge model	119
Modifications to half-space models	120
Discussion	122
Comparison of geodetic results with studies of seismicity and geology	122
Relation to other geodetic studies	124
Conclusion	125
Acknowledgments	126
References cited	126
Appendix 1: Corrections and adjustments to leveling data	127
Appendix 2: Data tables	129

ABSTRACT

Leveling surveys conducted before and after the 1989 Loma Prieta earthquake provide observations of the coseismic elevation changes. We use these data to define the spatial pattern of elevation change and to deduce the faulting geometry and distribution of slip. Both planar and curved (listric and negatively listric) faults produce elevation changes consistent with observations. Using an elastic half-space, we treat the data as correlated observations and find that 60 percent of the observed signal can be modeled by a planar rupture surface that extends from 6- to 12-km depth, is 32 km long and 7 km wide, and dips 64° SW. With a slip amplitude of 3.6 m, this model fault produces a geodetic moment of 2.6×10^{19} N-m. A larger dip-slip component is found northwest of the epicenter (rake, 144°) and a larger strike-slip component southeast of the epicenter (rake, 157°). Models with larger rake variations (>40°) marginally reduce the fit to the data but require a seismic moment of only 1.8×10^{19} N-m. The rupture plane lies 2 km southwest of the aftershock zone. When a low-modulus layer or wedge is added to the model for consistency with the seismic *P*-wave-velocity structure, the fault deepens and locates adjacent to the aftershock zone, coming within 1.5 km of the hypocenter.

INTRODUCTION

Precise geodetic leveling surveys conducted both before and after the 1989 Loma Prieta earthquake provide observations of the coseismic elevation changes. Although no active program of vertical-deformation monitoring using leveling has been pursued along this section of the San Andreas fault zone, previous leveling surveys for topographic-control and land-subsidence studies have been used together with postearthquake releveling to construct the coseismic elevation changes. Station separation for more than half of this extensive network of vertical-control bench marks is about 1 km.

In this study, we focus on the broad-scale pattern of vertical deformation and its interpretation in terms of fault geometry and slip. We use simple uniform-slip elastic-dislocation models to approximate the rupture surface at depth. In two different approaches, we treat the leveling observations as either independent or correlated elevation changes. We compare our models incorporating a heterogeneous elastic structure with the half-space models for consistency with the seismic-velocity models of Eberhart-Phillips and others (1990). We then compare the model rupture surface with seismologic, geologic, and other geodetic observations.

DATA

LEVELING NETWORK

The leveling network circumscribes the southern Santa Cruz Mountains and encloses most of the aftershock zone (fig. 1). The network spans 15 to 20 km (one hypocentral depth) on each side of the San Andreas fault and 67 km along strike. Postearthquake surveys were chosen to give maximum coverage of the aftershock zone and the area of expected vertical deformation. The leveling routes cross the San Andreas and Sargent faults in four places. The network is divided into seven routes (inset, fig. 1), each approximately parallel or perpendicular to the San Andreas fault.

Preearthquake leveling surveys were performed by both the U.S. National Geodetic Survey (NGS) and the U.S. Geological Survey (USGS) between 1948 and 1989. Postearthquake surveys were conducted from February through June 1990. We treat all of the vertical deformation occurring between the preearthquake and postearthquake surveys as "coseismic," noting that little postearthquake slip was observed between October 1989 and June 1990 (Behr and others, 1990; Langbein, 1990).

LEVELING ERRORS

Leveling can be contaminated by both systematic and random errors. Systematic errors generally produce a correlation between observed geodetic tilt and topographic slope, as is true for miscalibrated leveling rods (Jackson and others, 1981; Stein, 1981) and is sometimes true for atmospheric-refraction errors (Stein and others, 1986). Random errors have several causes: inaccurate readings of the leveling instrument caused by atmospheric scintillation and ground vibrations, incorrectly entered numerical values (blunders), random variations in the degree to which the instrument and rods are out of plumb, and so on. The NGS corrects all data for level collimation, rod

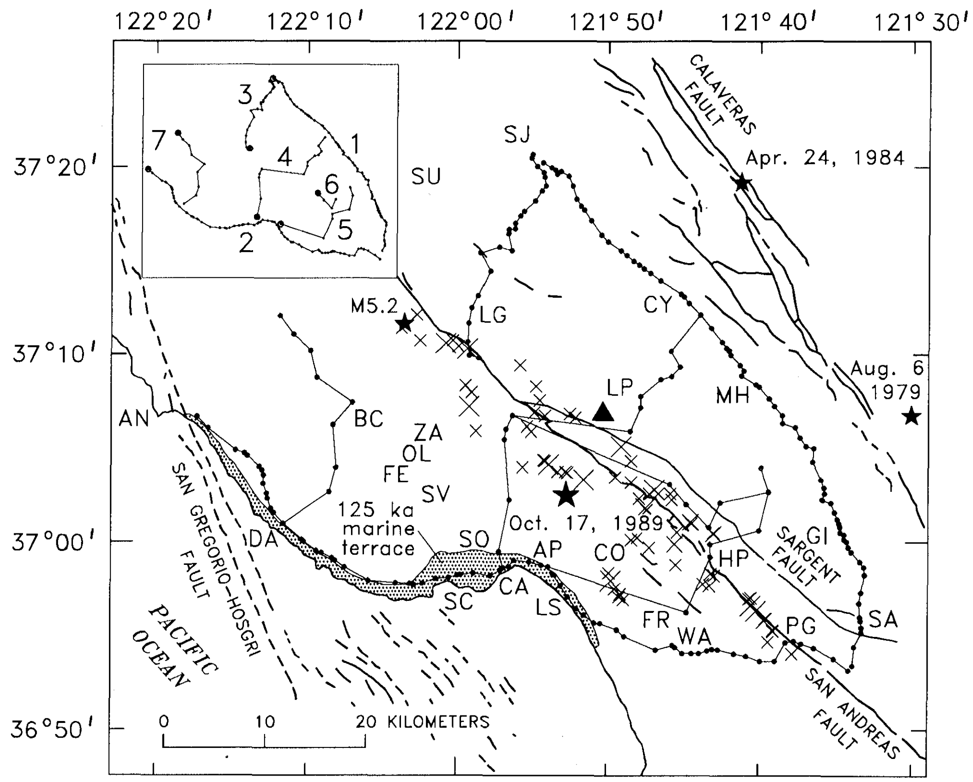

Figure 1.—Schematic map of Loma Prieta region, Calif., showing location of leveling network of 211 bench marks. Inset shows locations of leveling routes 1 through 7; bench marks (dots) indicate zero-distance points in profiles shown in figure 7. Stars, epicenters of Loma Prieta (Oct. 17, 1989; M_s=7.1), Coyote Lake (Aug. 6, 1979; M_s=5.9), and Morgan Hill (Apr. 24, 1984; M_L=6.1) earthquakes; crosses, epicenters of Loma Prieta aftershocks of M>2. Quaternary faults (dashed where inferred) from Jennings (1975). AN, Point Año Nuevo; AP, Aptos; BC, Boulder Creek; CA, Capitola; CO, Corralitos; CY, Coyote; DA, Davenport; FE, Felton; FR, Freedom; GI, Gilroy; HP, Hecker Pass; LG, Los Gatos; LP, Loma Prieta (triangle); LS, La Selva Beach; MH, Morgan Hill; OL, Olympia; PG, Pajaro Gap; SA, Sargent; SC, Santa Cruz; SJ, San Jose; SO, Soquel; SU, Sunnyvale; SV, Scotts Valley; WA, Watsonville; ZA, Zayante.

calibration, thermal expansion of the rod tapes, earth tides and associated gravitational effects, and atmospheric refraction. For the 1990 surveys, the thermal and refraction corrections were computed from the observed temperature gradient at the leveling instrument.

In contrast, the third-order USGS leveling data are not corrected for refraction, earth tides, or thermal-expansion effects. Refraction, collimation, and rod-calibration errors, which can lead to systematic errors detectable in third-order work, are evaluated by searching for height-dependent correlations. Profiles of elevation change and topography are shown in figure 2 for leveling routes 4 (fig. 2*A*) and 7 (fig. 2*B*), both of which cross substantial topography and show no correlation (positive or negative) between the tilt of elevation change and topographic slope. No such correlations are recognizable in the other coseismic data, although errors of ≤100 mm would be difficult to detect in the presence of large tectonic deformation.

Random error can be gaged from the height difference between adjacent bench marks when they are double-run (leveling in both directions), and from circuit misclosures.

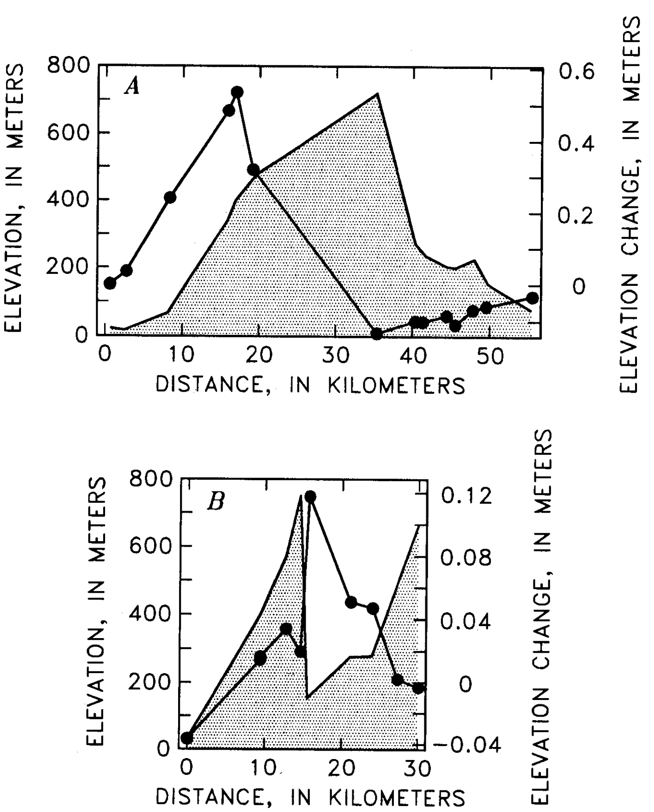

Figure 2.—Profiles of topography (shaded curve) and coseismic elevation change (dots) along leveling routes 4 (*A*) and 7 (*B*) (see inset, fig. 1). No consistent positive or negative correlation between topography and elevation change is observed.

Random error accumulates with the square root of distance, expressed as $\alpha\sqrt{L}$, where α (in millimeters per kilometer$^{1/2}$) is computed from the double-run sections and L is the length of each section (in kilometers). The observed α values listed in table 1 are derived from the statistics of all double-run sections and have been normalized to a distance of 1 km. The maximum allowable discrepancy between the forward and backward runs of each double-run section is the field tolerance, β. If this field tolerance is not met, the section must be rerun until the forward and backward runs agree to within the tolerance. In practice, arithmetic means of several runs are used for final elevation differences when the field tolerance cannot be met after several attempts. If random errors are normally distributed, then $\alpha = \frac{1}{3}\beta$. Generally, $\alpha < \frac{1}{3}\beta$ because the errors are not normally distributed or because the number of double-run sections used to compute α is small.

We have assigned α values to each survey on the basis of observed circuit misclosures. In the absence of large blunders or length-dependent systematic errors, observed circuit misclosures give an estimate of the random survey error. The accuracy of the 1990 surveys can be determined by examining five closed circuits. All the circuits are mapped in figure 3, and the observed misclosure, length, and allowable misclosure for each circuit are listed in table 2.

The assigned α values (table 1) are computed from the misclosures of circuits by the formula

$$\alpha^2 = \frac{1}{n}\sum \frac{e_i^2}{L_i}, \tag{1}$$

where e_i is the misclosure (in millimeters), L_i is the length (in kilometers) of the *ith* circuit, and n is the number of circuits (Bomford, 1971, p. 816). Generally, this calculation leads to more conservative assignments of error than does the observed α value. Where circuit-closure data are unavailable, the α value is assigned by setting the ratio β/α equal for all first-order surveys. All third-order surveys have been assigned an α value on the basis of the single preearthquake circuit 5 misclosure, which yields a 7-mm/$\sqrt{\text{km}}$ mean error, whereas the expected error for third-order levels is 12 mm/$\sqrt{\text{km}}$. Because circuit 5 was closed with several rod pairs, this small misclosure is consistent with an absence of rod-calibration error. Pure errors represented by circuit misclosures have been used to scale the relative precision of each survey.

The error assigned to each coseismic elevation change is based on survey precision and on the uncertainty and magnitude of the subsidence corrections (see app. 1). Relative uncertainties, δ_i, for each coseismic data point are computed as

$$\delta_i^2 = \alpha_{\text{post}}^2 + \alpha_{\text{pre}}^2 + (\gamma S_i)^2, \tag{2}$$

Table 1.—*Specifications for leveling surveys*

[Agencies: NGS, U.S. National Geodetic Survey; USGS, U.S. Geological Survey. Assigned α values are derived from circuit misclosures. n.a., not available]

Leveling route (inset, fig. 1)	Survey agency and designation	Survey date	Order of leveling (run)	Field tolerance, β (mm)	Observed α value (mm)	Assigned α value (mm)
1	NGS L25239.1	Jan.–Feb. 1990	1st (single)	4.0	0.77	2.5
	NGS L25172, L25174	Feb.–Mar. 1989	1st (single)	4.0	.84	2.5
	NGS L22841	July–Sept. 1972	1st (double)	3.0	.98	1.9
	NGS L21038, L21016.1, L21026.2	Mar.–May 1967	1st (double)	4.0	1.67	2.5
2	NGS L25239.1, L25239.2	Feb. 1990	1st (single)	4.0	.11	2.5
	NGS L25251.8	June 1990	1st (single)	4.0	1.32	2.5
	NGS L25174	Mar. 1989	1st (single)	4.0	.84	2.5
	NGS L24298	1978	1st (double)	3.0	.89	1.9
	NGS L22841, L22869	July–Oct. 1972	1st (double)	3.0	.89	1.9
3	NGS L25239.3	Feb.–Mar. 1990	1st (single)	4.0	1.30	2.5
	NGS L21016.9	Jan.–Mar. 1967	1st (double)	4.0	1.67	2.5
	NGS L18119.9	Dec. 1960	1st (double)	4.0	2.25	2.5
4	NGS L25239.4	Mar.–Apr. 1990	1st (single)	4.0	.80	2.5
	USGS PV 80, PV 208, PV 220	1948/53	3d single)	n.a.	n.a.	6.8
5	NGS L25239.6	Apr. 1990	1st (single)	4.0	.75	2.5
	USGS PV 220, PV 208	1953	3d (single)	n.a.	n.a.	6.8
6	NGS L25239.5	Apr. 1990	1st (single)	4.0	1.50	2.5
	USGS PV 220	1953	3d (single)	n.a.	n.a.	6.8
7	NGS L25251.7, L25251.8	May–June 1990	1st (single)	4.0	1.72	2.5
	USGS PV 218	1953/54	3d (single)	n.a.	n.a.	6.8

where α_{post} is the α value for the postearthquake survey, α_{pre} is the α value for the preearthquake survey, S_i is the subsidence correction for the *ith* data point, and γ is a parameter that depends on our confidence in the estimated subsidence rate. For points with a subsidence correction based on extensometer data, γ=0.15; for all other points, we assign γ=0.33.

The relative uncertainty indicates the relative importance of the elevation change at a point *i* with respect to any other point *j*. The uncertainty between two adjacent points *i* and *i*+1 is given by

$$\sigma_{(i,i+1)} = \left[(\delta_i^2 + \delta_{i-1}^2)L\right]^{1/2} \tag{3}$$

where *L* is the survey distance between the two points (in kilometers). The coseismic elevation changes and their relative uncertainties are listed in table 3. Each bench mark is identified by its NGS archival reference number (ACRN).

The coseismic signal available for modeling is best described by a signal-to-noise (*S*/*N*) ratio. The observed elevation-change signal is based on section-elevation changes (each section consists of two adjacent bench marks). The signal for the *ith* section, ΔH_i, is given by the difference between the coseismic elevation changes of the two bench marks at each end, $\Delta H_i = dH_{i+1} - dH_i$. The total error, σ_i, for each ΔH_i is calculated from equation 3 and is proportional to the square root of the survey length of the section and to the square root of the sum of squares of the uncertainties of the two observations. The *S*/*N* ratio is given by

$$\frac{S}{N} = \left[\frac{1}{n}\sum_i^n\left(\frac{\Delta H_i}{\sigma_i}\right)^2\right]^{1/2}, \tag{4}$$

where *n* is the total number of sections used in the calculation (table 4). The *S*/*N* ratio is ≤3 for 81 percent of all the sections in the network (leveling routes 1, 2, 5, 7). The area of large signal near the epicenter has a moderate *S*/*N* ratio of 4 to 6, because the coseismic elevation changes are derived from less precise preearthquake surveys that have poor spatial resolution and larger uncertainty (leveling routes 3, 4, 6). The *S*/*N* ratio of the entire Loma Prieta leveling-data set is 3.3, despite the high quality and resolution of the 1990 surveys. In effect, the leveling routes around the periphery of the network receive a higher weight by virtue of their high precision and bench-mark density, whereas those in the interior of the network receive a relatively lower weight. If all the data were of equal precision and density, the interior routes of the network would have had much larger *S*/*N* ratios.

OBSERVED COSEISMIC ELEVATION CHANGE

The observed coseismic elevation changes are mapped in figure 4*A*. Maximum uplift of 550 mm occurs just to the northwest of the epicenter, on the west side of the San Andreas fault (fig. 1). Maximum subsidence of 100 mm occurs at both the northeast and southwest ends of the network. Maximum coastal uplift occurs where the bench marks are closest to the San Andreas fault. Along the northwest section of the coastline, between Santa Cruz (SC, fig. 1) and Point Año Nuevo (AN, fig. 1), the observations show little or no uplift. To the east of the San Andreas fault, a broad 50-mm downwarp extends along the fault zone.

Repeated coseismic vertical deformation may give rise to the observed height of the coastal marine terraces. Noting the similarity between terrace-uplift profiles and the vertical deformation predicted by Lisowski and others' (1990) coseismic model of the earthquake, Anderson (1990), Valensise and Ward (1991), and Valensise (1992) suggested that Loma Prieta-type events, if repeated every 300 to 600 yr, could produce the observed terrace deformation. The observed coseismic elevation changes from the earthquake are plotted along with the observed long-term vertical deformation of the youngest (125 ka) marine terrace in figure 5*A*. At distances greater than 25 km south of Point Año Nuevo, the two profiles are similar, although the terrace deformation is broader, partly because the leveling route does not everywhere coincide with the terrace's inner edge. Within 25 km of Point Año Nuevo, the uplift recorded by the terrace is not observed coseismically.

An alternative interpretation of the long-term uplift is uniform coastward tilting normal to the San Andreas fault. If this interpretation is correct, then the terrace heights would be inversely proportional to their distance from the fault, unrelated to parameters of the earthquake. Terrace height as a function of distance normal to the San Andreas fault is plotted in figure 5*B*. Uniform tilting is seen to be a plausible explanation for the terrace height, except near the San Gregorio-Hosgri fault at Point Año Nuevo. Thus, although the similarity of the coseismic deformation to the 125-ka deformation suggests that permanent uplift associated with dip slip on the San Andreas fault is recorded by the terraces, uniform regional tilting may also account for the terrace uplift. In both cases, discrepancies near the San Gregorio-Hosgri fault may be due to dip-slip motion on the San Gregorio-Hosgri fault or to obliquity

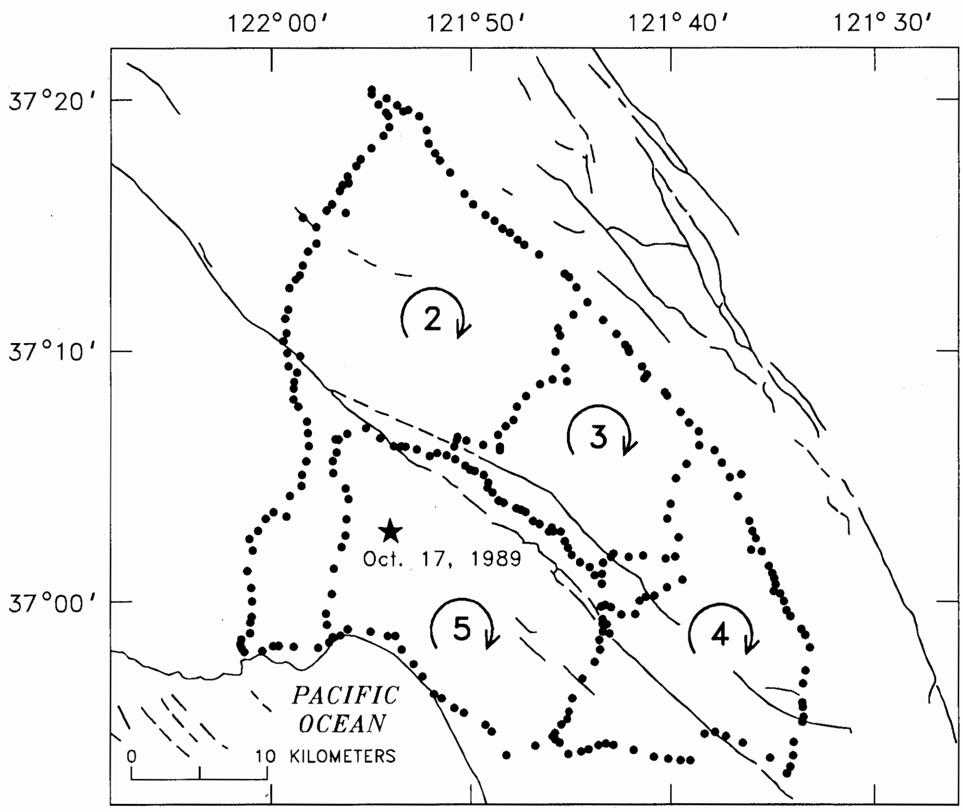

Figure 3.—Schematic map of Loma Prieta region, Calif., showing locations of leveling circuits (numbered loops) formed by 1990 releveling survey. Circuit misclosures computed in clockwise direction as indicated are listed in table 1. Leveling circuit 5 is closed by both preearthquake and postearthquake leveling. Circuit 1 is the outer perimeter loop.

Table 2.—*Leveling circuits and misclosures*

[Observed misclosure is computed in clockwise direction. Allowable misclosure is based on normal random error, $\alpha = \frac{1}{3}\beta$. NGS, U.S. National Geodetic Survey]

Circuit (fig. 3)	Date	Circuit length (km)	Observed misclosure (mm)	Allowable misclosure (mm)
1	1990	79.9	−51.34	±17.9
2	1990	146.0	−38.82	±16.1
3	1990	81.3	+15.86	±12.0
4	1990	90.5	−9.82	±12.7
5	1990	105.0	−18.56	±13.7
5	[1]1953/72	105.0	−70.00	[2]±123.0

[1]5 km of the preseismic loop is closed with an NGS 1972 height difference.
[2]Based on α=12 mm/$\sqrt{\text{km}}$.

of the long-term San Andreas fault slip, as proposed by Valensise and Ward (1991).

MODELING ELEVATION CHANGES

To model the observed coseismic elevation changes, we constructed a series of three-dimensional models, each of which utilizes an elastic-half-space Earth structure and model faults with uniform slip. We first construct planar rectangular model faults and search for the model that best fits the observations; the data are considered to be independent point elevation changes. Next, we allow the model fault to take on listric and negatively listric shapes. In an additional experiment, we consider the observed elevation changes to be correlated and model the section-elevation changes between adjacent bench marks. In our final series of models, we examine faults with alongstrike variations in rake.

To assess the influence of nonhomogeneous elastic Earth structure, we then tested several two-dimensional boundary-element models. In these tests, we compute the vertical displacement for a set of points aligned perpendicular to the strike of a model thrust fault embedded in a nonhomogeneous elastic medium. These displacements are then modeled with a two-dimensional elastic half-space, to deduce the correction that should be applied to our three-dimensional-half-space results to account for nonhomogeneous Earth structure. These nonhomogeneous-elastic-media calculations are designed to test the effects of a realistic Earth structure on the basis of calculated seismic-velocity models of the Loma Prieta region. We consider both a layered elastic structure and a wedge-shaped low-modulus region.

ELASTIC-HALF-SPACE MODELS

PLANAR ONE-RAKE MODEL

The earthquake rupture can be described as a superposition of moment-tensor point sources buried within a uniform elastic half-space (Ward and Barrientos, 1986; Barrientos and others, 1987). The model-fault geometry and source parameters are fixed; the uniform slip is defined by a least-squares inversion. When the data are considered to be independent point elevation changes, a constant elevation-change offset is also determined by inversion. Because the coseismic elevation changes are independent of a datum (zero-level elevation change is unknown), the model must include an elevation-change offset that, together with the slip amplitude, best fits the observations (in a second approach, the need for an elevation-change offset is eliminated by constructing elevation-change differences between adjacent bench marks). The data are weighted by the square of the observed errors, σ_0, which are proportional to the relative uncertainties, $\sigma_0 = \sqrt{L_c}\delta_i$, where L_c is a characteristic length scale for the network (L_c≈10 km). Note that we model the elevation change of each bench mark, which is treated as independent, and there are no correlations between bench marks. The characteristic length scale is chosen so that the *S/N* ratio calculated both by section and by bench mark is the same; without the characteristic length scale, the magnitude of the signal is unbounded, owing to the arbitrary datum.

To account for correlations in the leveling observations, we also model the section-elevation changes. In these models, differencing the coseismic elevation changes of adjacent bench marks eliminates the elevation-change offset, and so we invert only for the slip amplitude, with the section-elevation changes weighted by the square of the uncertainties given by equation 3. Each section has a length scale (the leveled distance between adjacent bench marks), and the characteristic network length scale L_c is not required. Before inverting the section-elevation changes, we remove bench marks that create spikes, and sections with excessive tilt. Spikes, defined by adjacent sections that have large tilts of opposite sign, indicate a disturbed bench mark or leveling-observation blunder. Steps in the leveling data indicate blunders in the leveling observations and are characterized by individual sections that have excessively large tilt. For spikes, the causative bench mark is removed, and a new section is formed by differencing the bench marks on either side. The magnitude of tilt that is used to define spikes and steps is chosen to maximize the percentage of signal modeled, while at the same time removing as few of the data as possible (fig. 6).

Each model fault is described by eight fixed model parameters. The location of the model fault is designated by the coordinates of its upper northwest corner; the latitude, longitude, and vertical depth of this corner locate the fault in space. The fault area is described by an alongstrike length and a downdip width. The strike is defined as the angle measured clockwise from north, and the rake is measured on the fault surface counterclockwise from the strike azimuth. The dip is the acute angle between horizontal and the fault surface.

Our systematic forward search of parameter space begins by finding the best-fitting planar model fault. In this initial phase of modeling, we make no assumptions about fault geometry or location, as might be derived from aftershock locations, focal mechanisms, or previous studies. Instead, we adopt strikes and rakes that reflect the general strike of the San Andreas fault in the Loma Prieta region and a reverse-oblique style of faulting. These and all other model parameters, however, are assigned large ranges in the initial parameter-space search. During successive parameter-space searches, these ranges are narrowed, guided by the values that produce the best fit to the data.

NONPLANAR ONE-RAKE MODEL

For curved fault shapes, one additional parameter is required. The downdip fault shape in cross section can be described by the relation $x=b_1z+b_2z^2$, where x is the horizontal distance perpendicular to the fault strike in the direction of dip (Ward and Barrientos, 1986), z is the depth, and b_1 and b_2 describe the cross-sectional shape of the fault surface: b_1 is the cotangent of the dip at the upper edge of the fault, and b_2 is the fault curvature. When b_2=0, the model fault is planar (fig. 7*A*); when b_2>0, the model fault is listric (fig. 7*B*); and when b_2<0, the model fault is negatively listric, a "shoulder thrust" in geologic parlance (fig. 7*C*). We examine fault curvature over a narrower range of initial parameters, using our acquired knowledge of the best-fitting planar-fault geometry. The ranges of parameters tested are listed in table 5.

TWO-RAKE MODEL

In an additional but limited modeling run, two new parameters are added to the model. By introducing an alongstrike segmentation, we create northwestern and southeastern fault segments with independent rakes. Slip is constrained to be uniform for both segments and is determined by inversion. Because Beroza (1991), Steidl and others (1991), and Wald and others (1991) modeled variations in rake in their analyses of strong-motion seismic data, we test whether the leveling observations also constrain variations in rake. This new parametrization is used to determine the best rakes and relative segment lengths for our best-fitting planar-model geometry and for perturbations to it.

ELASTIC-HALF-SPACE RESULTS

All models are ranked according to their misfit to the observations. Model misfits are characterized by a reduced χ^2 term here called the misfit-to-noise (*M*/*N*) ratio, computed as

$$\frac{M}{N}=\left[\frac{1}{n-N_f}\sum_{i}^{n}\left(\frac{\Delta H_o-\Delta H_c}{\sigma_o}\right)^2\right]^{1/2}, \tag{5}$$

where ΔH_0 is the observed elevation change, ΔH_c is the calculated elevation change, σ_0 is the observed error, n is the number of bench marks, and N_f is the number of free model parameters computed from the data (N_f=10, planar; N_f=11, curved; N_f=12, two-rake, because we have used the data to find the best values of all the parameters). For the section-elevation-change models, the values of ΔH_0 and ΔH_c refer to section-elevation changes, the observed error is calculated by using equation 3, and n is the number of sections modeled. If a model fits the observations to within the noise level of the data, then $M/N\leq1.0$. Our best-fitting one-rake model has an *M*/*N* ratio of 1.62 for independent data and 1.57 for correlated data, and the segmented two-rake model has an *M*/*N* ratio of 1.33 for independent data. Because all of these models have *M*/*N* ratios >1.0, we have not modeled all the observed signal. The fit is improved by 4 percent when the data are treated as correlated observations, as indicated by the percentage of signal modeled. Árnadóttir and others (1992) also found solutions for both correlated and independent data similar to our models, but the misfits they reported are larger. We calculate an *M*/*N* ratio of 1.61 for Árnadóttir and others' best model. Our use of the characteristic length scale, when modeling the data as independent observations, properly scales that problem, and so we obtain *M*/*N* ratios comparable to those in the models with correlated data. Because we have removed spikes and steps from the data before modeling the section-elevation changes, the data set that we invert may differ slightly from that of Árnadóttir and others. We have also removed the adjustment (see app. 1) to the third-order USGS data for the section-elevation-change models.

Parameter values and inversion results for the best-fitting planar, listric, and negatively listric model faults, the two-rake model fault, and the section-elevation-change models are listed in table 6. The uncertainties shown for the slip and moment are derived from the inversion and depend on the weighted rms residuals. Each one-rake fault fits the data equally well ($1.57\leq M/N\leq1.67$) and produces a similar moment release. With independent data, the two-rake model fault significantly improves the fit and greatly reduces the magnitudes of slip and moment. With correlated data, the two-rake model fault does not improve the

Table 3.—*Coseismic elevation changes along leveling routes*

[See inset, figure 1, for locations of leveling routes. ACRN, U.S. National Geodetic Survey archival reference number. A constant can be freely added to all elevation-change observations. Note that duplicate bench marks are listed at overlapping end points of leveling routes]

ACRN	Survey distance (km)	Latitude °N.	Longitude °W.	Coseismic elevation change (mm)	Relative uncertainty, δ_i (mm)
Leveling route 1					
HS5161	0.000	37.3519	121.9169	18.2	4.3
HS5160	.598	37.3489	121.9175	15.1	4.3
HS2891	1.745	37.3414	121.9111	8.7	4.4
HS2886	2.598	37.3461	121.9036	12.4	4.5
HS5162	4.166	37.3411	121.8958	5.4	4.6
HS2828	4.787	37.3394	121.8914	1.8	4.6
HS2826	4.968	37.3381	121.8906	1.0	4.6
HS2825	5.086	37.3378	121.8894	1.1	4.6
HS2822	5.383	37.3361	121.8894	.3	4.5
HS5163	5.709	37.3378	121.8864	.1	4.6
HS2813	6.972	37.3344	121.8764	−7.6	5.1
HS2814	8.568	37.3253	121.8697	−9.8	4.9
HS2811	10.085	37.3142	121.8678	−10.2	4.6
HS2810	10.957	37.3075	121.8625	−17.9	4.3
HS2809	11.753	37.3022	121.8581	−16.6	4.6
HS2806	13.031	37.2944	121.8506	−24.9	4.0
HS2796	15.012	37.2797	121.8364	−33.6	4.0
HS2795	15.846	37.2744	121.8308	−34.9	4.0
HS2792	15.982	37.2736	121.8294	−35.0	4.0
HS2789	17.378	37.2653	121.8183	−30.7	4.0
HS2788	18.111	37.2617	121.8114	−31.3	4.0
HS2787	19.036	37.2564	121.8033	−33.5	4.0
HS4926	19.609	37.2533	121.7981	−36.0	4.0
HS5164	19.615	37.2536	121.7981	−41.1	4.0
HS2785	20.301	37.2494	121.7917	−27.6	4.1
HS2784	21.212	37.2450	121.7842	−29.5	4.0
HS5165	22.505	37.2381	121.7719	−31.5	4.0
HS4141	24.649	37.2261	121.7506	−32.6	4.0
HS2778	25.464	37.2225	121.7450	−31.9	4.0
HS2776	26.325	37.2167	121.7392	−31.5	4.0
HS2775	27.865	37.2061	121.7281	−28.6	4.0
HS2773	29.592	37.1942	121.7156	−31.7	4.0
HS2769	31.084	37.1836	121.7047	−32.3	4.0
HS2771	31.091	37.1839	121.7047	−32.9	4.0
HS5166	32.057	37.1769	121.6978	−31.9	4.0
HS2768	32.432	37.1744	121.6947	−31.5	4.0
HS5167	32.881	37.1714	121.6919	−31.9	4.0
HS2762	34.168	37.1619	121.6831	−32.0	4.0
HS2757	34.957	37.1569	121.6775	−37.5	4.0
HS2758	35.919	37.1525	121.6808	−42.5	4.0
HS2759	35.930	37.1525	121.6805	−42.4	4.0
HS2761	36.014	37.1525	121.6805	−41.5	4.0
HS2754	37.913	37.1433	121.6639	−37.2	4.0
HS2753	38.236	37.1411	121.6614	−36.3	4.0
HS2751	39.739	37.1303	121.6500	−34.6	4.0
HS5168	40.908	37.1228	121.6428	−32.7	4.0
HS5169	41.933	37.1156	121.6353	−31.3	4.0
HS2745	43.419	37.1031	121.6222	−27.5	4.0
HS2743	44.781	37.0956	121.6156	−16.7	4.0
HS2742	44.826	37.0953	121.6156	−17.1	4.0
HS5170	46.147	37.0850	121.6086	−18.7	4.0
HS5171	47.156	37.0853	121.5997	−17.6	4.0
HS2738	47.740	37.0719	121.6011	−26.0	4.0
HS2737	49.664	37.0561	121.5922	−18.8	4.0
HS2736	50.366	37.0500	121.5892	−15.1	4.0
HS2733	51.125	37.0439	121.5864	−13.3	4.0
HS2727	52.380	37.0367	121.5917	−8.2	4.0
HS2725	53.422	37.0344	121.5811	−11.8	4.0
HS5172	54.449	37.0258	121.5769	−11.2	4.0
HS2724	55.119	37.0203	121.5736	−13.6	4.0
HS2723	55.512	37.0172	121.5719	−7.9	4.0
HS5143	56.083	37.0125	121.5700	−7.6	4.0
HS2720	56.822	37.0078	121.5706	−6.4	4.0
HS2721	57.287	37.0069	121.5669	−6.7	4.0
HS2722	57.320	37.0069	121.5672	−6.3	4.0
HS2719	57.607	37.0058	121.5658	−7.1	4.0
HS2718	57.664	37.0025	121.5653	−7.2	4.0
HS5144	58.146	37.0006	121.5631	−8.9	4.0
HS3323	58.200	37.0006	121.5636	−10.1	4.0
GU2195	58.785	36.9950	121.5611	−8.7	4.0
GU2192	59.329	36.9908	121.5583	−8.5	4.0
GU2190	60.917	36.9811	121.5483	−10.5	4.0
GU2189	61.564	36.9775	121.5444	−14.8	4.0
GU2188	62.363	36.9692	121.5417	−18.0	4.1
GU2180	63.974	36.9544	121.5442	−16.3	4.1
GU2178	65.207	36.9442	121.5464	−15.3	4.1
GU4096	65.308	36.9433	121.5467	−12.0	4.0
GU2177	66.625	36.9311	121.5469	−14.5	4.0
GU2176	66.879	36.9286	121.5469	.2	4.0
GU2174	67.554	36.9219	121.5467	17.0	4.0
GU2175	67.791	36.9208	121.5472	23.0	4.0
GU2173	68.173	36.9178	121.5467	.0	4.0
Leveling route 1—Continued					
GU2172	68.187	36.9172	121.5467	5.5	4.0
GU2171	68.274	36.9172	121.5467	−6.3	4.0
GU2167	69.904	36.9042	121.5553	−27.7	4.0
GU2154	71.743	36.8878	121.5567	−39.2	4.0
GU2151	72.394	36.8825	121.5600	−42.3	4.0
GU4097	74.431	36.8922	121.5742	−21.4	4.0
Leveling route 2					
GU4097	0.000	36.8922	121.5742	−21.4	4.0
GU2161	2.766	36.9014	121.5975	−31.6	4.0
GU2162	4.252	36.9067	121.6128	−37.5	4.1
GU2163	5.070	36.9094	121.6203	−51.3	4.0
GU2226	6.117	36.9092	121.6308	−50.3	4.0
GU2229	8.532	36.8917	121.6425	−78.2	4.0
GU2231	10.120	36.8922	121.6600	−88.8	4.0
GU2232	11.305	36.8944	121.6728	−104.5	4.0
GU2233	12.923	36.8975	121.6900	−103.7	4.0
GU2235	14.374	36.9008	121.7056	−104.8	4.0
GU4098	14.966	36.9014	121.7117	−90.2	4.0
GU2237	15.546	36.9003	121.7181	−94.9	4.0
GU2239	16.468	36.8986	121.7275	−88.0	4.0
GU2240	17.132	36.8972	121.7344	−82.5	4.0
GU2242	17.952	36.8956	121.7444	−83.1	4.0
GU2245	19.356	36.9033	121.7536	−70.7	3.6
GU2246	19.720	36.9053	121.7564	−68.0	5.8
GU2248	21.899	36.9003	121.7764	−44.6	3.0
GU2260	26.209	36.9103	121.8117	−7.8	3.4
GU2262	27.316	36.9156	121.8194	−5.8	3.3
GU2264	29.151	36.9225	121.8375	15.7	5.2
GU2265	29.794	36.9250	121.8444	20.2	3.2
GU2266	31.156	36.9317	121.8569	32.1	4.6
GU2269	32.092	36.9361	121.8639	16.5	3.8
GU2268	32.100	36.9361	121.8639	24.3	3.6
GU2273	33.700	36.9483	121.8733	53.9	9.0
GU2276	34.877	36.9572	121.8817	108.9	3.5
GU2277	36.273	36.9669	121.8914	137.8	6.1
GU2279	37.317	36.9756	121.8972	166.7	5.0
GU2278	37.457	36.9758	121.8975	165.0	4.3
GU2281	37.958	36.9764	121.9031	170.4	6.5
GU2282	38.207	36.9758	121.9044	159.0	5.0
GU2283	39.528	36.9792	121.9181	151.6	7.0
GU2285	41.374	36.9814	121.9364	150.6	7.7
GU2286	42.225	36.9769	121.9431	132.0	7.4
GU2287	42.767	36.9753	121.9494	118.2	7.0
GU2290	43.234	36.9731	121.9528	112.0	5.3
GU2289	44.452	36.9683	121.9636	86.8	5.5
GU2291	46.234	36.9692	121.9842	80.8	7.3
GU2294	47.406	36.9692	121.9967	73.9	6.0
GU1941	47.786	36.9683	122.0014	65.0	7.6
GU1944	48.822	36.9656	122.0117	35.4	3.5
GU3223	50.089	36.9656	122.0244	37.3	3.9
GU1945	50.331	36.9647	122.0250	45.9	4.0
GU1954	52.171	36.9614	122.0411	25.8	3.1
GU1959	53.149	36.9589	122.0511	19.4	3.0
GU1960	53.944	36.9611	122.0556	15.8	3.0
GU1964	55.451	36.9622	122.0728	10.5	3.0
GU1970	58.303	36.9644	122.1033	1.6	3.0
GU1972	60.897	36.9747	122.1300	.5	3.0
GU1974	61.947	36.9811	122.1397	10.2	3.0
GU1975	62.447	36.9833	122.1436	6.9	3.0
GU1976	63.587	36.9878	122.1550	−.5	3.0
GU1978	64.232	36.9903	122.1617	3.0	3.0
GU1979	66.032	36.9986	122.1764	5.3	3.0
HT1572	66.418	37.0011	122.1792	6.1	3.0
HT1568	69.463	37.0153	122.2000	−3.7	3.0
HT1567	70.723	37.0247	122.2108	−4.1	3.0
HT1566	71.272	37.0286	122.2144	−1.6	3.0
HT1565	71.391	37.0292	122.2156	−5.9	3.0
HT1564	72.456	37.0372	122.2194	−1.5	3.0
HT1563	73.464	37.0431	122.2208	−2.7	3.0
HT1562	74.448	37.0517	122.2244	−2.8	3.0
HT1559	75.468	37.0597	122.2242	−1.9	3.0
HT1558	75.930	37.0636	122.2253	4.5	3.0
HT1557	76.345	37.0669	122.2281	1.0	3.0
HT1556	78.305	37.0778	122.2428	4.7	3.0
HT1555	78.635	37.0800	122.2453	−3.7	3.0
HT1552	80.343	37.0833	122.2558	−4.4	3.0
HT1547	82.141	37.1044	122.2872	−.5	3.0
HT1545	83.794	37.1142	122.3006	−5.4	3.0

Table 3.—*Coseismic elevation changes along leveling routes*—Continued

ACRN	Survey distance (km)	Latitude °N.	Longitude °W.	Coseismic elevation change (mm)	Relative uncertainty, δ_i (mm)
		Leveling route 3			
HS3165	0.000	37.1706	121.9889	37.1	4.0
HS3174	2.091	37.1678	121.9786	71.6	4.0
HS3160	1.793	37.1833	121.9908	−1.9	4.0
HS3154	4.014	37.2008	121.9900	−17.9	4.0
HS3150	5.706	37.2147	121.9869	−56.1	4.0
HS3145	6.958	37.2242	121.9800	−108.0	4.0
HS3140	10.143	37.2469	121.9653	−144.9	4.1
HS3141	10.232	37.2469	121.9653	−136.5	4.1
HS3188	12.161	37.2636	121.9769	−59.7	4.2
HS3132	12.845	37.2681	121.9561	−95.5	4.1
HS3271	14.161	37.2669	121.9408	−126.4	4.4
HS3131	14.676	37.2819	121.9444	−81.9	4.5
HS3130	15.162	37.2856	121.9436	−57.0	7.1
HS3127	15.868	37.2869	121.9375	−66.0	7.4
HS3125	16.486	37.2908	121.9383	−75.8	9.4
HS3124	17.504	37.2978	121.9308	−76.9	14.6
HS3122	18.045	37.3019	121.9267	−95.3	17.4
HS3120	19.473	37.3108	121.9164	−111.3	25.0
HS3118	20.888	37.3194	121.9072	9.9	32.5
HS3117	21.617	37.3244	121.9017	20.8	33.3
HS3109	22.509	37.3319	121.9025	−6.4	39.9
HS3108	22.814	37.3347	121.9036	.2	41.5
HS2891	23.822	37.3414	121.9111	8.7	40.7
		Leveling route 4			
GU2287	0.000	36.9753	121.9494	118.2	7.0
GU4169	1.933	36.9906	121.9567	150.3	7.0
HS5196	7.398	37.0358	121.9431	342.3	7.0
HS5202	15.016	37.0947	121.9492	570.4	7.0
HS5203	15.934	37.1022	121.9464	620.4	7.0
HS5205	18.230	37.1144	121.9389	395.2	7.0
HS5224	34.410	37.1025	121.8056	−86.3	7.0
HS5229	39.352	37.1236	121.7942	−65.2	7.0
HS5231	40.445	37.1322	121.7917	−69.9	7.0
HS5233	43.345	37.1483	121.7708	−56.3	7.0
HS5235	44.533	37.1519	121.7597	−83.2	7.0
HS5238	46.850	37.1603	121.7489	−47.3	7.0
HS5239	48.527	37.1722	121.7583	−41.0	7.0
HS2775	54.309	37.2061	121.7281	−28.6	7.0
		Leveling route 5			
HS5281	0.000	37.0681	121.6589	−62.2	7.0
HS5283	2.786	37.0453	121.6519	−48.2	7.0
HS5285	7.981	37.0108	121.6619	−35.8	7.0
GU4175	15.066	36.9972	121.7167	−5.4	7.0
GU4177	16.759	36.9861	121.7169	39.3	7.0
GU4185	25.263	36.9353	121.7422	−60.3	7.0
GU2278	48.142	36.9758	121.8975	165.0	7.0
		Leveling route 6			
HS5283	0.000	37.0453	121.6519	−48.2	7.0
HS5247	7.309	37.0344	121.7072	−82.0	7.0
HS5252	11.399	37.0133	121.7172	−58.9	7.0
HS5256	14.701	37.0325	121.7428	−40.6	7.0
HS5262	18.295	37.0508	121.7619	−16.8	7.0
HS5205	39.535	37.1144	121.9389	395.2	7.0
		Leveling route 7			
HT1568	0.000	37.0153	122.2000	−3.7	7.0
HT3637	9.170	37.0444	122.1494	47.8	7.0
HT3636	9.189	37.0444	122.1489	49.4	7.0
HT3633	12.315	37.0672	122.1400	66.1	7.0
HT3631	14.278	37.1083	122.1442	52.3	7.0
HT3595	17.254	37.1286	122.1217	150.1	7.0
HT3600	22.709	37.1500	122.1636	83.7	7.0
HT3603	25.685	37.1739	122.1694	80.1	7.0
HT3607	28.969	37.1914	122.1908	34.7	7.0
HT3612	31.738	37.2069	122.2053	30.0	7.0

Table 4.—*Signal-to-noise ratios along leveling routes*

Leveling route (inset, fig.1)	Number of sections	Signal-to-noise ratio
1	86	2.1
2	71	2.8
3	22	5.5
4	13	6.5
5	6	2.9
6	5	4.1
7	9	2.4
1–7	212	3.3

fit to the observations but can provide an equally good fit with 13 percent less moment. Each model fault is about 34 km long, stretching over just half the length of the aftershock zone of October 1989. The fault strikes 127°–129°, similar to the aftershock zone (Dietz and Ellsworth, 1990), and approximately parallels the Santa Cruz Mountains section of the San Andreas fault. The depth of burial of the upper edge of each fault surface is 4 to 5 km; deeper faults are preferred when modeling with correlated data. The planar model fault dips 60°, approximately the average dip of each of the nonplanar model faults; with correlated data, the faults dip slightly steeper. With independent data, the model faults lie above and to the west of the main-shock hypocenter and aftershocks, whereas with correlated data they lie at the west edge of the aftershock zone but still do not intersect the hypocenter. The closest distance between any typical good-fitting model fault and the main-shock hypocenter is 6 km. Contours of observed, predicted, and residual (observed minus predicted) elevation changes are mapped in figure 4 for the best-fitting planar one-rake model fault with independent data. Profiles of the elevation changes for the one- and two-rake model faults are plotted along with the observations in figures 8*A* and 8*B*, respectively. In five places, notable misfits are visible in the one-rake model: (1) at the Sargent fault crossing on leveling route 1 (inset, fig. 1), (2) near the San Andreas fault crossing on leveling route 2, (3) in the center of leveling route 3, (4) near the Sargent fault on leveling route 6, and (5) near the Sargent fault on leveling route 4. These misfits may occur where nontectonic or secondary deformation has disturbed the bench marks. If, for example, we remove a small fraction (13 percent) of the bench marks in the network at sites where notable misfits to our best model fault occur, then the *M*/*N* ratio is reduced to 1.13 for the one-rake planar model fault. The two-rake model fault, however, explains the misfits on leveling routes 2 and 6.

To examine the variation in our best parameter values and the inversion results with independent data, we select an acceptable range of *M*/*N* ratios above the minimums for the one-rake planar, listric, and negatively listric model faults. The acceptable ranges in the fixed parameters and the corresponding inversion results for each model fault at an M/N ratio of the best value plus 5 percent are listed in table 7. Depth of burial is well constrained between 4- and 6-km depth. Strike is constrained to a 5° range that at its upper bound includes the strike of the observed aftershock locations. For planar model faults, acceptable dips vary only slightly, whereas for nonplanar model faults, the dip of the upper edge of the rupture surface is not well constrained. Our results do not indicate a preference between planar and nonplanar model faults within the range of curvatures tested. The inversion results indicate a consistent determination of the moment release, whereas slip amplitude varies by a factor of as much as 2. Because the geodetic moment is proportional to the product of the fault area and the slip amplitude ($M_0=\mu As$, where μ is the elastic rigidity, A is the fault area, and s is the average slip amplitude), models with similar moment release and fault length exhibit a tradeoff between slip amplitude and fault width. The distance between the fault surface and the hypocenter is consistently greater than 4 km. The best-fitting faults do not pass through the main-shock hypocenter. The best-fitting model fault that passes within 1 km of the main shock is listric and has an M/N ratio of 2.54, whereas the best-fitting one-rake model fault has an M/N ratio of 1.61. Results of the section-elevation-change models, though within 5 percent of the M/N ratio for models with independent data, are omitted from table 5 and indicate somewhat different parameter values. We note that model discrimination is weaker, and the acceptable range of parameters values is larger, with correlated data.

Use of a two-rake model fault significantly improves the fit by reducing the M/N ratio from 1.61 to 1.33 with independent data. Although we have added two new degrees of freedom to the model, the improvement in fit is significant above the 99-percent-confidence level. We follow the method of Barrientos and others (1987, 1989) to analyze the significance of this improvement in fit. The geometry of the two-rake model fault changes only slightly from that of the one-rake model fault: The dip is slightly greater at 62°, the depth of burial is 4.5 km, and the

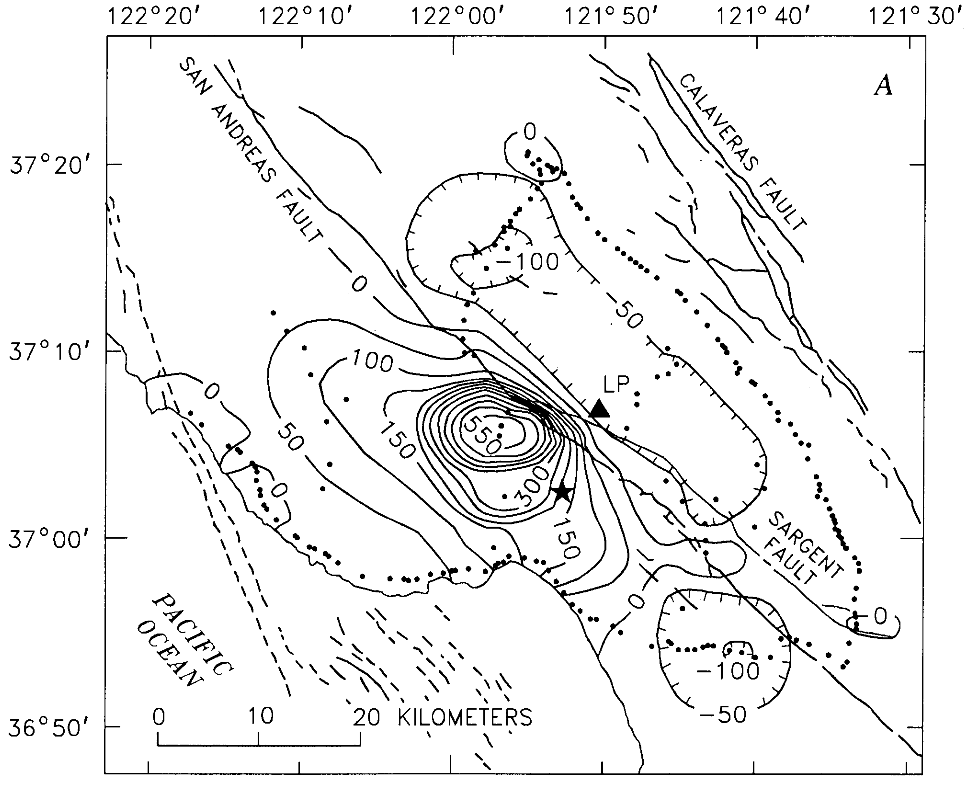

Figure 4.—Schematic map of Loma Prieta region, Calif., showing contours of observed (A), predicted (B), and residual (C) (observed minus predicted) coseismic elevation change. Predicted and residual elevation changes for one-rake planar model fault are listed in table 4. Star, epicenter of Loma Prieta earthquake of October 17, 1989 (M_s=7.1); triangle, Loma Prieta; dots, bench marks. Map in figure 4C was constructed by contouring residual elevation changes, not by subtracting predicted from observed contours. Residual and observed contours are valid only where they are adjacent to bench marks. Contour intervals: 50 mm (figs. 4A, 4B), 20 mm (fig. 4C; shaded where positive).

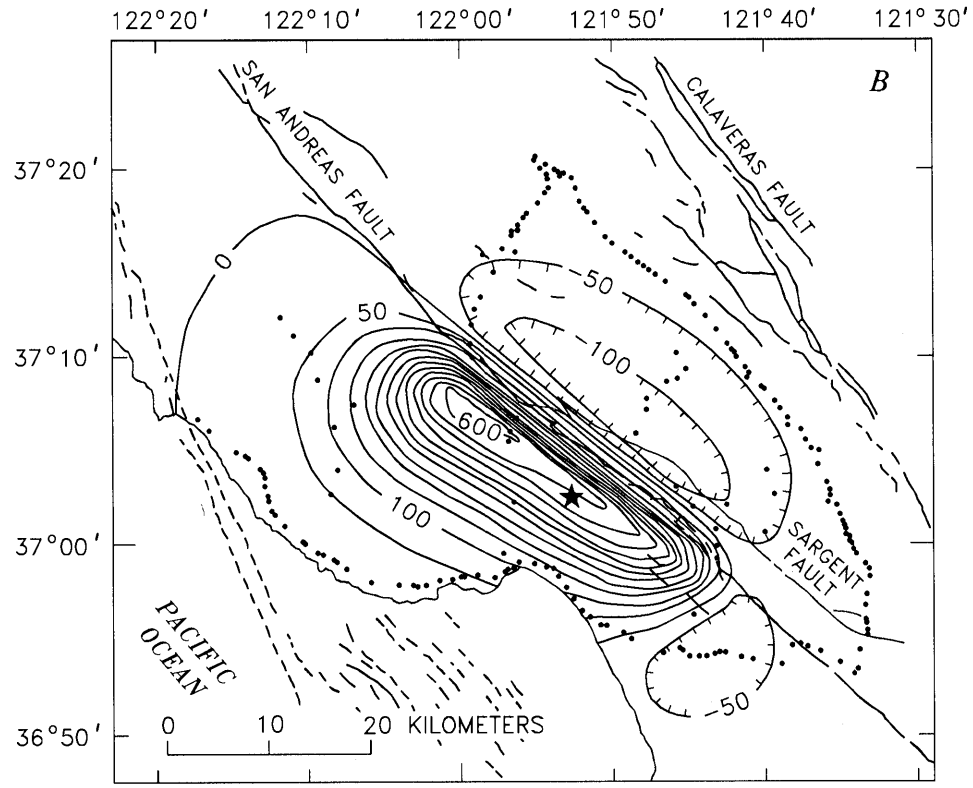

Figure 4.—Continued

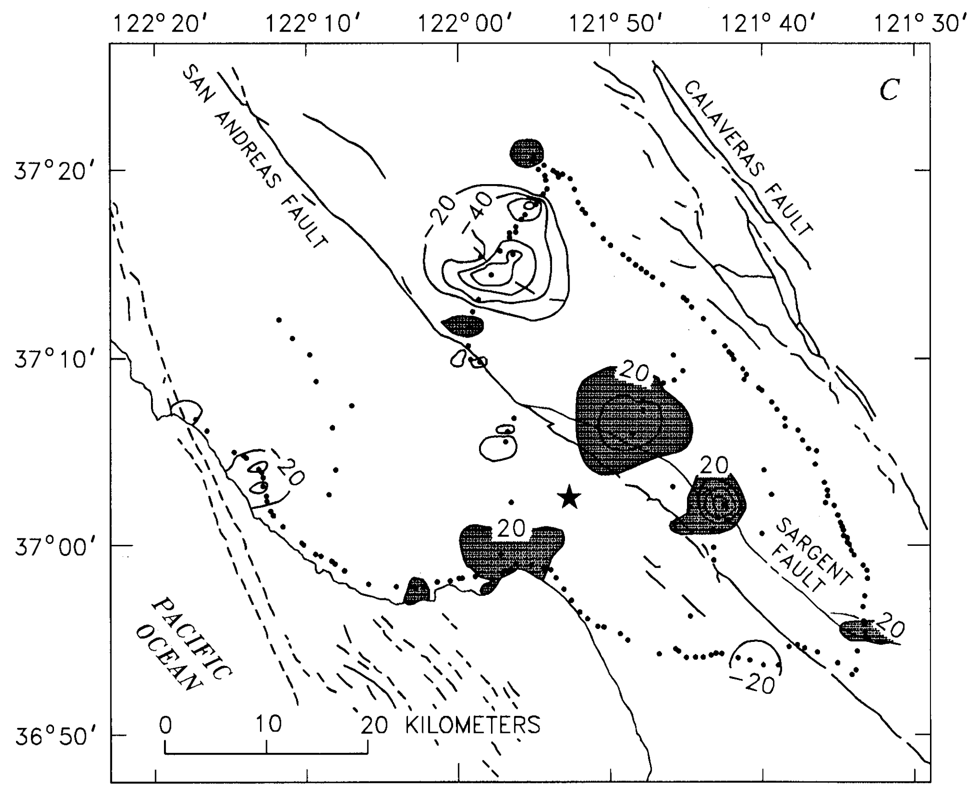

Figure 4.—Continued

length is 37 km. The segment lengths are equal (18.5 km each) and have rakes of 116° in the northwest and 163° in the southeast, similar to the average rake values determined from modeling of strong-motion data (115° NW., 156° SE.; Steidl and others, 1991). The two-rake model fault is illustrated in figure 9. With correlated data, the best two-rake model fits the data no better than the one-rake model. We prefer the two-rake model because it produces the same data misfit with a lower moment—it is a more efficient source. Furthermore, the greater width of the two-rake model fault is more consistent with the spatial extent of the aftershock zone. In comparison with the two-rake model with independent data, the variation in rake is subtle (13°) for the section-elevation-change model. A still more efficient source is obtained if we use the two-rake model with independent data to model the section-elevation changes; then, the M/N ratio is 1.64, and the seismic moment is 1.8×10^{19} N-m.

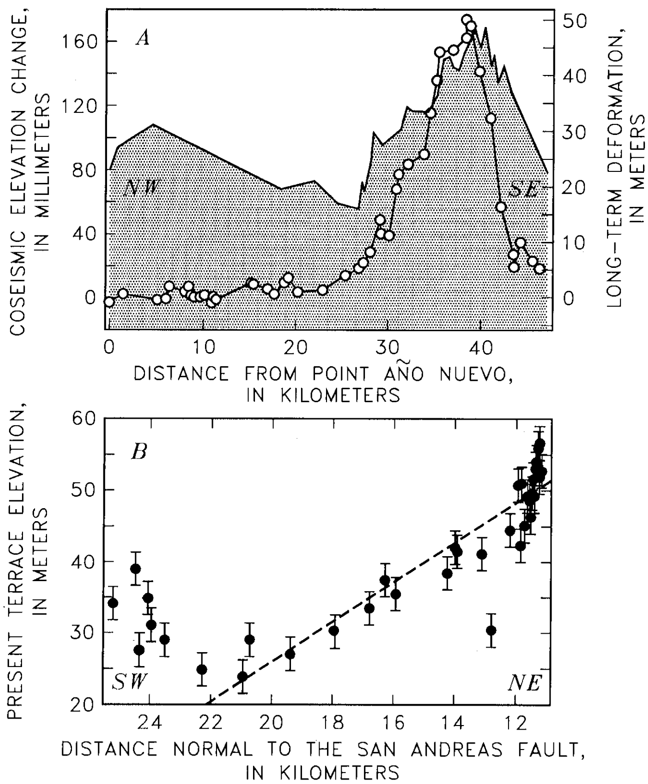

Figure 5.—Marine-terrace deformation. *A*, Profiles of coseismic (circles) and long-term (shaded curve) coastal deformation; long-term deformation is derived from 125-ka marine terrace. Profile is projected along lat N. 115° E. from Point Año Nuevo. Note that leveling route does not everywhere coincide with inner edge of terrace (see fig. 1) *B*, Terrace elevation as a function of perpendicular distance from the San Andreas fault. Dashed line shows linear fit to data, excluding first seven data points.

SENSITIVITY OF RESULTS TO DATA DISTRIBUTION

Because peak-elevation changes are measured on few bench marks and are derived from third-order preearthquake levelings (route 4, inset, fig. 1), we examine how these data influence the goodness of fit of one-rake models with independent data. When we remove leveling route 4, our best-fitting planar-fault geometry

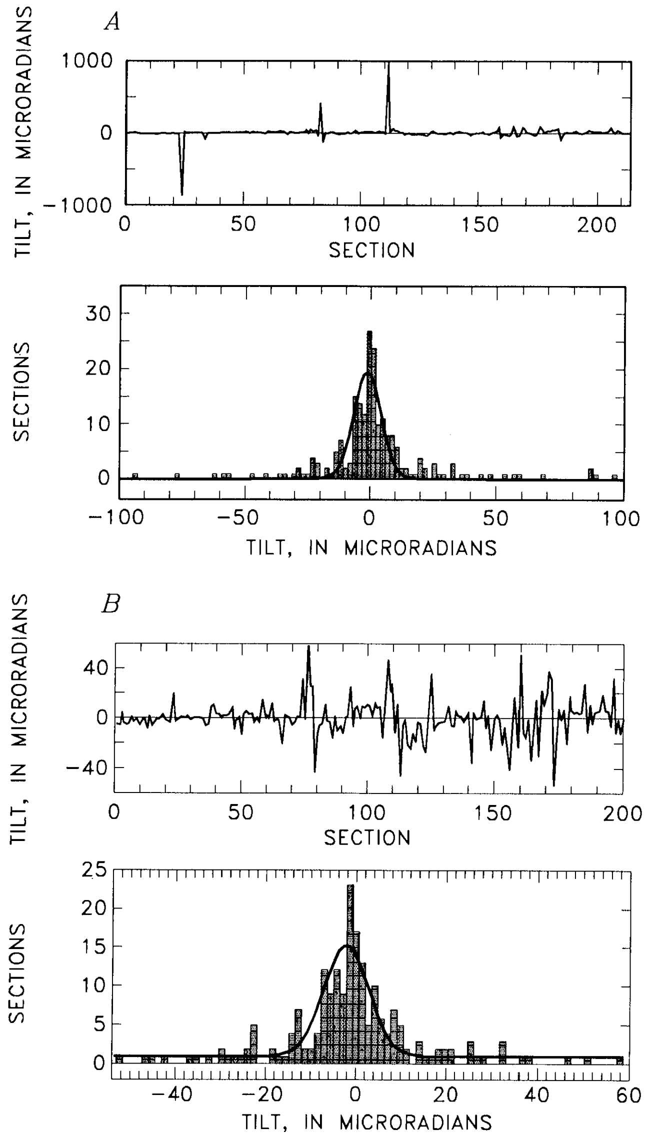

Figure 6.—Coseismic section-elevation changes, showing tilt by section (upper plot) and histogram of tilt populations (lower plot). *A*, Entire data set. Tilt population: standard deviation, 8 microradians; mean, -1 microradian. *B*, Data set with four bench marks with spikes greater than 40 microradians and eight sections with steps greater than 70 microradians omitted. Tilt population: standard deviation, 7 microradians; mean, -2 microradians. Tilt limits: spikes, 40 microradians; steps, 70 microradians. Note that tilt limits are 5 and 9 times the original standard deviation, respectively, and that only 5 percent of data are omitted.

(table 6) gives the same *M/N* ratio as with all the data, indicating that the best-model selection is insensitive to these data.

If all third-order leveling and data with large subsidence corrections are removed (leveling routes 3–7, inset, fig. 1), the precise first-order surveys (leveling routes 1, 2) that circumscribe the aftershock zone remain. Using only these observations increases the acceptable range of fault parameters. The best-fitting planar one-rake model obtained using all the data (table 6), however, remains among the best-fitting models. Marginally better fits can be obtained by changing the fault geometry as follows: length, <34 km; width, <9 km; strike, <128°; dip, >50°, and rake, >145°; however, these faults are displaced still farther to the southwest of the aftershock zone. Faults with a width >10 km, a strike >130°, a dip <50°, a rake <140°, and a depth <5 km are precluded when only leveling routes 1 and 2 are used. Thus, the less precise data from the interior of the network do not dictate the modeling results, although including them limits the range of acceptable models.

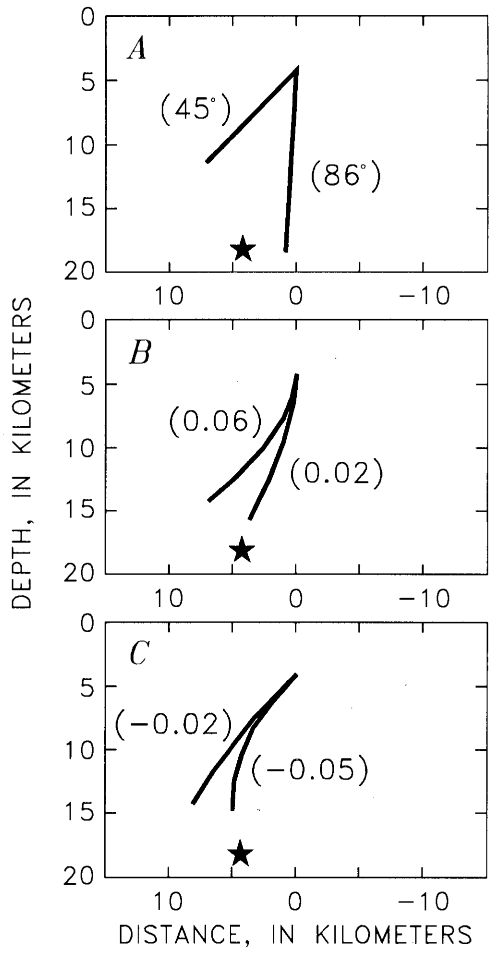

Figure 7.—Profiles of model faults: (*A*) planar, (*B*) listric, and (*C*) negatively listric. In figure 7*A*, maximum and minimum dips are shown; in figures 7*B* and 7*C*, maximum and minimum curvatures are shown. Dip of upper edge of fault is 85° in figure 7*B* and 45° in figure 7*C*. Downdip fault widths are arbitrary. Star, location of hypocenter relative to strikeline.

If the model fault is restricted to lie within the aftershock zone, a substantial misfit results. Translating the best-fitting fault perpendicular to strike 2 km to the northeast, and increasing the dip to 65° and the downdip width to 13 km, so that the fault approximately coincides with the aftershock zone and the main-shock hypocenter, the minimum *M/N* ratio we obtain is 3.01, representing an 86-percent increase in the average misfit relative to our best-fitting fault. Increasing the fault dip from 60° through 65°–70° produces large misfits adjacent to the east side of the San Andreas fault, resulting from excessively large subsidence (leveling routes 3–6, inset, fig. 1). Increasing the downdip width of the fault produces too much deformation in the far field at any of the three dips tested, too much uplift along the coast (leveling route 2), and too much subsidence inland (leveling route 1); in addition, the peak uplift along leveling route 4 cannot be modeled with a wider fault.

The section-elevation-change models place nearly all weight on the leveling routes at the periphery of the network, owing to the high bench-mark density; the interior leveling routes receive less weight because the section lengths are longer than those of the exterior leveling routes (see eq. 3). For section-elevation changes, the exterior data have 50 times the weight of the interior data, whereas with independent elevation changes, the exterior data have 17 times the weight of the interior data. The fact that wider variation in parameter values is acceptable for the section-elevation-change models stems from the absence of constraints furnished by the large signal of the interior data, consistent with results of the data-sensitivity tests.

NONHOMOGENEOUS ELASTIC MODELS

Next, we examine the systematic bias inherent in the use of an elastic half-space in place of more realistic Earth structure. Eberhart-Phillips and others (1990) demonstrated a marked velocity gradient with depth in the southern Santa Cruz Mountains: Seismic *P*-wave velocities range from 3.2 to 5.6 km/s in the uppermost 3 to 5 km, increasing to 6.5 to 6.8 km/s below 10- to 15-km depth. Reches and Zoback (1990) argued that strain is concentrated in the low-modulus (low velocity) layer. To test whether the modulus contrast caused by the velocity and associated rock-density gradient influences the deduced fault geometry and slip, we carry out a suite of simple boundary-element tests.

Table 5.—*Ranges of parameters of one-rake model faults*

[Dip on nonplanar faults is for upper edge of fault surface. Latitude and longitude are for vertical projection onto the Earth's surface of northwest corner of upper edge of fault surface. Strike is measured clockwise from north. Rake is measured on fault surface counterclockwise from strike azimuth. Downdip fault shape is described by the relation $x=b_1z+b_2z^2$, where x is the horizontal distance perpendicular to strike in the direction of dip and z is the depth]

Parameter	Planar fault	Listric fault	Negatively listric fault
Length (km)	20→40	30→35	30→35
Width (km)	3→24	7→16	6→12
Dip (°)	45→86	66→85	45→59
Latitude (°N.)	37.127→37.265	37.149→37.184	37.147→37.177
Longitude (°W.)	122.099→121.939	122.027→121.983	122.031→121.990
Depth (km)	0→9	1→6	3→5
Strike (°)	120→140	125→130	126→130
Rake (°)	120→160	140→150	140→150
b_2 (km^{-1})	0	.02→0.06	−.05→ −0.02
Number of models computed.	64,000	32,000	32,000

Table 6.—*Best-fitting uniform-elastic-half-space models*

[Length is measured along strike. Width is measured downdip. Latitude and longitude are for vertical projection onto the Earth's surface of northwest corner of upper edge of fault surface. Depth is to upper edge of fault surface. Strike is measured clockwise from north. Rake is measured on fault surface counterclockwise from strike azimuth. Downdip fault shape is described by the relation $x=b_1z+b_2z^2$, where x is the horizontal distance perpendicular to strike in the direction of dip and z is the depth. Distance to hypocenter is closest approach between fault surface and hypocentral location of Dietz and Ellsworth (1990). Geodetic moment is based on shear modulus $\mu=3.23\times10^{10}$ Pa]

	Fixed parameters										Inversion results			
Fault style	Length (km)	Width (km)	Dip, upper edge (°)	Dip, lower edge (°)	Latitude (°N.)	Longitude (°W.)	Depth (km)	Strike (°)	Rake (°)	b_2 (km^{-1})	Distance to hypocenter (km)	Slip (m)	Geodetic moment (10^{19} N-m)	M/N ratio
Independent data														
Planar	34	9	60	60	37.161	122.013	4	128	145	0.000	6	2.9±0.1	2.9±0.1	1.62
Listric	34	11	75	45	37.159	122.014	4	127	143	.040	5	2.4±0.1	2.9±0.1	1.67
Negatively listric.	34	6	51	72	37.159	122.021	5	127	142	−.045	8	4.3±0.1	2.8±0.1	1.61
Two-rake planar.	[1]37	9	62	62	37.164	122.014	4.5	128	[2]116/163	.000	6	2.1±0.1	2.2±0.1	1.33
Correlated data														
Planar	31	4	66	66	37.136	121.971	7	129	155	0.000	7	7.4±0.4	3.0±0.2	1.57
Two-rake planar.	32	7	64	64	37.140	121.972	6	129	[2]144/157	.000	6	3.6±0.2	2.6±0.2	1.57

[1]Two-rake fault is segmented halfway along strike; each segment is 18.5 km long.
[2]First rake value applies to northwest segment, and second to southeast segment.

LAYERED MODEL

We conducted three experiments to assess the effects of the modulus contrast at Loma Prieta. In the first experiment, we considered a dip-slip fault of infinite length along strike embedded in a layer over a half-space, using the boundary-element program of King and Ellis (1990). Shear and normal stresses were prescribed to be continuous across the layer interface. Taking a 5-km-thick layer velocity of 4 km/s and a density of 2,700 kg/m^3, with an underlying-half-space velocity of 6.7 km/s and a density of 3,000 kg/m^3, yields a contrast in Young's modulus, E, between the half-space and the layer of 3 (3.6×10^{10} Pa above and 11.2×10^{10} Pa below). Poisson's ratio is 0.25 in both the layer and the underlying half-space. In our test, we used a contrast in Young's modulus of 5 to examine the maximum possible effects of the weak layer. Uniform slip was imposed on a 65°-dipping fault extending from 6- to 18-km depth. The vertical deformation calculated for this model was then inverted, assuming a uniform half-space.

WEDGE MODEL

In the second experiment, we replaced the low-modulus layer with a wedge extending from the San Andreas fault 10 km to the west and extending vertically from the surface to a depth of 7 km, (see Eberhart-Phillips and Stuart, 1992). The wedge exaggerates the observed across-fault modulus contrast, particularly near the surface, and thus furnishes an upper-bound case to assess how nonhomogeneous Earth models affect the fault parameters. Both the layer and wedge models are approximations to features observed in Eberhart-Phillips and others' (1990) seismic-velocity model. Young's modulus in the wedge is 3.5×10^{10} Pa, and in the surrounding medium 8.8×10^{10} Pa, for a contrast of 2.5. Note that the fault contacts the wedge at a depth of 5 to 7 km (fig. 10*E*). Poisson's ratio within the wedge is 0.333, and in the surrounding medium 0.258.

In the third experiment, we retained the wedge geometry but imposed a uniform shear-stress drop on the fault, rather than uniform fault slip. This condition, also used by Eberhart-Phillips and Stuart (1992), results in tapered slip. For an elastic half-space, the condition produces maximum slip at the center of the fault; in the wedge model,

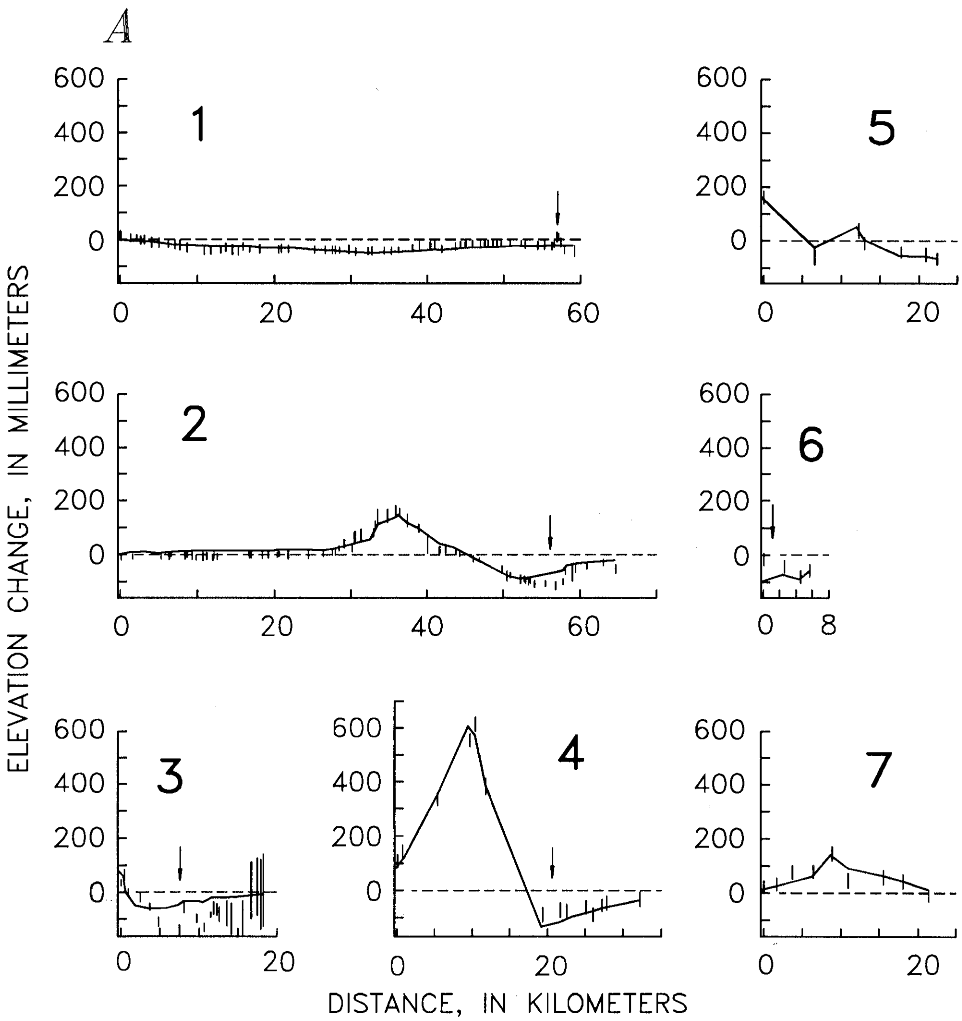

Figure 8.—Profiles of best one-rake (*A*) and two-rake (*B*) planar model faults and observed coseismic elevation changes along leveling routes 1 through 7 (see inset, fig. 1). Vertical bars indicate relative uncertainty of determinations; note that relative uncertainties are large where substantial subsidence corrections have been made (for example, profile 3). Arrows indicate locations where notable misfits occur; note that misfits are substantially reduced for two-rake model fault (fig. 8*B*).

slip is concentrated near the top of the fault because the wedge is more compliant than its surroundings.

MODIFICATIONS TO HALF-SPACE MODELS

Models with a nonhomogeneous elastic structure reduce the misfit of the geodetic fault plane to the aftershock zone and main-shock hypocenter. In the layered model, the location of the upper edge of the fault, its dip, and the slip amplitude are nearly unaffected by the low-modulus layer. The upper edge of the fault, however, locates 1 km too shallow, and the lower depth is as much as 2.3 km too shallow. Thus, if a contrast in Young's modulus of as much as 5 is appropriate for Loma Prieta, then faults would extend 2 to 3 km deeper and be slightly steeper than those deduced by half-space models. Inclusion of the low-modulus layer therefore moves faults several kilometers closer to the main-shock hypocenter than do half-space models (compare figs. 10*B*, 10*D*).

Similarly, imposing uniform slip on the fault in the wedge model results in the fault locating 1 km to the east of its former position, and the fault width increases by several kilometers. With the uniform-shear-stress wedge model, the fault again is found to locate 1 km farther east than for a half-space; in addition, the fault width is found to increase by 4 to 5 km, the slip is reduced by 25 to 30 percent, and the dip may increase slightly (<5°). The effect of these changes is shown in figure 10*E*. The fault lies closer to the aftershock zone and main-shock hypocenter, although the locations of the fault and aftershocks do not coincide. The improvements in fit to the aftershock zone gained by considering a nonhomogeneous structure are illustrated in figure 11, which also shows the dependence of the fit on hypocentral distance for elastic-half-space planar model faults.

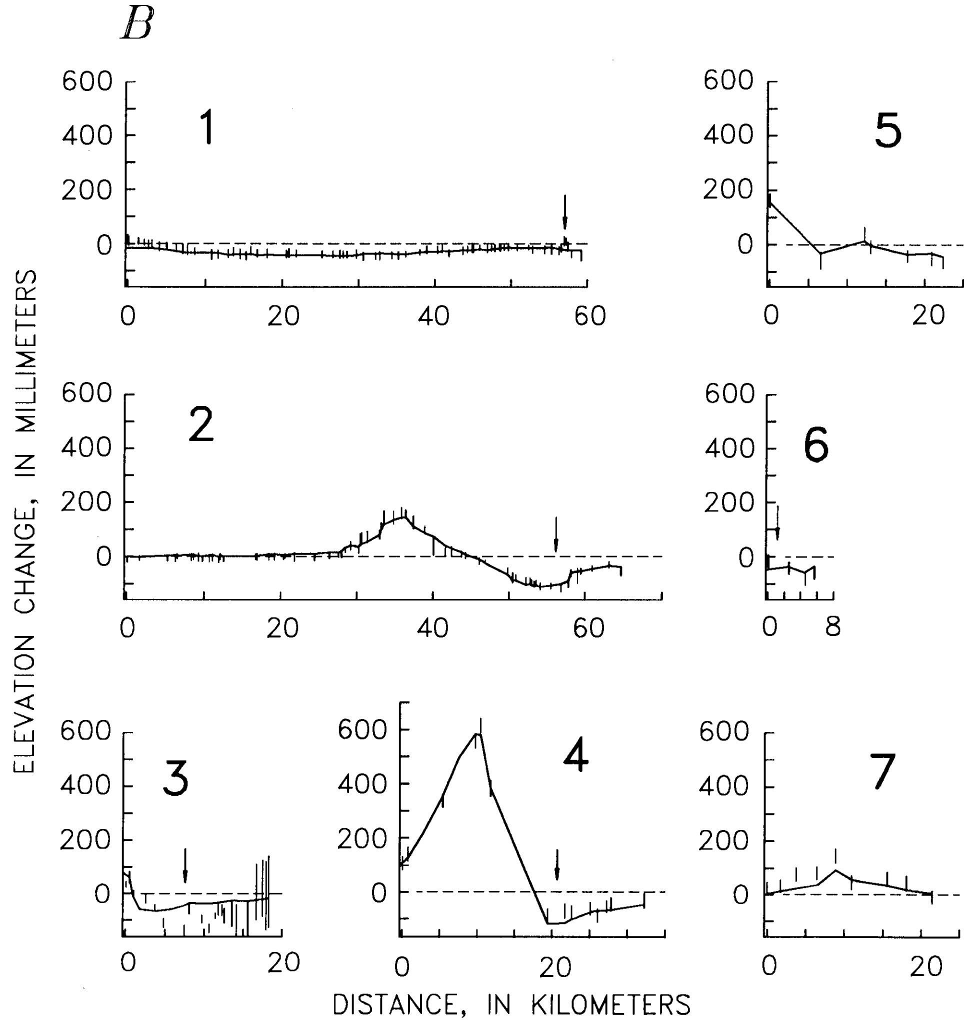

Figure 8.—Continued

Table 7.—*Ranges of parameters for uniform-elastic-half-space models*

[Dip on nonplanar faults is for upper edge of fault surface. Latitude and longitude are for vertical projection onto the Earth's surface of northwest corner of upper edge of fault surface. Strike is measured clockwise from north. Rake is measured on fault surface counterclockwise from strike azimuth. Downdip fault shape is described by the relation $x=b_1z+b_2z^2$, where x is the horizontal distance perpendicular to strike in the direction of dip and z is the depth. Geodetic moment is based on shear modulus $\mu=3.23\times10^{10}$ Pa]

Fixed parameter	Planar fault	Listric fault	Negatively listric fault
Length (km)	32→35	30→35	31→35
Width (km)	9→11	7→12	6→10
Dip (°)	57→60	66→85	48→55
Latitude (°N.)	37.153→37.167	37.147→37.172	37.148→37.169
Longitude (°W.)	122.023→122.003	122.031→121.997	122.027→121.998
Depth (km)	4→5	4→6	4→5
Strike (°)	126→129	125→130	126→129
Rake (°)	139→147	140→150	140→150
b_2 (km^{-1})	0	.020→0.060	-.045→ −0.020
Number of models	641	200	90
	Inversion results		
Distance to hypocenter (km).	5→7	4→7	6→8
Slip (m)	2.3→3.0	2.1→4.2	2.5→4.6
Geodetic moment (10^{19} N-m).	2.6→3.0	2.6→3.4	2.6→3.1
M/*N* ratio	1.62→1.70	1.67→1.75	1.61→1.69

Although all non-half-space models move the fault closer to the aftershock zone, none moves it far enough, and so we have made the modulus contrast as large as permitted by the velocity data of Eberhart-Phillips and others (1990). We note that the uniform-shear-stress-drop model produces about the same geodetic moment as the uniform-slip model because the increased fault width is compensated by the decreased slip. The top of the fault surface undergoes increased slip in the presence of the more compliant wedge under the uniform-shear-stress-drop assumption, a plausible result for an individual earthquake. Over many earthquake cycles, however, uniform slip from

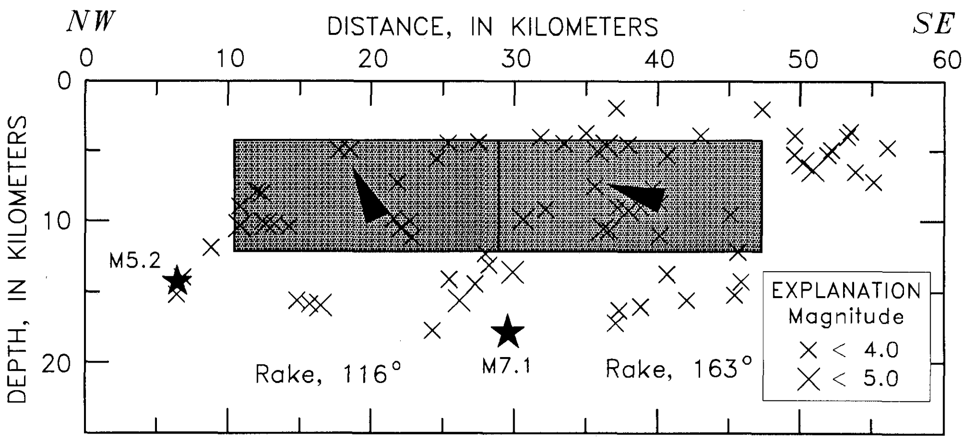

Figure 9.—Alongstrike cross section of two-rake model fault from southwest side. Arrowheads indicate slip direction of hanging-wall block. Stars, main shock and largest aftershock. Fault motion is primarily dip slip to northwest of hypocenter and primarily strike slip to southeast of hypocenter.

the Earth's surface to the base of the seismogenic layer must prevail, and so it is unclear which assumption best represents the Loma Prieta rupture.

DISCUSSION

COMPARISON OF GEODETIC RESULTS WITH STUDIES OF SEISMICITY AND GEOLOGY

The seismic-source mechanism and waveforms of the 1989 Loma Prieta earthquake appear to have simple characteristics, in comparison with those of other earthquakes of similar magnitude, such as the 1988 M=6.7 Armenia earthquake (Kanamori and Satake, 1990). Nevertheless, seismologic studies of the Loma Prieta mechanism suggest a range of source parameters, some of which are compatible with our geodetic results. The source mechanisms found in 10 such studies are compared with the results of our elastic-half-space modeling with independent data in table 8. Four of these studies provide estimates of the strike, dip, and rake that fall within our acceptable model range: the first-motion mechanisms of Plafker and Galloway (1989) and Oppenheimer (1990), and the body-wave inversions of Choy and Boatwright (1990) and Langston and others (1990). Of the 10 studies, 5 report a fault dip and seismic moment consistent with our acceptable model range, and most of the studies agree with our values of strike and rake. The seismologic determination of the source dip, however, is least consistent with our results. The 10 studies report dips ranging from 53° to 85°, and several studies have solutions with dips ≥70°, a value that produces significant misfits to the leveling observations. Seismic values of the fault rake, which range from 110° to 155°, also exceed our acceptable model range. Seismic moments derived from surface-wave analy-

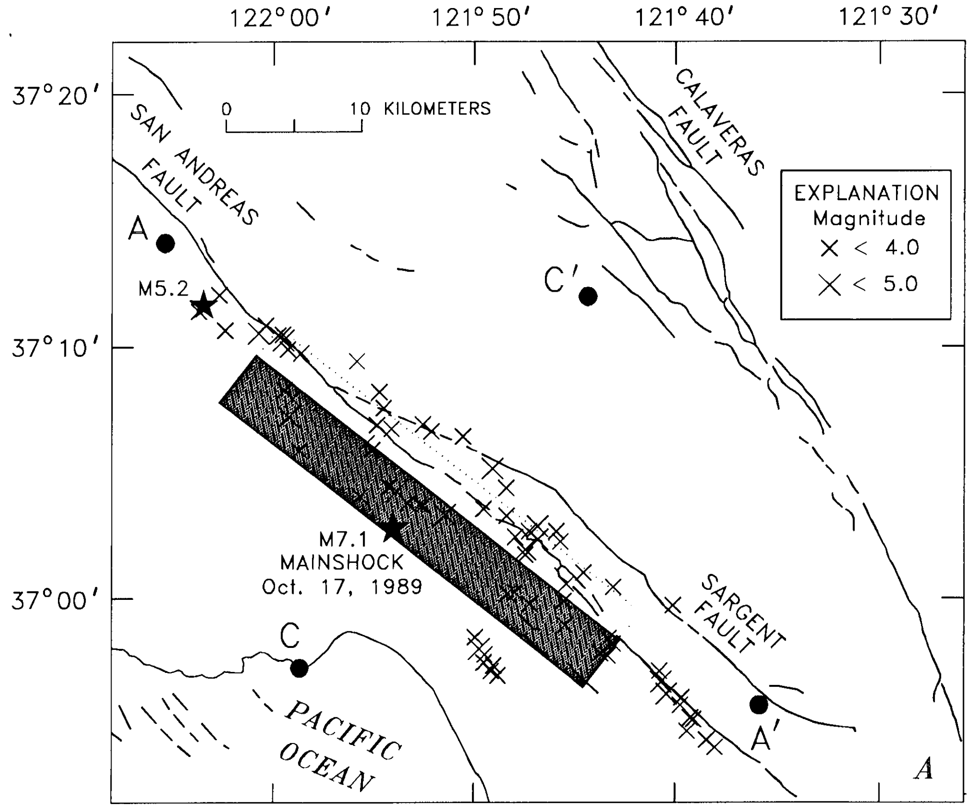

Figure 10.—Schematic map (A) and cross sections (B–F) of Loma Prieta region, Calif., showing locations of aftershocks of M≥3 (Dietz and Ellsworth, 1990) and vertical projection of best-fitting planar model fault (shaded rectangle). Dotted line, updip projection. Quaternary faults (dashed where inferred) from Jennings (1975). Cross sections C–C' (figs. 10B–10E) show updip projection of fault surface (dotted line) and locations of the San Andreas (SA) and Sargent (S) faults. B, Results for elastic-half-space two-rake model fault with independent data. C, Results for elastic-half-space two-rake model fault with correlated data: D, Corrections for low-modulus layer (shaded area) over half-space. E_1, E_2, Young's modulus. E, Corrections for low-modulus wedge (shaded area) in half-space. E_1, E_2, Young's modulus. F, Alongstrike projection of fault surface. Bold rectangle, elastic half-space; dotted rectangle, layer over half-space; long-dashed rectangle, wedge in half-space; short-short-long-dashed rectangle, model fault with correlated data.

ses (Romanowicz and Lyon-Caen, 1990; Zhang and Lay, 1990) and from the body-wave solutions of Barker and Salzberg (1990), Nábělek (1990), and Kanamori and Satake (1990), however, agree with the calculated geodetic moment. Seismic moments derived from data at different frequencies and from different studies vary by a factor of as much as 2.

The consistency between the seismic and geodetic results can be addressed further by examining the spatial relation between the geodetically determined fault surface and the main shock and its aftershocks. Dietz and Ellsworth (1990) found that the aftershock distribution is approximately planar, extending upward from the main-shock hypocenter along a 65°-dipping zone that is 4 to 5 km wide perpendicular to strike. Along strike, Loma Prieta aftershocks tend to cluster around the periphery of a central zone that is depleted of aftershocks. The observed vertical-deformation field is best modeled by a rupture surface approximately parallel to and southwest of the aftershock zone, with a homogeneous elastic Earth structure and independent data. Correlated data reduce this discrepancy and place the fault closer to the aftershock zone. Models that lie within the aftershock zone increase the misfit to the correlated observations by 3 percent. Our models of nonhomogeneous elastic structure also suggest a significant reduction of the misfit of the geodetic fault plane to the aftershock zone and main-shock hypocenter. Our best-fitting planar model faults are mapped in figure 10, with aftershocks of $M \geq 3$ from Dietz and Ellsworth (1990). In map view, the epicenter nearly bisects the fault plane along strike, consistent with bilateral rupture as modeled by Beroza (1991), Steidl and others (1991), and Wald and others (1991). The updip projection of the model fault surface at its northwest terminus coincides with the trace of the San Andreas fault; at its southeast end, the updip projection is equidistant between the Sargent and San Andreas faults. Most aftershock activity is clustered approximately 4 to 5 km northeast and below our elastic-half-space model fault (fig. 10*B*). Including correlations in the leveling data or nonhomogeneous elastic structure improves the fit to the aftershocks, as shown in figures 10*C* through 10*F*. Our acceptable range of latitudes and longitudes allows the elastic model fault to move less than 2 km perpendicular to strike, and the results of our nonhomogeneous tests indicate that the half-space solutions may shift the fault plane 1 km perpendicular to strike.

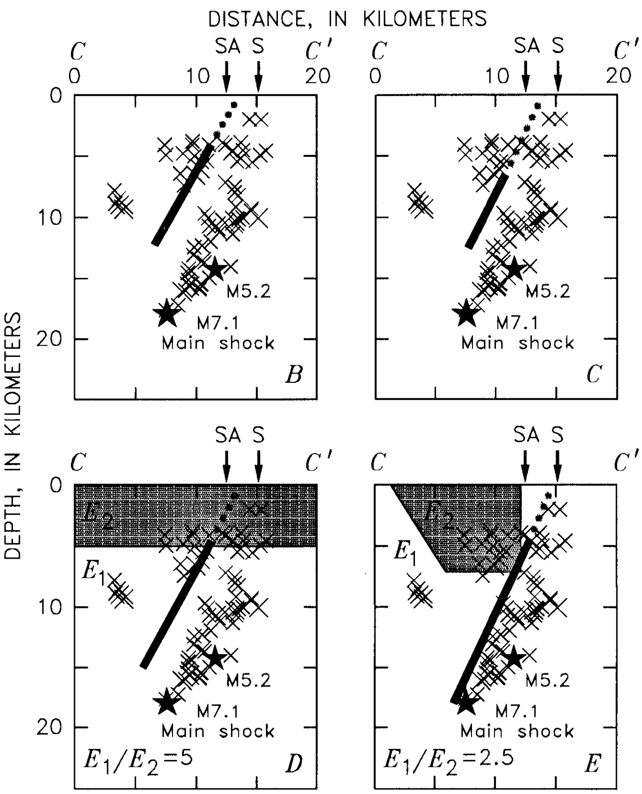

Figure 10.—Continued

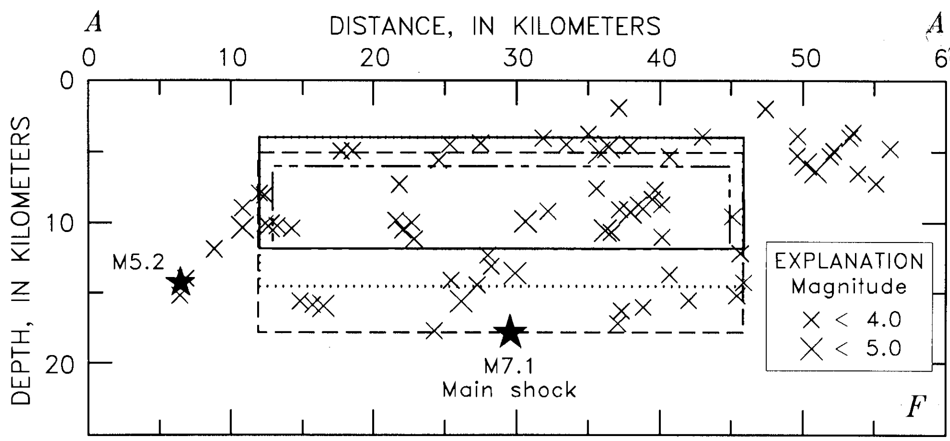

Figure 10.—Continued

Thus, if our two-dimensional nonhomogeneous models are appropriate for the Loma Prieta region, then the combined results indicate that the discrepancy between the position of the geodetic fault plane and the aftershock zone is small (~1 km). In modeling with correlated data, this discrepancy becomes insignificant.

Studies of teleseismic body waves place centroidal depths between 8 and 16 km, shallower than the main-shock hypocenter, which is presumably the depth of rupture initiation (table 8). These teleseismic studies generally only weakly constrain the spatial extent of significant slip on the fault plane. Modeling of local strong-motion seismic data provides better resolution, and these studies suggest that moment release is concentrated in two zones lying between about 9- and 16-km depth (Beroza, 1991; Steidl and others, 1991; Wald and others, 1991). The location of the rupture surface, as constrained by vertical geodetic data and corrections for nonhomogeneous elastic structures, suggests that significant moment release occurred from 6- to 18-km depth, moderately consistent with these interpretations of the strong-motion data.

Focal mechanisms of aftershocks are diverse over short spatial scales. Oppenheimer (1990) presented focal mechanisms for a representative sample of aftershocks; the variations in and distinctness of the aftershock mechanisms, in comparison with the main-shock mechanism, could mean that the aftershocks occurred on structures adjacent to the main-shock rupture surface. The misfit of our model faults to the aftershock zone, however, could also be due to unmodeled three-dimensional variations in elastic modulus or to greater variations in fault geometry or slip distribution. Inaccurate velocity models used to locate the aftershocks might also explain part of this misfit.

The oblique slip inferred from geodetic observations is consistent with the abundance of young (Pliocene-Quaternary) fold structures and reverse faults identified throughout the Santa Cruz Mountains. The Loma Prieta rupture occurred within a structural domain, bounded by the San Gregorio-Hosgri fault in the west, the Ben Lomond, Zayante, and Vergeles faults in the southwest, and a discontinuous series of faults east of the San Andreas fault (Aydin and Page, 1984) that is characterized by southwest-dipping faults and northwest-trending folds. At the surface, the fault features indicate both strike-slip and reverse displacements. The surface projection of model faults compatible with the vertical geodetic data could match either the Sargent or the San Andreas fault.

RELATION TO OTHER GEODETIC STUDIES

A geodetic model (Lisowski and others, 1990) derived from precise electronic distance measurement (EDM), Global Positioning System (GPS) vectors, and very long baseline interferometry (VLBI) observations is not fully consistent with our best-fitting model fault (table 8). Lisowski and others modeled the offsets in the relative positions of geodetic stations, using an elastic dislocation, and determined the source mechanism: strike, 136°; dip, 70°; rake, 144°; geodetic moment, 3.0×10^{19} N-m. The rake and moment of their solution are consistent with our results, whereas the strike and dip do not fall within our acceptable model range. Their model has a strike slightly different from that of the aftershock zone, producing a close fit to the aftershocks in the northwest but a misfit of about 2 km in the southeast. Although their model agrees better with the locations of aftershocks, it has an *M*/*N* ratio of 2.4 (twice as large as that of our best fitting model) when used to model the coseismic elevation changes. Likewise, our model doubles the average misfit of their obser-

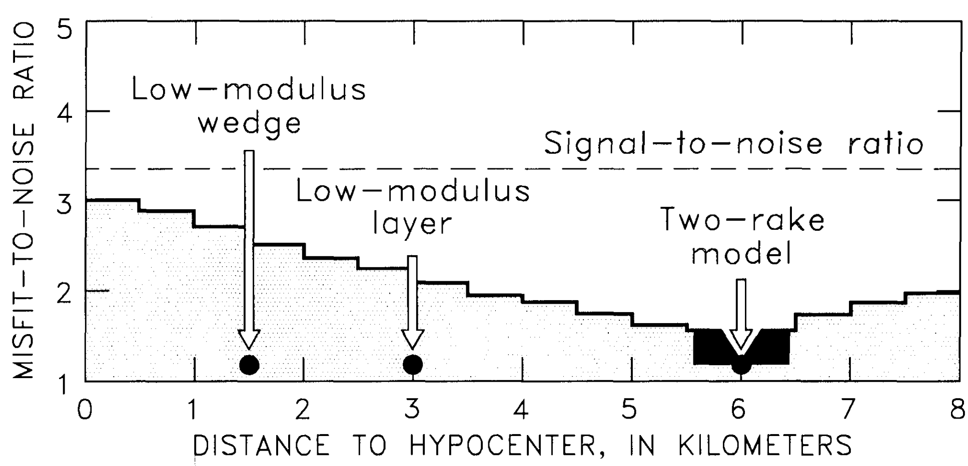

Figure 11.—Misfit-to-noise ratio for one-rake (shaded area) and two-rake (black area) planar model faults versus distance to hypocenter. Best-fitting faults are those with smallest misfit-to-noise ratio and a corresponding hypocentral distance of 6 km. Two-rake model substantially reduces misfit of elevation change. Low-modulus layer and wedge reduce misfit of model fault surface to aftershock zone.

Table 8.—*Comparison of fault parameters from seismologic studies with the results of our elastic-half-space modeling*

[Boldface values are consistent with our ranges of model parameters listed at bottom. Strike is measured clockwise from north. Rake is measured on fault surface counterclockwise from strike azimuth. Depth from *P*-wave first-motion data is depth to rupture initiation; depth from body-wave data is average depth; and depth from body- and surface-wave data is centroidal depth, using a 4-km radius. Do., ditto]

Strike (°)	Dip (°)	Rake (°)	Seismic moment (10^{19} N-m)	Depth (km)	Type of data	Reference
120–140	**55–85**	**125–155**	- -	18	*P*-wave first motions -----------	Oppenheimer (1990).
122–138	**60–80**	**115–145**	- -	19	do -------------------------	Plafker and Galloway (1989).
130	73	**146**	**2.8**	18	Body waves --------------------	Barker and Salzberg (1990).
125–135	**60–70**	**135–145**	2.0–2.2	**12–16**	do -------------------------	Choy and Boatwright (1990).
117–127	**53–63**	**139–149**	2.1–2.4	**8**	do -------------------------	Langston and others (1990).
126–130	61–65	127–131	**3.0–3.1**	**11–12**	do -------------------------	Nábělek (1990).
126	66	138	1.7	**10**	do -------------------------	Romanowicz and Lyon-Caen (1990).
132–144	71–81	110–130	1.5–2.5	**10–12**	do -------------------------	Ruff and Tichelaar (1990).
125–129	70–75	**130–144**	**2.5–3.0**	**15**	Body and surface waves-------	Kanamori and Satake (1990).
122–132	61–71	127–137	**2.8–3.8**	20	Surface waves -----------------	Romanowicz and Lyon-Caen (1990).
125–135	65–75	**130–140**	**2.9–3.9**	**12–22**	do -------------------------	Zhang and Lay (1990).
136	70	**142–147**	**2.6–3.4**	**11**	Horizontal deformation--------	Lisowski and others (1990).
126–129	57–60	139–147	2.6–3.0	8	Vertical deformation (elastic half-space).	This study.

vations. Future studies that combine both geodetic data sets are needed to find the fault geometry and source mechanism that are most consistent with all the observations.

CONCLUSION

Observations of coseismic elevation changes associated with the 1989 Loma Prieta earthquake favor a rupture surface extending from 6- to 12-km depth, dipping 64°. With a geodetic moment of 2.6×10^{19} N-m, slip direction on this rupture surface ranges in rake from 144° northwest of the epicenter to 157° southeast of the epicenter, with a slip amplitude of 3.6 m. A two-rake model fault produces the same fit to the observations as a one-rake model fault, with 13 percent less moment. Thus, the two-rake model fault is a more efficient source of surface deformation and, in our judgment, more probable. With independent data, two-rake models with a rake variation greater than 40° can be found that offer smaller model misfit and less moment.

The rupture surface determined by our half-space modeling lies 1 to 2 km southwest of most aftershocks and is 6 km from the main-shock hypocenter. With independent data, preferred model faults lie still farther away from the aftershock zone, whereas with correlated data, faults can be found within the aftershock zone that produce only a few-percent increase in model misfit.

The strength of the section-elevation-change modeling is that the correlation of the leveling observations is incorporated into the analysis. Although the section-elevation-change modeling is more sensitive to outliers (such as spikes and steps), we have found that these features can be objectively purged. The weakness of the section-elevation-change modeling stems from the uniquely inhomogeneous distribution of the Loma Prieta data set, in which most of the signal is contained in a few long sections in the interior of the network. Although the influence of these sections is modest with independent data, it is almost nonexistent in the section-elevation-change modeling. Thus, most of the signal we seek to explain with the section-elevation-change modeling has no influence on model selection, and our ability to discriminate among candidate model faults is greatly diminished.

Two-dimensional models with nonhomogeneous elastic structure reduce the misfit between the geodetic fault plane and the aftershock zone, suggesting that more complex (three dimensional) models of the modulus structure of the crust might bring the geodetic and seismic observations into even-better accord. Using a low-modulus layer or wedge model instead of a uniform half-space also deepens and steepens the fault.

The connection between the Loma Prieta rupture surface at depth and the known faults mapped at the Earth's surface remains unclear. Because both listric and negatively listric faults are permitted by the vertical geodetic data, a connection can be inferred to either the San Andreas or the Sargent fault. Further study of the localized anomalous elevation changes seen in some of the leveling data, along with observations of surface displacements northeast of the San Andreas fault (Haugerud and Ellen, 1990), may provide the necessary evidence to infer a connection to shallow surface faults.

ACKNOWLEDGMENTS

All of the postearthquake leveling was funded by the USGS, NGS, and Santa Cruz County Public Works Department. We thank the NGS leveling crew, including Richard Hattesohl, Leonard Bergman, Don Breidenbach, Jim Palo, Scott Hanford, Chris Jacobs, and Verland Pierson, for their expertise in performing a careful and timely leveling job and in releveling after the earthquake. Emery Balazs helped to define and organize the leveling project at the NGS. Gary Perasso provided field-summary books and helpful discussions on the USGS leveling data. Kim Vester provided access to and information about Santa Cruz County leveling data. Accurate subsidence corrections could not have been made without the depth-to-water and extensometer data provided by the Santa Clara Valley Water Conservation District, with the assistance of Adele Sheperd and Lauren Mall. Robert Johnson of the Monterey County Flood Control and Water Conservation District supplied additional depth-to-water data for Monterey County. We greatly appreciate the guidance and encouragement of Wayne Thatcher and the contributions of Geoffrey C.P. King and Jian Lin in creating and testing, respectively, the boundary-element program, and the generosity of Donna Eberhart-Phillips for sharing her finite-element results with us. Thoughtful reviews of the manuscript were provided by Mike Lisowski, David Oppenheimer, and Richard Snay.

REFERENCES CITED

Anderson, R.S., 1990, Evolution of the northern Santa Cruz Mountains by advection of crust past a San Andreas Fault bend: Science, v. 249, no. 4967, p. 397–401.

Árnadóttir, Thora, Segall, Paul, and Matthews, M.V., 1992, Resolving the discrepancy between geodetic and seismic fault models for the 1989 Loma Prieta, California, earthquake: Seismological Society of America Bulletin, v. 82, no. 5, p. 2248–2255.

Aydin, Atilla, and Page, B.M., 1984, Diverse Pliocene-Quaternary tectonics in a transform environment, San Francisco Bay region, California: Geological Society of America Bulletin, v. 95, no. 11, p. 1303–1317.

Bakun, W.H., Clark, M.M., Cockerham, R.S., Ellsworth, W.L., Lindh, A.G., Prescott, W.H., Shakal, A.F., and Spudich, Paul, 1984, The 1984 Morgan Hill, California, earthquake: Science, v. 225, no. 4659, p. 288–291.

Barker, J.S., and Salzberg, D.H., 1990, Long-period and broad-band teleseismic body-wave modeling of the October 18, 1989 Loma Prieta earthquake: Geophysical Review Letters, v. 17, no. 9, 1409–1412.

Barrientos, S.E., Stein, R.S., and Ward, S.N., 1987, Comparison of the 1959 Hebgen Lake, Montana, and the 1983 Borah Peak, Idaho, earthquakes from geodetic observations: Seismological Society of America Bulletin, v. 77, no. 3, p. 784–808.

———1989, Errata; comparison of the Hebgen Lake, Montana and the 1983 Borah Peak, Idaho, earthquakes from geodetic observations: Seismological Society of America Bulletin, v. 79, no. 6, p. 2018.

Behr, Jeffrey, Bilham, Roger, Bodin, Paul, Burford, R.O., and Bürgmann, Roland, 1990, Aseismic slip on the San Andreas fault south of Loma Prieta: Geophysical Research Letters, v. 17, no. 9, p. 1445–1448.

Beroza, G.C., 1991, Near-source modeling of the Loma Prieta earthquake; evidence for heterogeneous slip and implications for earthquake hazard: Seismological Society of America Bulletin, v. 81, no. 5, p. 1603–1621.

Bomford, Guy, 1971, Geodesy: Oxford, U.K., Oxford University Press, 855 p.

Choy, G.L., and Boatwright, John, 1990, Source characteristics of the Loma Prieta, California, earthquake of October 18, 1989 from global digital seismic data: Geophysical Research Letters, v. 17, no. 8, p. 1183–1186.

Dietz, L.D., and Ellsworth, W.L., 1990, The October 17, 1989, Loma Prieta, California, earthquake and its aftershocks; geometry of the sequence from high-resolution locations: Geophysical Research Letters, v. 17, no. 9, p. 1417–1420.

Eberhart-Phillips, D.M., Labson, V.F., Stanley, W.D., Michael, A.J., and Rodriguez, B.D., 1990, Preliminary velocity and resistivity models of the Loma Prieta earthquake region: Geophysical Research Letters, v. 17, no. 8, p. 1235–1238.

Eberhart-Phillips, D.M., and Stuart, W.D., 1992, Material heterogeneity simplifies the picture; Loma Prieta: Seismological Society of America Bulletin, v. 82, no. 4, p. 1964–1968.

Haugerud, R.A., and Ellen, S.D., 1990, Coseismic ground deformation along the northeast margin of the Santa Cruz Mountains, stop 7 *of* Schwartz, D.P., and Ponti, D.J., eds., Field guide to neotectonics of the San Andreas fault system, Santa Cruz Mountains, in light of the 1989 Loma Prieta earthquake: U.S. Geological Survey Open-File Report 90–274, p. 32–36.

Jackson, D.D., Lee, W.B., and Liu, C.-C., 1981, Height dependent errors in southern California leveling, *in* Simpson, D.W., and Richards, P.G., eds., Earthquake prediction; an international review: Washington, D.C., American Geophysical Union, p. 457–472.

Jennings, C.W., compiler, 1975, Fault map of California: Sacramento, California Division of Mines and Geology, scale 1:750,000.

Kanamori, Hiroo, and Satake, Kenji, 1990, Broadband study of the 1989 Loma Prieta earthquake: Geophysical Research Letters, v. 17, no. 8, p. 1179–1182.

King, G.C.P., and Ellis, Michael, 1990, The origin of large local uplift in extensional regions: Nature, v. 348, no. 6303, p. 689–693.

King, N.E., Savage, J.C., Lisowski, Michael, and Prescott, W.H., 1981, Preseismic and coseismic deformation associated with the Coyote Lake, California, earthquake: Journal of Geophysical Research, v. 86, no. B2, p. 892–898.

Langbein, J.O., 1990, Post-seismic slip on the San Andreas fault at the northwestern end of the 1989 Loma Prieta earthquake rupture zone: Geophysical Research Letters, v. 17, no. 8, p. 1223–1226.

Langston, C.A., Furlong, K.P., Vogfjord, K.S., Clouser, R.H., and Ammon, C.J., 1990, Analysis of teleseismic body waves radiated from the Loma Prieta earthquake: Geophysical Research Letters, v. 17, no. 9, p. 1405–1408.

Lisowski, Michael, Prescott, W.H., Savage, J.C., and Johnston, M.J.S., 1990, Geodetic estimate of coseismic slip during the 1989 Loma Prieta, California, earthquake: Geophysical Research Letters, v. 17, no. 9, p. 1437–1440.

Nábělek, J.L., 1990, Rupture process of the October 18, 1989 Loma

Prieta earthquake from broadband teleseismic body waves [abs.]: Seismological Research Letters, v. 61, no. 1, p. 46.
Oppenheimer, D.H., 1990, Aftershock slip behavior of the 1989 Loma Prieta, California earthquake: Geophysical Research Letters, v. 17, no. 8, p. 1199–1202.
Plafker, George, and Galloway, J.P., eds., 1989, Lessons learned from the Loma Prieta, California, earthquake of October 17, 1989: U.S. Geological Survey Circular 1045, 48 p.
Poland, J.F., and Ireland, R.L., 1988, Land subsidence in the Santa Clara Valley, California, as of 1982: Washington, D.C., U.S. Government Printing Office, 61 p.
Prescott, W.H., King, N.E., and Gu Guohua, 1984, Preseismic, coseismic, and postseismic deformation associated with the 1984 Morgan Hill, California, earthquake, *in* Bennett, J.H., and Sherburne, R.W., eds., The 1984 Morgan Hill, California earthquake: California Division of Mines and Geology Special Publication 68, p. 137–148.
Reasenberg, P.A., and Ellsworth, W.L., 1982, Aftershocks of the Coyote Lake, California, earthquake of August 6, 1979; a detailed study, Journal of Geophysical Research, v. 87, no. B13, p. 10637–10655.
Reches, Ze'ev, and Zoback, M.D., 1990, Theoretical analysis of the deformation of a layered sequence above a fault—preliminary application to the Loma Prieta earthquake, chap. 10 *of* Nur, Amos, Mavko, Gary, and Zoback, Mark, eds., Stanford rock physics and borehole geophysics, v. 40, p.X1–X22.
Romanowicz, B.A., and Lyon-Caen, Hélène, 1990, The Loma Prieta earthquake of October 18, 1989; results of teleseismic mantle and body wave inversion: Geophysical Research Letters, v. 77, no. 8, p. 1191–1194.
Ruff, L.J., and Tichelaar, B.W., 1990, Moment tensor rate functions for the 1989 Loma Prieta earthquake: Geophysical Research Letters, v. 17, no. 8, p. 1187–1190.
Steidl, J.H., Archuleta, R.J., and Hartzell, S.H., 1991, Rupture history of the 1989 Loma Prieta, California, earthquake: Seismological Society of America Bulletin, v. 81, no. 5, 1573–1602.
Stein, R.S., 1981, Discrimination of tectonic displacement from slope-dependent errors in geodetic leveling from southern California, 1953–1979, *in* Simpson, D.W., and Richards, P.G., eds., Earthquake prediction; an international review: Washington, D.C., American Geophysical Union, p. 441–456.
Stein, R.S., Whalen, C.T., Holdahl, S.R., Strange, W.E., and Thatcher, Wayne, 1986, Saugus-Palmdale, California, field test for refraction error in historical leveling surveys: Journal of Geophysical Research, v. 91, no. B9, p. 9031–9044.
Valensise, Gianluca, 1994, Geologic assessment of the relative contribution of strike-slip faulting, reverse-slip faulting, and bulk squeezing in the creation of the central Santa Cruz Mountains, California, *in* Simpson, R.W., ed., The Loma Prieta, California, earthquake of October 17, 1989—tectonic processes and models: U.S. Geological Survey Professional Paper 1550–F, p. 17–34.
Valensise, Gianluca, and Ward, S.N., 1991, Long-term uplift of the Santa Cruz coastline in response to repeated earthquakes along the San Andreas fault: Seismological Society of America Bulletin, v. 81, no. 5, p. 1694–1704.
Wald, D.J., Helmberger, D.V., and Heaton, T.H., 1991, Rupture model of the 1989 Loma Prieta earthquake from the inversion of strong motion and broadband teleseismic data: Seismological Society of America Bulletin, v. 81, no. 5, p. 1540–1572.
Ward, S.N., and Barrientos, S.E., 1986, An inversion for slip distribution and fault shape from geodetic observations of the 1983 Borah Peak, Idaho, earthquake: Journal of Geophysical Research, v. 91, no. B5, p. 4909–4919.
Zhang, Jiajun, and Lay, Thorne, 1990, Source parameters of the 1989 Loma Prieta earthquake determined from long-period Rayleigh waves: Geophysical Research Letters, v. 17, no. 8, p. 1195–1198.

APPENDIX 1: CORRECTIONS AND ADJUSTMENTS TO LEVELING DATA

To isolate the elevation change associated with the earthquake ("coseismic"), each survey route must be corrected to eliminate other sources of elevation change, on the basis of knowledge of subsidence caused by ground-water withdrawal during the coseismic time interval, and on the preearthquake rate of subsidence. In some places, the preearthquake subsidence pattern can easily be attributed to tectonic or nontectonic sources (for example, water withdrawal); in other places, disturbed bench marks can lead to unpredictable patterns. Leveling routes 1 through 3 (inset, fig. 1) have preearthquake leveling histories; whereas leveling routes 4 through 7 do not. Leveling routes 4 through 7 are primarily located in mountainous regions and are unlikely to be influenced by ground-water-withdrawal-induced subsidence.

Land subsidence due to ground-water withdrawal in San Jose is documented by leveling surveys and compaction monitoring. Multiple releveling projects during 1934–67 have documented approximately 2.5 m of land subsidence in San Jose. In 1960, the USGS installed several extensometers (corehole compaction-measuring devices; Poland and Ireland, 1988) in San Jose and Sunnyvale, five of which remain in operation today and are maintained by the Santa Clara Valley Water Conservation District. These extensometers provide an excellent record of the compacting aquifer system and, in comparison with leveling data, confirm that land subsidence is compensated by compaction at depths of 61 to 305 m. The land subsidence, which is correlated with ground-water withdrawal and an associated water-table decline, has slowed drastically since the introduction of substantial surface-water imports during the late 1960's (Poland and Ireland, 1988). An example extensometer record for well 7S/1E–16C11 in San Jose is shown in figure 12, along with depth-to-water data for the period 1982–90. Note that during the coseismic interval 1989–90 along leveling route 1, the aquifer system shows a net expansion or land-surface rebound.

To correct leveling routes 1 through 3 (inset, fig. 1) for nontectonic subsidence effects, we use both preearthquake leveling and extensometer data. Subsidence-rate functions are determined from preearthquake leveling surveys, and subsidence corrections are computed by multiplying the subsidence-rate functions by the coseismic time intervals. In this correction, subsidence rates are implicitly assumed to remain constant over time. Near the extensometer sites where subsidence is greatest, however, the observed rates vary over time; for bench marks near the extensometer sites, the subsidence-rate functions have been modified by the observed rate changes. Preearthquake leveling data for routes 1 through 3 are plotted in figure 13. The preearthquake interval for leveling route 1 (1967–89) spans both the August 6, 1979, M_L=5.9 Coyote Lake, Calif., earthquake and the April 24, 1984, M_L=6.1 Morgan Hill, Calif., earthquake (King and others, 1981; Reasenberg and Ellsworth, 1982; Bakun and others, 1984; Prescott and others, 1984). Although the vertical deformation along leveling route 1 from these two events is small (+8 to -10 mm), we remove their contributions to elevation change. Bench marks seated in bedrock presumably are least affected by nontectonic subsidence and so are used to establish the zero-elevation-change datum for the preearthquake surveys. The San Jose subsidence basin is evident in the profiles for leveling routes 1 (1967–89) and 3 (1960–67), and subsidence rates apparently decline after 1967. Subsidence-rate modifications are made for all bench marks that lie within this subsidence basin. To correct for subsidence-rate changes, the subsidence-rate functions are multiplied by a rate-correction factor, which is the ratio of the subsidence rate during the coseismic interval to that during the preearthquake interval. Average subsidence rates and rate-correction factors along leveling routes 1 and 3 are listed in table 9; these average rates are derived from readings of the two extensometers at the San Jose site. Extensometer-tape readings for the period 1982–90 are listed in table 10; increasing values indicate compaction during the period between readings, whereas decreasing values indicate expansion. Poland and Ireland (1988) discussed extensometers and presented compaction data for the period 1960–81.

Depth-to-water records for wells along leveling routes 1 and 2 (inset, fig. 1) were examined to assess the validity of our assumption of constant subsidence rates in areas outside the San Jose subsidence basin. The locations of the 16 wells whose histories we examined are shown in figure 13. The coupling of land subsidence to water-table fluctuations is not spatially uniform; except in one well, no large water-table fluctuations were noted that would require a modification of the subsidence rates represented by the leveling data outside the San Jose area. Well 12S/2E–15E01 (fig. 13*B*) near Watsonville (WA, fig. 1) has a larger ratio of subsidence to water-table decline than that observed in San Jose, possibly indicating that subsidence is particularly sensitive to the water table there. The ratio of subsidence to water-table decline, and the total water-table decline during the period 1978–89, are used to predict subsidence of the junction-point bench mark between these two preearthquake surveys and thus to adjust the datum level for the preearthquake leveling survey along route 2.

Corrected coseismic profiles along leveling routes 1 through 3 were computed by subtracting the subsidence-correction functions from the observed-elevation-change profiles. The correction functions may not contain all the bench marks of the coseismic survey, and so they are interpolated for missing points. Because subsidence basins and the subsidence patterns determined from preearthquake leveling have primarily short spatial wavelengths, elevation-change profiles generally are smoother after correction. Reduction of the short-wavelength com-

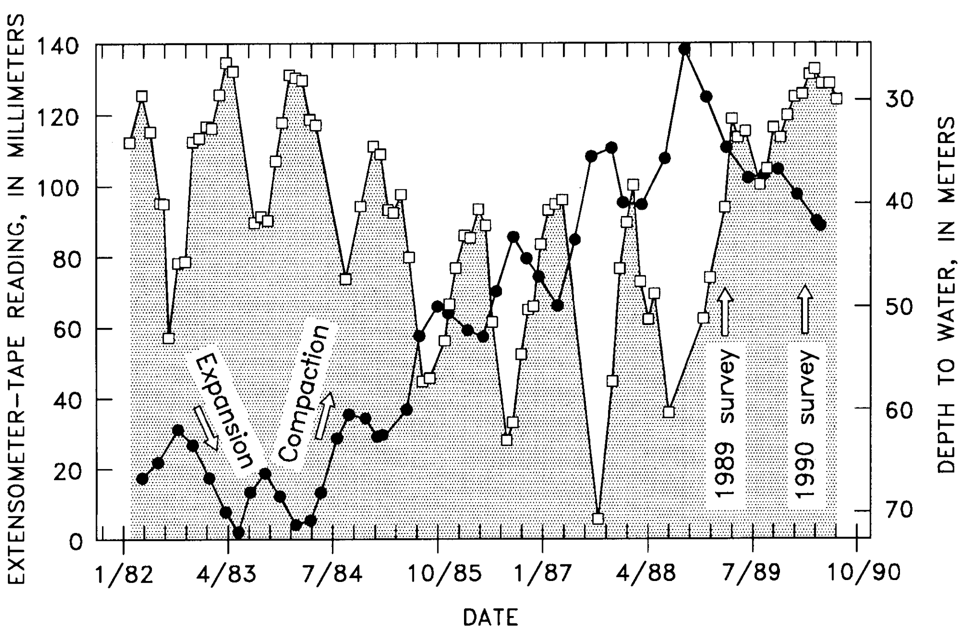

Figure 12.—Extensometer readings (circles) and depth-to-water records (squares) for 305-m-deep well 7S/1E–16C11 in San Jose. Increasing readings indicate compaction, whereas decreasing readings indicate expansion of aquifer system in depth range 0–305 m.

ponents serves as a test of the efficacy of the correction. The corrections for leveling routes 1 through 3 are all well behaved, except at the north end of leveling route 2 between 55 and 84 km. We believe that this problem originates in the north half of the 1972 survey, where a height-dependent error may have occurred; thus, we neglected the subsidence correction for this area. The observed and corrected elevation changes and the correction functions along leveling routes 1 through 3 are plotted in figure 14.

For the network to be self-consistent, overlapping end points of each survey route must have the same coseismic elevation change. To accomplish this agreement, we adjust the third-order USGS data. The test for the efficacy of these adjustments is that the circuit misclosure of the adjusted data must be smaller than that of the observed data. We use the original field data from the USGS surveys and thus remove all previous USGS adjustments.

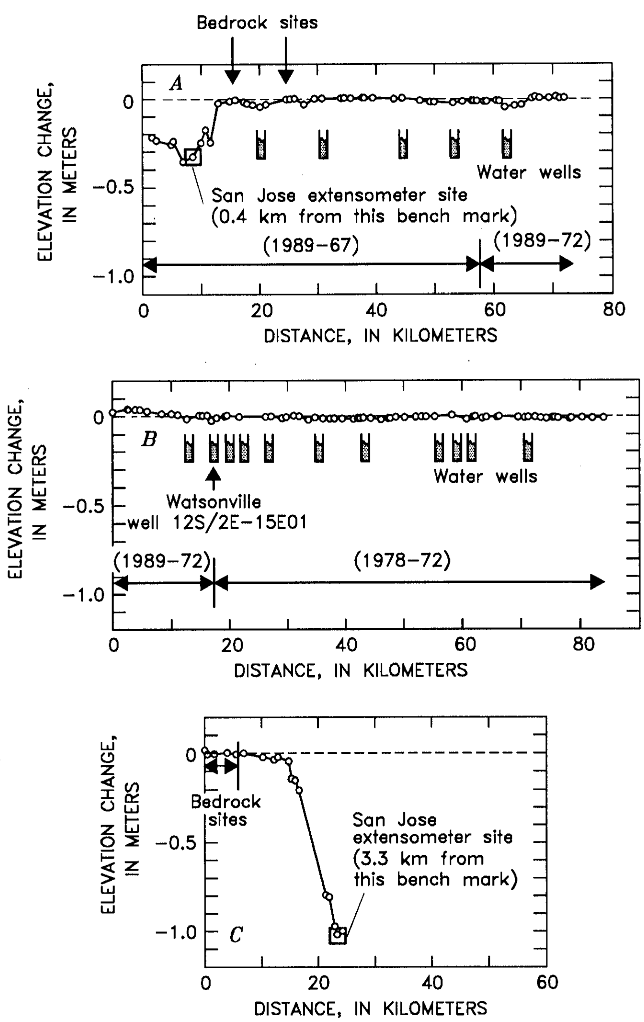

Figure 13.—Preearthquake leveling data along routes 1 (*A*, 1989–67/72), 2 (*B*, 1989–72, 1978–72), and 3 (*C*, 1967–60) (see inset, fig. 1), showing locations of bedrock, water wells, and bench marks closest to San Jose extensometer site.

The end point of leveling route 4 has an unadjusted coseismic mismatch with leveling routes 1 and 2 of 115 mm, which, using the assigned α value (see table 1), is about twice as great as the expected random error for the length of this leveling route. We apply an adjustment of 2 mm/km to the 1953 elevations along leveling route 4, so that the adjusted coseismic elevation changes match at both ends. At the junction of leveling routes 5 and 6, the mismatch is 46 mm, which is about the expected random error at this point for both leveling routes. The misfit is divided equally, and so leveling route 6 is adjusted by 0.5 mm/km and leveling route 5 by 0.6 mm/km. After these adjustments, the computed circuit misclosure for the preearthquake circuit is reduced from -70 to +15 mm. These adjustments reduce the 1953 circuit misclosure to that of the precise 1990 survey (-19 mm; see table 2). The adjusted and subsidence-corrected coseismic elevation changes used in our modeling, and their relative uncertainties, are listed in table 3; each bench mark is identified by its ACRN. The elevation changes listed in table 3 are relative to an arbitrary datum, and so a constant can be added to all the bench marks. Specifications for all the data listed in table 3 are listed in table 1.

APPENDIX 2: DATA TABLES

All the postearthquake elevation-change observations made by the NGS are listed in tables 11 through 24, along with the corresponding historical leveling data, our corrections, and some additional data that were analyzed for use in the subsidence corrections. The title of each table corresponds to the survey titles as named during the 1990 survey.

Tables 11 through 13 contain only NGS orthometric heights for which all standard NGS corrections have been applied. These heights, however, may differ from current NGS data-base values because some heights were obtained from unadjusted ("print file") elevations. Also included in these tables are our earthquake and subsidence corrections to the coseismic elevation changes; these corrections are omitted from the orthometric heights listed in these tables. The coseismic correction was computed by assuming right-lateral slip on a vertical fault for both the 1979 Coyote Lake and 1984 Morgan Hill earthquakes. For the 1979 Coyote Lake earthquake, we used 0.33 m of slip on a 20-km-long fault plane extending from 4- to 12-km depth. For the 1984 Morgan Hill earthquake, we used 0.76 m of slip on a 25-km-long fault plane extending from 4- to 10-km depth (King and others, 1981; Reasenberg and Ellsworth, 1982; Bakun and others, 1984; Prescott and others, 1984). Tables 14 through 24 contain NGS, USGS, and Santa Cruz County leveling data.

The USGS data are all from surveys dated 1953, although a few are actually from 1948. In some places, both

Table 9.—*Average subsidence rates along leveling routes 1 and 3*

[First, the average of the first and second readings of the cable extensometer after manual oscillation was computed; then, this average was combined with the reading of the pipe extensometer to compute the average subsidence rate]

Leveling route (inset, fig. 1)	Survey interval	Average subsidence rate (mm/yr)	Rate-correction factor (Coseismic rate/ preearthquake rate)
1	1989–90	−18.67	−1.28
	1967–89	14.57	---
3	1967–90	13.31	.07
	1960–67	181.93	---

1953 observed and adjusted heights are listed. The adjusted heights are the observed heights adjusted by us as described here; the observed heights are the original field observations with the original USGS adjustments removed. The USGS heights were measured with a three-wire leveling instrument and one 3-yd (3 m)-long, single-piece leveling rod; some rod-calibration tables are available. Leveling was conducted between NGS bench marks and adjusted to closure with previous NGS heights for those bench marks.

The Santa Cruz County data are all surveys dated "1970." Although the precise dates for these surveys are unknown, we were told by Santa Cruz County officials that they were conducted during the late 1960's and early 1970's. The heights were measured with a three-wire leveling instrument and a folding leveling rod ("Philadelphia rod") ruled in hundredths of feet; we do not know whether the rods had been calibrated. Leveling was conducted between USGS bench marks and adjusted to closure with previous USGS heights for those bench marks. Original unadjusted heights may be obtained from the Santa Cruz County Public Works Department, Office of the Surveyor, where the original leveling books are kept. The designations listed for the Santa Cruz bench marks are in the form of a height (in feet), an equal sign, and a integer designation (for example, "271.52=301"); the actual stampings on the marks are simply the height (in feet). The integer following the equal sign is the index number given to that bench mark by Santa Cruz County. The index numbers are used to find the adjusted heights listed in an index-card file and to locate the bench marks on a map in the Office of the Surveyor.

We did not use coseismic elevation changes constructed from the Santa Cruz County data for several reasons. Extensive research on the original field books is required, and the quality of the data is uncertain. Three leveling rods were used during the surveys, only one of which is still available for calibration, and the correspondence between rod serial numbers and particular surveys is uncertain. Tilt of elevation change and slope of topography appear to be correlated along several of the leveling routes that we examined, indicating a rod-calibration problem.

The locations of all the bench marks at which coseismic elevation changes were measured (both those used in this study and those not used) are shown in figure 15.

Table 10.—*Extensometer-tape readings in two wells in San Jose for the period 1982–90*

[F.O., first reading of tape, before manual oscillation; M.O., second reading of tape, after counterweight was manually oscillated]

Date	Well 7S/1E–16C11 pipe (305 m) (mm)	Well 7S/1E–16C5 cable (277 m)	
		F.O. (mm)	M.O. (mm)
1/22/82	- -	0.00	0.31
3/26/82	.00	−7.01	−10.97
6/4/82	4.27	−12.80	−8.84
8/27/82	14.02	−8.84	3.66
10/18/82	- -	2.74	.31
10/28/82	9.45	2.74	.31
1/10/83	−.30	- -	- -
3/25/83	−9.75	- -	−15.54
5/18/83	−15.54	−23.47	−21.34
7/15/83	−3.96	−21.95	−8.23
9/15/83	1.53	−8.53	−.30
11/17/83	−5.18	−10.06	−9.45
1/30/84	−13.41	−13.72	−13.41
4/6/84	−12.19	−16.15	−12.50
5/29/84	−4.27	−17.07	−3.35
7/26/84	11.28	−3.05	7.01
9/17/84	18.29	8.23	17.07
11/27/84	16.77	12.80	16.15
1/16/85	11.58	9.75	12.80
2/27/85	12.50	- -	- -
3/27/85	- -	10.36	10.97
5/20/85	19.51	10.67	20.42
7/19/85	40.24	20.12	36.88
9/30/85	48.77	37.49	44.50
11/22/85	46.64	43.28	43.89
2/13/86	41.76	40.23	40.54
4/24/86	39.93	30.78	37.19
6/17/86	53.04	35.97	46.94
8/29/86	68.58	47.55	58.52
10/27/86	62.18	55.17	55.17
12/19/86	57.00	53.95	54.56
3/9/87	48.77	49.99	49.99
5/21/87	67.97	48.77	63.70
8/5/87	91.44	- -	- -
8/10/87	- -	61.57	81.99
9/17/87	- -	81.38	85.95
10/27/87	93.88	80.77	- -
12/15/87	78.34	67.06	68.89
3/7/88	77.73	- -	- -
3/8/88	- -	66.75	70.41
6/9/88	90.83	70.10	78.64
9/8/88	121.62	79.25	97.23
9/12/88	- -	97.23	- -
9/15/88	- -	97.23	98.76
12/7/88	108.21	86.87	91.44
3/6/89	93.88	88.09	70.10
6/8/89	85.35	61.26	69.49
9/5/89	86.57	68.88	76.20
10/20/89	88.09	66.14	61.27
1/9/90	80.77	60.66	49.07
4/4/90	73.15	48.16	- -
4/16/90	- -	48.46	44.50
4/23/90	71.63	- -	- -

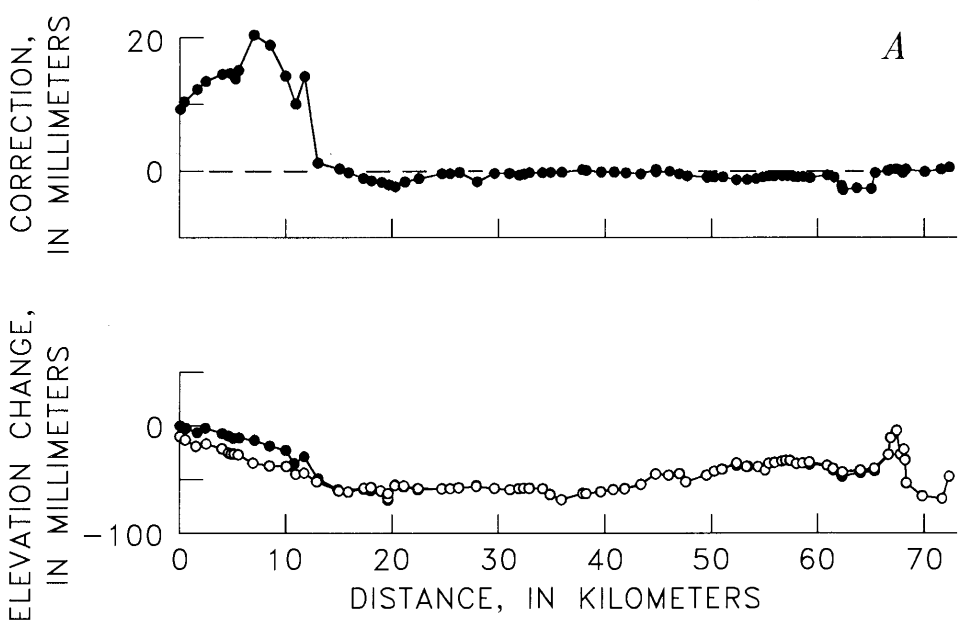

Figure 14.—Observed (dots) and corrected (circles) coseismic elevation changes and correction functions along leveling routes 1 (*A*), 2 (*B*), and 3 (*C*) (see inset, fig. 1, for locations). Note change of scale between correction function and elevation changes in figures 14*A* and 14*B* but not in figure 14*C*.

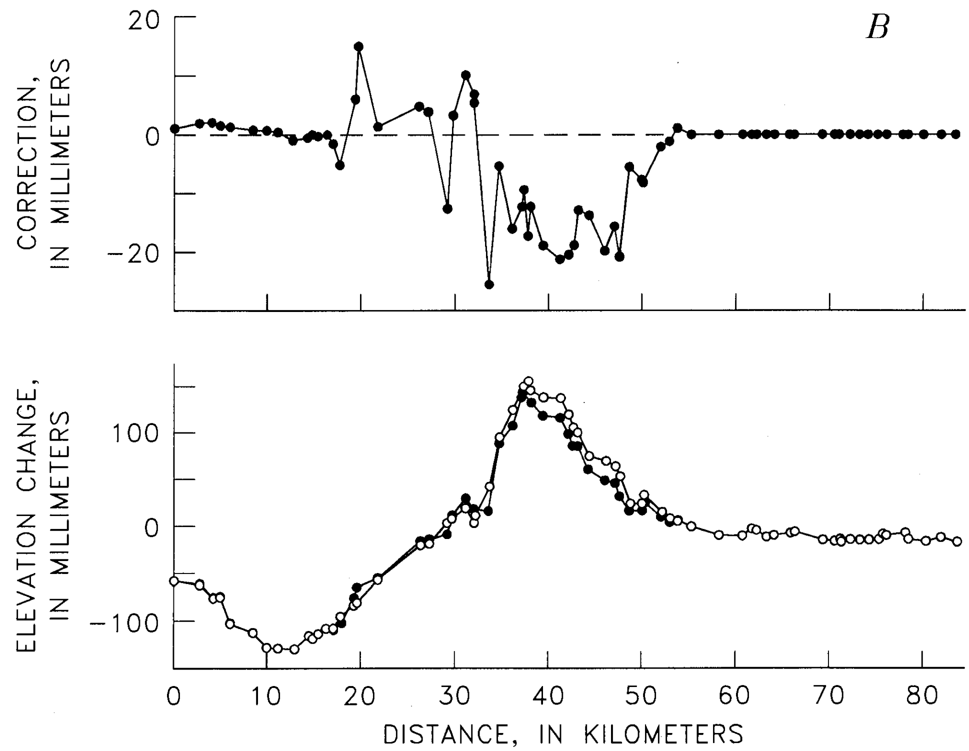

Figure 14.—Continued

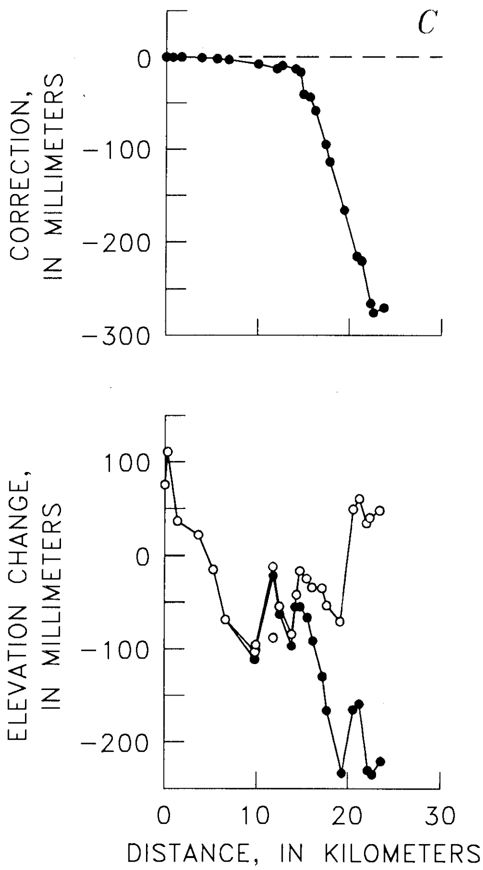

Figure 14.—Continued

Table 11.—*Leveling observations along a line from San Jose through Gilroy and Sargent to Watsonville*

ACRN	Designation	Latitude N.	Longitude W.	Leveled distance (km)	Orthometric height (m) 1967 (3–5) L21038, L21016.1, L21016.2	1968 (10–11) L21602	1969 (3–10) L219691, L21746	1972 (7–9) L22841	1989 (2–7) L2517.2, L2517.4	1990 (1–2) L25239.1	Subsidence correction (mm)	Earthquake correction (mm)
HT0651	V 1197	37°47′33″	122°16′07″	−69.693	- - -	- - -	2.62559	- - -	2.56716	- - -	- - -	- - -
HT0648	U 469	37°47′26″	122°15′32″	−68.804	- - -	- - -	3.77282	- - -	3.72073	- - -	- - -	- - -
HT0649	Oakland 6	37°47′15″	122°15′15″	−67.980	- - -	- - -	- - -	- - -	3.21844	- - -	- - -	- - -
HT0020	Oakland 8 reset	37°47′20″	122°14′24″	−66.407	- - -	- - -	- - -	- - -	16.86315	- - -	- - -	- - -
HT3546	K 1444	37°46′53″	122°14′01″	−65.067	- - -	- - -	- - -	- - -	10.13692	- - -	- - -	- - -
HT3547	L 1444	37°46′35″	122°13′31″	−64.108	- - -	- - -	- - -	- - -	12.70819	- - -	- - -	- - -
HT0012	Oakland 7	37°46′09″	122°13′43″	−63.295	- - -	- - -	4.63102	- - -	4.60421	- - -	- - -	- - -
HT0010	Q 148 reset	37°46′19″	122°13′21″	−62.224	- - -	- - -	5.88354	- - -	5.85996	- - -	- - -	- - -
HT0008	20 G	37°46′09″	122°13′06″	−61.648	- - -	- - -	6.06521	- - -	6.04251	- - -	- - -	- - -
HT0003	San Leandro NW base	37°45′48″	122°12′34″	−60.679	- - -	- - -	2.70758	- - -	2.67620	- - -	- - -	- - -
HT0002	N 554	37°45′18″	122°12′02″	−59.486	- - -	- - -	1.91654	- - -	1.89311	- - -	- - -	- - -
HT3555	M 1444	37°45′02″	122°11′42″	−58.777	- - -	- - -	- - -	- - -	3.56099	- - -	- - -	- - -
HT0281	M 554	37°44′39″	122°11′17″	−57.872	- - -	- - -	3.52047	- - -	3.49978	- - -	- - -	- - -
HT0252	K 738 reset	37°44′16″	122°10′50″	−56.828	- - -	- - -	7.56252	- - -	7.53342	- - -	- - -	- - -
HT0253	941 4711 tidal 6	37°44′25″	122°10′47″	−56.424	- - -	- - -	7.08717	- - -	7.06291	- - -	- - -	- - -
HT0245	L 554	37°44′06″	122°10′27″	−55.636	- - -	- - -	12.27936	- - -	12.25369	- - -	- - -	- - -
HT3556	U 1435	37°43′53″	122°10′09″	−55.022	- - -	- - -	- - -	- - -	12.95211	- - -	- - -	- - -
HT3557	X 1435	37°43′25″	122°09′39″	−53.865	- - -	- - -	- - -	- - -	15.80825	- - -	- - -	- - -
HT0241	K 554	37°43′06″	122°09′28″	−53.171	- - -	- - -	15.93973	- - -	15.90496	- - -	- - -	- - -
HT0239	T 1197	37°42′40″	122°08′58″	−52.027	- - -	- - -	12.63164	- - -	12.59509	- - -	- - -	- - -
HT0240	M 148	37°42′28″	122°08′46″	−51.549	- - -	- - -	- - -	- - -	11.50655	- - -	- - -	- - -
HT0238	J 554	37°42′08″	122°08′18″	−50.574	- - -	- - -	12.24255	- - -	12.21673	- - -	- - -	- - -
HT0237	H 554	37°41′27″	122°07′36″	−48.888	- - -	- - -	11.13984	- - -	11.11455	- - -	- - -	- - -
HT1876	Q 1256	37°41′13″	122°07′15″	−48.178	- - -	- - -	- - -	- - -	13.97392	- - -	- - -	- - -
HT0236	L 148	37°41′09″	122°07′17″	−47.988	- - -	- - -	14.61744	- - -	14.58750	- - -	- - -	- - -
HT1866	R 1256	37°40′56″	122°06′59″	−47.387	- - -	- - -	- - -	- - -	11.92283	- - -	- - -	- - -
HT0223	S 1197	37°40′35″	122°06′33″	−46.417	- - -	- - -	16.35982	- - -	16.33930	- - -	- - -	- - -
HT0226	K 148	37°39′58″	122°05′55″	−44.946	- - -	- - -	22.49624	- - -	22.46721	- - -	- - -	- - -
HT3558	V 1435	37°39′36″	122°05′29″	−43.970	- - -	- - -	- - -	- - -	25.59443	- - -	- - -	- - -
HT0208	N 1197	37°39′22″	122°05′12″	−43.337	- - -	- - -	21.92241	- - -	21.90318	- - -	- - -	- - -
HT0207	V 591	37°39′16″	122°05′06″	−43.117	- - -	- - -	20.49403	- - -	20.47668	- - -	- - -	- - -
HT0201	P 1197	37°38′46″	122°04′31″	−41.858	- - -	- - -	13.29236	- - -	13.27336	- - -	- - -	- - -
HT0200	Q 1197	37°38′31″	122°04′14″	−41.252	- - -	- - -	12.84962	- - -	12.82873	- - -	- - -	- - -
HT3559	C 1447	37°38′03″	122°03′42″	−40.036	- - -	- - -	- - -	- - -	7.15201	- - -	- - -	- - -
HT0197	R 1197 reset	37°37′30″	122°03′05″	−38.626	- - -	- - -	- - -	- - -	4.53620	- - -	- - -	- - -
HT2434	X 1446	37°37′33″	122°03′02″	−38.575	- - -	- - -	- - -	- - -	6.19229	- - -	- - -	- - -
HT3562	F 1447	37°36′39″	122°02′06″	−36.356	- - -	- - -	- - -	- - -	16.70963	- - -	- - -	- - -
HT0187	253	37°36′21″	122°01′34″	−35.336	- - -	- - -	25.63398	- - -	25.61522	- - -	- - -	- - -
HT0185	M 1197	37°36′04″	122°01′28″	−34.320	- - -	- - -	20.44525	- - -	20.42730	- - -	- - -	- - -
HT2446	Y 1446	37°35′34″	122°01′07″	−33.109	- - -	- - -	- - -	- - -	17.96061	- - -	- - -	- - -
HT0184	B 46 reset	37°35′40″	122°00′59″	−32.687	18.02171	- - -	18.08764	- - -	18.07497	- - -	- - -	- - -
HT0182	50.5	37°35′08″	122°00′13″	−31.187	15.32380	- - -	15.38993	- - -	15.37849	- - -	- - -	- - -
HS3384	L 177	37°34′56″	121°59′43″	−30.387	16.02651	- - -	16.08962	- - -	16.07170	- - -	- - -	- - -
HS3383	K 177	37°34′46″	121°59′04″	−29.352	19.91230	- - -	19.96777	- - -	19.89738	- - -	- - -	- - -
HS3382	Niles AZ MK	37°34′42″	121°58′54″	−29.121	19.47716	- - -	19.53420	- - -	19.48375	- - -	- - -	- - -
HS3381	F 148	37°34′43″	121°58′53″	−29.063	22.58309	- - -	22.64050	- - -	22.59410	- - -	- - -	- - -
HS3549	R 874	37°34′41″	121°58′19″	−28.230	29.28733	- - -	29.34630	- - -	29.31619	- - -	- - -	- - -
HS3379	Q 874	37°34′30″	121°58′20″	−27.840	27.25989	- - -	27.31696	- - -	27.28474	- - -	- - -	- - -
HS3565	Switch	37°34′21″	121°58′11″	−27.448	25.61108	- - -	25.66508	- - -	25.62402	- - -	- - -	- - -
HS3375	T 591	37°34′09″	121°57′55″	−26.871	24.82369	- - -	24.87956	- - -	24.83114	- - -	- - -	- - -
HS3374	B 148 reset	37°33′47″	121°57′32″	−26.054	- - -	- - -	- - -	- - -	22.58554	- - -	- - -	- - -
HS3370	M 886	37°32′30″	121°57′18″	−23.616	17.87337	- - -	17.93522	- - -	17.91673	- - -	- - -	- - -
HS5153	K 1447	37°32′05″	121°57′14″	−22.805	- - -	- - -	- - -	- - -	22.11553	- - -	- - -	- - -
HS3337	D 175	37°31′26″	121°56′59″	−21.450	15.26510	- - -	15.32480	- - -	15.32068	- - -	- - -	- - -
HS3335	F 1076	37°31′00″	121°56′45″	−20.514	8.85408	- - -	8.91096	- - -	8.90941	- - -	- - -	- - -
HS5154	D 1447	37°30′48″	121°56′41″	−20.068	- - -	- - -	- - -	- - -	10.13647	- - -	- - -	- - -
HS5155	J 1447	37°30′23″	121°56′25″	−19.280	- - -	- - -	- - -	- - -	10.67165	- - -	- - -	- - -
HS2880	N 874	37°29′15″	121°55′53″	−17.047	13.86164	- - -	13.90928	- - -	13.90672	- - -	- - -	- - -
HS2877	Q 591 reset	37°28′39″	121°55′33″	−16.023	- - -	- - -	13.14489	- - -	13.14609	- - -	- - -	- - -
HS4395	C 1371	37°27′34″	121°55′10″	−13.702	- - -	- - -	- - -	- - -	4.08388	- - -	- - -	- - -
HS2856	D 1076	37°27′07″	121°54′46″	−12.603	3.71923	- - -	3.75836	- - -	3.75451	- - -	- - -	- - -
HS2852	Jacklin RM 1	37°26′21″	121°54′23″	−11.066	3.32197	- - -	3.36280	- - -	3.34855	- - -	- - -	- - -
HS2851	M 874	37°26′10″	121°54′20″	−10.752	3.94223	- - -	3.98305	- - -	3.97993	- - -	- - -	- - -
HS5156	G 1447	37°25′55″	121°54′17″	−10.246	- - -	- - -	- - -	- - -	5.60388	- - -	- - -	- - -
HS5157	D 176 reset	37°25′40″	121°54′30″	−9.547	- - -	- - -	- - -	- - -	4.52166	- - -	- - -	- - -
HS2849	Z 174	37°25′33″	121°54′12″	−8.940	5.24552	- - -	5.29129	- - -	5.27474	- - -	- - -	- - -
HS2969	Milpitas	37°25′31″	121°54′12″	−8.866	5.30201	- - -	5.34227	- - -	5.33907	- - -	- - -	- - -
HS2968	Milpitas RM 1	37°25′31″	121°54′11″	−8.851	5.62744	- - -	5.66884	- - -	5.66102	- - -	- - -	- - -
HS2848	L 874	37°24′58″	121°54′03″	−7.777	8.19467	- - -	8.27074	- - -	8.24521	- - -	- - -	- - -
HS2847	G 554	37°24′50″	121°54′01″	−7.524	10.09069	- - -	10.13329	- - -	10.11783	- - -	- - -	- - -
HS3086	K 179 reset	37°24′30″	121°53′20″	−6.091	- - -	- - -	- - -	- - -	14.99672	- - -	- - -	- - -
HS5158	M 1447	37°24′15″	121°53′59″	−4.898	- - -	- - -	- - -	- - -	11.20016	- - -	- - -	- - -
HS5159	N 1447	37°23′17″	121°53′54″	−3.135	- - -	- - -	- - -	- - -	15.13748	- - -	- - -	- - -
HS2840	X 147	37°22′44″	121°53′50″	−2.118	19.14230	- - -	19.15978	- - -	19.06579	- - -	- - -	- - -
HS2838	B 1076	37°22′06″	121°53′47″	−0.963	16.98160	- - -	16.96284	- - -	16.84116	- - -	- - -	- - -
HS5161	G 1448	37°21′07″	121°55′01″	0.000	- - -	- - -	- - -	- - -	17.22686	17.22686	9.81	- - -
HS2835	C 1121 reset	37°21′41″	121°53′42″	0.088	18.22893	- - -	18.18108	- - -	18.00880	- - -	- - -	- - -
HS5160	L 1447	37°20′56″	121°55′03″	0.598	- - -	- - -	- - -	- - -	22.74936	22.74729	10.78	- - -
HS2833	U 174	37°21′06″	121°53′28″	1.173	19.41924	- - -	19.37769	- - -	19.22744	- - -	- - -	- - -
HS2891	Z 111 reset 1962	37°20′29″	121°54′40″	1.745	23.22841	- - -	- - -	- - -	23.05946	23.05275	12.64	3.10
HS2885	Z 876 reset	37°20′58″	121°53′59″	2.060	- - -	- - -	19.75525	- - -	19.59935	- - -	- - -	- - -
HS2886	B 112	37°20′46″	121°54′13″	2.598	22.14169	- - -	- - -	- - -	21.94914	21.94754	14.02	3.21
HS5162	E 1447	37°20′28″	121°53′45″	4.166	- - -	- - -	- - -	- - -	23.47840	23.47067	14.82	- - -
HS2828	P 7 reset 1965	37°20′22″	121°53′29″	4.787	26.51995	- - -	26.46974	- - -	26.30861	26.29759	15.14	3.66

Table 11.—*Leveling observations along a line from San Jose through Gilroy and Sargent to Watsonville*—Continued

ACRN	Designation	Latitude N.	Longitude W.	Leveled distance (km)	Orthometric height (m) 1967 (3–5) L21038, L21016.1, L21016.2	1968 (10–11) L21602	1969 (3–10) L219691, L21746	1972 (7–9) L22841	1989 (2–7) L2517.2, L2517.4	1990 (1–2) L25239.1	Subsidence correction (mm)	Earthquake correction (mm)
HS2826	D 886	37°20′17″	121°53′26″	4.968	26.45147	- - -	26.40250	- - -	26.23949	26.22769	15.17	3.63
HS2825	A 326 reset 1970	37°20′16″	121°53′22″	5.086	- - -	- - -	- - -	- - -	25.69628	25.68429	14.90	- - -
HS2822	M 177	37°20′10″	121°53′22″	5.383	27.34161	- - -	27.29548	- - -	27.14673	27.13324	14.23	4.59
HS5163	I 19=96 reset 1976	37°20′16″	121°53′11″	5.709	- - -	- - -	- - -	- - -	23.70753	23.69523	15.60	- - -
HS2813	A 1122	37°20′04″	121°52′35″	6.972	27.00560	- - -	26.92388	- - -	26.69688	26.68216	20.90	5.17
HS2814	San Jose AZ MK	37°19′31″	121°52′11″	8.568	29.61819	- - -	29.54719	- - -	29.34023	29.32154	19.12	5.45
HS2811	B 149	37°18′51″	121°52′04″	10.085	30.56198	- - -	30.50680	- - -	30.36366	30.34000	14.52	6.13
HS2810	L 591	37°18′27″	121°51′45″	10.957	32.42800	- - -	32.38979	- - -	32.30360	32.26790	10.23	6.41
HS2809	2=J 19	37°18′08″	121°51′29″	11.753	36.57012	- - -	36.51550	- - -	36.37031	36.34033	14.63	6.54
HS2806	C 886 reset 1962	37°17′40″	121°51′02″	13.031	44.16217	- - -	44.17860	- - -	44.18479	44.13360	1.69	6.81
HS2796	A 1076	37°16′47″	121°50′11″	15.012	50.19516	- - -	50.21369	- - -	50.23496	50.17403	.70	6.83
HS2795	Q 877 reset 1964	37°16′28″	121°49′51″	15.846	64.08164	- - -	64.10134	- - -	64.13296	64.07007	–.03	7.04
HS2792	B 1121	37°16′25″	121°49′46″	15.982	53.18187	- - -	53.20085	- - -	53.23023	53.16702	–.17	7.14
HS2789	P 453	37°15′55″	121°49′06″	17.378	55.37796	- - -	55.40304	- - -	55.41240	55.35291	–.81	7.37
HS2788	R 174	37°15′42″	121°48′41″	18.111	54.71156	- - -	54.73644	- - -	54.73319	54.67250	–1.39	7.41
HS2787	QQ 453	37°15′23″	121°48′12″	19.036	57.36310	- - -	57.38652	- - -	57.38041	57.31731	–1.60	7.59
HS4926	JCT	37°15′12″	121°47′53″	19.609	- - -	- - -	- - -	- - -	58.85663	58.79086	–1.82	- - -
HS5164	JCT RM3	37°15′13″	121°47′53″	19.615	- - -	- - -	- - -	- - -	59.13915	59.06825	–1.82	- - -
HS2785	P 174	37°14′58″	121°47′30″	20.301	59.23695	- - -	59.25801	- - -	59.24368	59.18601	–2.08	7.58
HS2784	N 453	37°14′42″	121°47′03″	21.212	60.02265	- - -	60.03420	- - -	60.04362	59.98473	–1.42	7.39
HS5165	H 1447	37°14′17″	121°46′19″	22.505	- - -	- - -	- - -	- - -	65.40824	65.34790	–.88	- - -
HS4141	L 453	37°13′34″	121°45′02″	24.649	79.23240	- - -	79.23369	- - -	79.28453	79.22396	.03	6.59
HS2778	M 174	37°13′21″	121°44′42″	25.464	74.60063	- - -	74.60037	- - -	74.65133	74.59144	–.01	6.09
HS2776	P 19	37°13′00″	121°44′21″	26.325	77.65145	- - -	77.65462	- - -	77.70273	77.64330	.04	5.56
HS2775	L 174	37°12′22″	121°43′41″	27.865	79.83738	- - -	79.84146	- - -	79.85548	79.79742	–1.46	5.30
HS2773	Y 176	37°11′39″	121°42′56″	29.592	88.56798	- - -	88.56946	- - -	88.61912	88.55947	.07	4.79
HS2769	Perrys	37°11′01″	121°42′17″	31.084	91.36767	- - -	91.36921	- - -	91.41696	91.35666	.01	4.23
HS2771	Perrys RM 4	37°11′02″	121°42′17″	31.091	- - -	- - -	91.56066	- - -	91.60079	91.53994	.01	- - -
HS5166	A 1448	37°10′37″	121°41′52″	32.057	- - -	- - -	- - -	- - -	94.02074	93.96089	.07	- - -
HS2768	K 453 reset 1974	37°10′28″	121°41′41″	32.432	- - -	- - -	- - -	- - -	96.86834	96.80890	.09	- - -
HS5167	B 1448	37°10′17″	121°41′31″	32.881	- - -	- - -	- - -	- - -	98.37293	98.31317	.12	- - -
HS2762	J 453	37°09′43″	121°40′59″	34.168	101.44952	- - -	101.45073	- - -	101.50033	101.44053	.20	1.45
HS2757	A 177	37°09′25″	121°40′39″	34.957	102.87953	- - -	102.87917	- - -	102.93175	102.86655	.29	.90
HS2758	A 1077 X	37°09′09″	121°40′51″	35.919	105.35747	105.45392	105.35041	- - -	105.40869	105.33849	.29	–.16
HS2759	B 1077 X	37°09′09″	121°40′50″	35.930	105.58296	105.67947	105.57601	- - -	105.63412	105.56405	.33	–1.07
HS2761	C 1077 X	37°09′09″	121°40′50″	36.014	102.74605	102.84134	102.73934	- - -	102.79502	102.72574	.25	–1.46
HS2754	R 19	37°08′36″	121°39′50″	37.913	106.83633	106.93251	106.83503	- - -	106.88920	106.82443	.45	–1.93
HS2753	RV 2501	37°08′28″	121°39′41″	38.236	107.53127	107.62476	107.53570	- - -	107.57909	107.51500	.24	–2.32
HS2751	D 1080	37°07′49″	121°39′00″	39.739	106.96565	107.06415	106.96679	- - -	107.01052	106.94802	.13	–3.00
HS5168	N 1448	37°07′22″	121°38′34″	40.908	- - -	- - -	- - -	- - -	103.46770	103.40712	.10	- - -
HS5169	P 1448	37°06′56″	121°38′07″	41.933	- - -	- - -	- - -	- - -	99.96772	99.90848	.08	- - -
HS2745	E 1080	37°06′11″	121°37′20″	43.419	95.79480	95.88446	95.79689	- - -	95.83563	95.78015	.04	–4.89
HS2743	A 812	37°05′44″	121°36′56″	44.781	95.41833	95.51439	95.41404	- - -	95.46137	95.41688	.19	–6.02
HS2742	T 19 reset 1938	37°05′43″	121°36′56″	44.826	93.66576	93.76229	93.66226	- - -	93.71473	93.67007	.47	–6.24
HS5170	D 1448	37°05′06″	121°36′31″	46.147	- - -	- - -	- - -	- - -	87.24420	87.19758	.05	- - -
HS5171	C 1448	37°05′07″	121°35′59″	47.156	- - -	- - -	- - -	- - -	85.93072	85.88483	–.26	- - -
HS2738	G 1080	37°04′19″	121°36′04″	47.740	80.47289	80.54364	80.45440	- - -	80.49911	80.44464	–.45	–8.86
HS2737	C 812	37°03′22″	121°35′32″	49.664	74.75169	74.83194	74.74230	- - -	74.77397	74.72653	–.62	–9.08
HS2736	M 149	37°03′00″	121°35′21″	50.366	71.19232	71.26762	71.17744	- - -	71.21151	71.16765	–.76	–8.96
HS2733	Rucker reset 1957	37°02′38″	121°35′11″	51.125	- - -	69.28362	- - -	- - -	69.22693	69.18477	–.84	- - -
HS2727	E 812 reset 1973	37°02′12″	121°35′30″	52.380	- - -	- - -	- - -	- - -	67.49486	67.45765	–.96	- - -
HS2725	D 812	37°02′04″	121°34′52″	53.422	67.11539	67.19149	67.09881	- - -	67.12845	67.08759	–1.07	–8.35
HS5172	Q 1448	37°01′33″	121°34′37″	54.449	- - -	- - -	- - -	- - -	62.83462	62.79470	–.76	- - -
HS2724	N 149	37°01′13″	121°34′25″	55.119	61.93561	62.00800	61.91427	- - -	61.96063	61.91852	–.56	–7.66
HS2723	L 1193	37°01′02″	121°34′19″	55.512	- - -	61.11025	61.01426	- - -	61.05964	61.02322	–.54	- - -
HS5143	E 1448	37°00′45″	121°34′12″	56.083	- - -	- - -	- - -	- - -	60.67193	60.63577	–.51	- - -
HS2720	Z 19	37°00′28″	121°34′14″	56.822	62.80408	62.88158	- - -	- - -	62.83183	62.79699	–.47	–6.86
HS2721	Y 19	37°00′25″	121°34′01″	57.287	61.20904	61.28681	- - -	- - -	61.23684	61.20166	–.49	–6.42
HS2722	11	37°00′25″	121°34′02″	57.320	60.84984	60.92697	60.83076	- - -	60.87549	60.84059	–.60	-6.13
HS2719	P 149	37°00′21″	121°33′57″	57.607	- - -	- - -	- - -	- - -	59.86798	59.83225	–.59	- - -
HS2718	RV 22	37°00′09″	121°33′55″	57.664	60.49429	60.57143	- - -	- - -	60.52009	60.48431	–.58	–6.27
HS5144	F 1448	37°00′02″	121°33′47″	58.146	- - -	- - -	- - -	- - -	59.78645	59.74900	–.55	- - -
HS3323	D 1236	37°00′02″	121°33′49″	58.200	- - -	- - -	- - -	60.53572	60.55068	60.51207	–.55	–7.12
GU2195	C 1193	36°59′42″	121°33′40″	58.785	57.35129	57.42843	- - -	57.35129	57.37748	57.34027	–.51	–7.56
GU2192	Q 149 reset 1967	36°59′27″	121°33′30″	59.329	- - -	59.02364	- - -	58.94728	58.97008	58.93271	–.83	–7.99
GU2190	D 1193	36°58′52″	121°32′54″	60.917	- - -	53.80850	- - -	53.73351	53.76051	53.72144	–.56	–8.40
GU2189	RV 24	36°58′39″	121°32′40″	61.564	- - -	52.14657	- - -	52.06820	52.08874	52.04508	–.91	–8.87
GU2188	R 149	36°58′09″	121°32′30″	62.363	- - -	54.07306	- - -	53.98806	53.97888	53.93024	–2.65	–9.12
GU2180	E 1193	36°57′16″	121°32′39″	63.974	- - -	46.44321	- - -	46.35519	46.35174	46.30512	–2.29	–9.43
GU2178	F 1193	36°56′39″	121°32′47″	65.207	- - -	43.28335	- - -	43.19479	43.18976	43.14411	–2.37	–9.61
GU4096	M 1448	36°56′36″	121°32′48″	65.308	- - -	- - -	- - -	- - -	42.92262	42.88038	–2.21	- - -
GU2177	S 149	36°55′52″	121°32′49″	66.625	- - -	44.02923	- - -	43.95420	44.01788	43.97529	–.11	–8.99
GU2176	G 1193	36°55′43″	121°32′49″	66.879	- - -	46.00386	- - -	45.93814	45.97923	45.95170	.30	–8.93
GU2174	E 1236	36°55′19″	121°32′48″	67.554	- - -	- - -	- - -	44.81370	44.85771	44.84713	.45	–8.54
GU2175	SF 138	36°55′15″	121°32′50″	67.791	- - -	42.10530	- - -	- - -	42.09616	42.09158	.42	- - -
GU2173	K 1193	36°55′04″	121°32′48″	68.173	- - -	46.09696	- - -	46.04545	46.08843	46.06083	.37	–8.16
GU2172	12 41	36°55′02″	121°32′48″	68.187	- - -	46.38910	- - -	46.33795	46.37990	46.35768	.28	–7.65
GU2171	Sargent AZ MK	36°55′02″	121°32′48″	68.274	- - -	46.35530	- - -	46.29594	46.33384	46.29952	.02	–7.32
GU2167	G 1236	36°54′15″	121°33′19″	69.904	- - -	- - -	- - -	48.62907	48.67581	48.62064	.52	–6.97
GU2155	F 1236	36°53′42″	121°33′20″	70.975	- - -	- - -	- - -	43.90135	43.94900	43.93368	.55	–6.66
GU2154	B 1193	36°53′16″	121°33′24″	71.743	- - -	44.97181	- - -	44.90292	44.93956	44.87223	–.12	–6.24
GU2151	A 1193	36°52′57″	121°33′36″	72.394	- - -	45.68985	- - -	45.62485	45.67091	45.60102	.39	–5.56
GU4097	U 1448	36°53′32″	121°34′27″	74.431	- - -	- - -	- - -	- - -	54.58518	54.53649	.73	- - -
GU2161	K 812	36°54′05″	121°35′51″	77.197	- - -	- - -	- - -	40.90965	40.96978	40.91139	1.19	–4.96
GU2162	E 20	36°54′24″	121°36′46″	78.683	- - -	- - -	- - -	37.94356	38.01785	37.95440	2.01	–4.74
GU2163	L 1236	36°54′34″	121°37′13″	79.501	- - -	- - -	- - -	38.35744	38.43214	38.35483	2.02	–4.57
GU2226	M 1236	36°54′33″	121°37′51″	80.548	- - -	- - -	- - -	37.43106	37.50049	37.42382	1.67	–3.87
GU2229	N 1236	36°53′30″	121°38′33″	82.963	- - -	- - -	- - -	28.96355	29.02759	28.92277	1.33	–3.45
GU2230	W 149	36°53′28″	121°38′58″	83.574	- - -	- - -	- - -	29.28700	29.34896	29.21428	1.19	–3.11
GU2231	P 1236	36°53′32″	121°39′36″	84.551	- - -	- - -	- - -	24.90692	24.96232	24.84626	.76	–2.42
GU2232	Q 1236	36°53′40″	121°40′22″	85.736	- - -	- - -	- - -	19.23247	19.28686	19.15505	.68	–2.17

Table 11.—*Leveling observations along a line from San Jose through Gilroy and Sargent to Watsonville*—Continued

ACRN	Designation	Latitude N.	Longitude W.	Leveled distance (km)	Orthometric height (m)						Subsidence correction (mm)	Earthquake correction (mm)
					1967 (3–5) L21038, L21016.1, L21016.2	1968 (10–11) L21602	1969 (3–10) L219691, L21746	1972 (7–9) L22841	1989 (2–7) L2517.2, L2517.4	1990 (1–2) L25239.1		
GU2233	R 1236	36°53′51″	121°41′24″	87.354	---	---	---	18.88477	18.93404	18.80269	.35	−1.58
GU2235	Y 149	36°54′03″	121°42′20″	88.805	---	---	---	12.21096	12.24087	12.10724	−.82	−1.01
GU4098	V 1448	36°54′05″	121°42′42″	89.397	---	---	---	---	14.11705	13.99848	−.38	---
GU2237	S 1236	36°54′01″	121°43′05″	89.977	---	---	---	11.89650	11.94221	11.81938	.05	.00
GU2239	T 1236	36°53′55″	121°43′39″	90.899	---	---	---	10.35522	10.39775	10.28159	−.14	.00
GU2240	U 1236	36°53′50″	121°44′04″	91.563	---	---	---	8.63629	8.68082	8.57030	−.02	.00
GU2242	M 20 reset 1964	36°53′44″	121°44′40″	92.383	---	---	---	8.66899	8.68768	8.57506	−1.54	.00

Table 12.—*Leveling observations along a line from Watsonville to Santa Cruz*

[See figure 1 for locations. Number(s) in parentheses below year of survey indicate month(s) when survey was conducted. L-number is U.S. National Geodetic Survey designation. Subsidence correction applies to 1978–90 height difference]

ACRN	Designation	Latitude N.	Longitude W.	Leveled distance (km)	Orthometric height (m)			Subsidence correction (mm)
					1972 (7–9) L22841	1978 (5) L24298	1990 (2) L25239.2	
GU2242	M 20 reset 1964	36°53′44″	121°44′40″	0.000	8.69274	8.67814	8.57506	−1.54
GU2245	V 1236	36°54′12″	121°45′13″	1.404	10.18733	10.17828	10.09895	−5.23
GU2246	W 1236	36°54′19″	121°45′23″	1.768	7.46515	7.46053	7.39289	6.11
GU4162	H 249 reset 1979	36°54′28″	121°45′37″	2.204	---	---	8.12852	---
GU2248	X 1236	36°54′01″	121°46′35″	3.947	5.46739	5.45611	5.39828	15.16
GU4161	A 1455	36°53′39″	121°47′56″	6.166	---	---	7.10690	---
GU2260	Z 1236	36°54′37″	121°48′42″	8.257	22.37276	22.36318	22.34565	1.55
GU2262	A 1237	36°54′56″	121°49′10″	9.364	37.47246	37.46232	37.44568	5.03
GU2264	E 249	36°55′21″	121°50′15″	11.199	47.88581	47.86756	4.85577	3.88
GU2265	C 1237	36°55′30″	121°50′40″	11.842	36.09285	36.08243	36.09116	−12.69
GU2266	D 1237	36°55′54″	121°51′25″	13.204	15.87628	15.86939	15.89721	3.31
GU2269	RV 6	36°56′10″	121°51′50″	14.140	23.43842	23.42989	23.43879	10.52
GU2268	E 1237	36°56′10″	121°51′50″	14.148	23.37247	23.36326	23.37856	7.17
GU2272	C 249	36°56′52″	121°52′20″	15.636	---	---	35.90532	---
GU2273	F 1237	36°56′54″	121°52′24″	15.748	33.08911	33.06446	33.07778	5.78
GU2276	G 1237	36°57′26″	121°52′54″	16.925	37.22072	37.20603	37.29474	−25.77
GU2277	H 1237	36°58′01″	121°53′29″	18.321	31.53158	31.51163	31.61853	−5.42
GU2279	J 1237	36°58′32″	121°53′50″	19.365	30.37252	30.35453	30.49432	−16.16
GU2278	RV 5	36°58′33″	121°53′51″	19.505	29.78264	29.76600	29.90682	−12.16
GU2281	RV 4	36°58′35″	121°54′11″	20.006	32.16769	32.14712	32.28531	−9.40
GU2282	K 1237	36°58′33″	121°54′16″	20.255	34.82839	34.81040	34.94245	−17.43
GU2283	L 1237	36°58′45″	121°55′05″	21.576	40.88461	40.86311	40.98057	−12.16
GU2285	M 1237	36°58′53″	121°56′11″	23.422	22.61641	22.59380	22.70805	−19.33
GU2286	N 1237	36°58′37″	121°56′35″	24.273	24.54349	24.52137	24.61802	−21.60
GU2287	Z 212	36°58′31″	121°56′58″	24.815	19.40660	19.38520	19.46904	−20.60
GU2290	P 1237	36°58′23″	121°57′10″	25.282	16.45093	16.43249	16.51665	−19.13
GU2289	61.94	36°58′06″	121°57′49″	26.500	18.84766	18.82875	18.88675	−13.08
GU2291	55.79	36°58′09″	121°59′03″	28.282	16.97265	16.95073	16.99658	−14.04
GU2294	51.93	36°58′09″	121°59′48″	29.454	15.79953	15.77982	15.82329	−20.19
GU1941	R 1237	36°58′06″	122°00′05″	29.834	8.63581	8.61349	8.64272	−15.67
GU1944	S 1237	36°57′56″	122°00′42″	30.870	7.31218	7.29741	7.31251	−21.01
GU3223	941 3745 tidal 4	36°57′56″	122°01′28″	32.137	---	13.21725	13.23207	−5.58
GU1945	14	36°57′53″	122°01′30″	32.379	4.20406	4.18806	4.21113	−7.69

Table 13.—Leveling observations along a line from Santa Cruz through Los Gatos to San Jose

[See figure 1 for locations. Numbers in parentheses below year of survey indicate months when survey was conducted. L-numbers are U.S. National Geodetic Survey designations. Subsidence correction applies to 1967–90 height difference]

ACRN	Designation	Latitude N.	Longitude W.	Leveled distance (km)	Orthometric height (m)				Subsidence correction (mm)
					1954 (4–7) L15275.9, L15275.10	1960 (9–12) L18119.9, L18119.10	1967 (1–3) L21016.9, L21016.10, L21016.13	1990 (2–3) L25239.3	
GU3223	941 3745 tidal 4	36°57′56″	122°01′28″	0.000	---	---	---	13.23207	---
GU1945	14	36°57′53″	122°01′30″	.147	---	---	---	4.21146	---
GU1952	T 1237	36°58′05″	122°01′42″	.601	---	---	---	4.55344	---
GU4167	B 1455	36°58′15″	122°01′50″	1.042	---	---	---	4.41596	---
GU1953	W 212	36°58′26″	122°01′50″	1.472	---	---	---	6.58358	---
GU4163	C 1455	36°58′42″	122°01′24″	2.329	---	---	---	8.12574	---
GU4164	D 1455	36°59′10″	122°01′22″	3.365	---	---	---	12.63562	---
GU4165	E 1455	36°59′24″	122°01′15″	3.796	---	---	---	26.60844	---
GU4166	F 1455	36°59′58″	122°01′12″	4.970	---	---	---	78.09381	---
HT3563	G 1455	37°00′31″	122°01′13″	6.103	---	---	---	103.22221	---
HT3564	H 1455	37°01′14″	122°01′34″	7.519	---	---	---	135.67828	---
HT3565	J 1455	37°02′08″	122°01′13″	9.482	---	---	---	169.60427	---
HT3566	K 1455	37°02′34″	122°01′24″	10.349	---	---	---	156.57370	---
HT3567	M 1455	37°03′12″	122°02′19″	10.506	---	---	---	135.65247	---
HT3568	L 1455	37°03′18″	122°03′04″	10.662	---	---	---	156.30220	---
HT3569	N 1455	37°03′20″	122°03′31″	10.819	---	---	---	109.07614	---
HT3570	P 1455	37°03′19″	122°03′36″	10.975	---	---	---	106.74056	---
HT1429	L 249	37°03′05″	122°03′43″	11.132	---	---	---	91.08537	---
HT1430	RV 12	37°02′55″	122°03′48″	11.288	---	---	---	89.43701	---
HT3571	Q 1455	37°02′51″	122°00′53″	11.445	---	---	---	166.37080	---
HT3572	R 1455	37°03′19″	122°00′35″	12.525	---	---	---	174.13167	---
HT3573	S 1455	37°03′39″	122°00′11″	13.729	---	---	---	192.78908	---
HS4900	TRAILL	37°03′31″	121°59′35″	15.070	---	---	---	281.51432	---
HS5175	T 1455	37°04′19″	121°59′24″	15.560	---	---	---	248.10103	---
HS5176	U 1455	37°04′42″	121°58′43″	16.947	---	---	---	306.37117	---
HS5177	V 1455	37°05′10″	121°58′40″	17.909	---	---	---	346.31595	---
HS5178	W 1455	37°05′43″	121°58′30″	19.063	---	---	---	387.01594	---
HS5179	X 1455	37°06′20″	121°58′24″	20.378	---	---	---	370.64274	---
HS5180	Y 1455	37°06′48″	121°58′24″	21.425	---	---	---	423.19583	---
HS5181	Z 1455	37°07′20″	121°58′21″	22.477	---	---	---	469.51265	---
HS5182	A 1456	37°07′59″	121°58′48″	23.891	---	---	---	553.06745	---
HS5183	B 1456	37°08′16″	121°59′02″	24.628	---	---	---	543.58833	---
HS3171	R 1077 reset 1970	37°08′44″	121°59′03″	25.590	---	---	---	558.60804	---
HS5184	C 1456	37°09′06″	121°59′01″	26.676	---	---	---	485.80749	---
HS5185	D 1456	37°09′26″	121°58′52″	27.590	---	---	---	423.41982	---
HS5186	E 1456	37°09′42″	121°59′21″	28.580	---	---	---	365.70972	---
HS3165	P 878	37°10′14″	121°59′20″	29.779	322.14184	322.06118	322.07113	322.14841	.00
HS3174	R 878	37°10′04″	121°58′43″	30.300	205.79353	205.74637	205.73157	205.84335	.00
HS5187	F 1456	37°10′41″	121°59′39″	30.821	---	---	---	263.53229	---
HS3160	M 878	37°11′00″	121°59′27″	31.572	228.18700	228.13815	228.12361	228.16190	.00
HS5188	G 1456	37°11′41″	121°59′32″	32.974	---	---	---	203.69486	---
HS3154	K 878	37°12′03″	121°59′24″	33.793	203.28128	203.23991	203.23140	203.25366	.00
HS3150	D 177	37°12′53″	121°59′13″	35.485	135.17397	135.12746	135.11170	135.09580	.00
HS5189	H 1456	37°13′19″	121°58′57″	36.454	---	---	---	124.60494	---
HS3145	C 177	37°13′27″	121°58′48″	36.737	121.88043	121.83275	121.82025	121.75144	−1.01
HS5190	J 1456	37°13′55″	121°58′36″	37.904	---	---	---	112.04248	---
HS5191	K 1456	37°14′24″	121°58′20″	38.896	---	---	---	104.06291	---
HS3140	G 386	37°14′49″	121°57′55″	39.922	93.57815	93.53010	93.50326	93.39370	−4.86
HS4911	VASO-	37°14′50″	121°57′54″	39.975	---	---	---	92.90174	---
HS3141	G 875	37°14′49″	121°57′55″	40.011	93.31040	93.27220	93.24122	93.13894	−5.97
HS5192	L 1456	37°15′24″	121°57′51″	41.256	---	---	---	85.22922	---
HS3188	F 180	37°15′49″	121°58′37″	41.940	77.42417	77.38116	77.34461	77.31581	−9.29
HS3132	T 1122	37°16′05″	121°57′22″	42.624	---	71.64922	71.61770	71.55630	−6.11
HS5193	M 1456	37°16′26″	121°57′04″	43.424	---	---	---	67.62296	---
HS3271	A 887 reset 1962	37°16′01″	121°56′27″	43.940	---	---	71.65135	71.55339	−11.71
HS3131	S 1122	37°16′55″	121°56′40″	44.455	---	63.34012	63.27957	63.22391	−13.90
HS3130	E 875	37°17′08″	121°56′37″	44.941	61.54129	61.45800	61.30408	61.24838	−38.94
HS3127	U 176 reset 1940	37°17′13″	121°56′15″	45.647	58.95799	58.87831	58.71350	58.64586	−41.86
HS3125	D 875	37°17′27″	121°56′18″	46.265	59.19844	59.09533	58.87475	58.78229	−56.81
HS3124	T 176 reset 1962	37°17′52″	121°55′51″	47.283	---	---	52.26381	52.13361	−93.45
HS3122	S 176 reset 1962	37°18′07″	121°55′36″	47.824	---	---	50.23288	50.06486	−112.92
HS3120	R 176 reset 1962	37°18′39″	121°54′59″	49.252	---	---	42.33935	42.10389	−164.32
HS3118	P 176	37°19′10″	121°54′26″	50.667	34.32425	33.93393	33.12257	32.95738	−215.25
HS3117	D 877	37°19′28″	121°54′06″	51.396	31.00216	30.60606	29.77560	29.61618	−220.37
HS3109	C 112	37°19′55″	121°54′09″	52.288	30.60766	30.13155	29.13692	28.90626	−264.40
HS3108	B 875	37°20′05″	121°54′13″	52.593	28.52997	28.02726	26.99132	26.75623	−275.48
HS2891	Z 111 reset 1962	37°20′29″	121°54′40″	53.601	---	24.23590	23.22121	23.00027	−269.78
HS5160	L 1447	37°20′56″	121°55′03″	54.722	---	---	---	22.69595	---
HS5161	G 1448	37°21′07″	121°55′01″	55.311	---	---	---	17.17585	---

Table 14.—*Leveling observations along a line from Capitola through Loma Prieta to Coyote*

[See figure 1 for locations. Numbers in parentheses below year of survey indicate months when survey was conducted; month of 1953 survey is unknown. L-number is U.S. National Geodetic Survey designation; PV numbers are U.S. Geological Survey (USGS) field-summary-book designations. Obs., original field observations, with previous USGS adjustments removed; adj., observations adjusted for consistent coseismic network (see text)]

ACRN	Designation	Latitude N.	Longitude W.	Leveled distance (km)	Orthometric height (m) 1953 (obs.) PV 80, PV208, PV220	Orthometric height (m) 1953 (adj.) PV 80, PV208, PV220	Orthometric height (m) 1990 (3–4) L25239.4
GU2286	N 1237	36°58′37″	121°56′35″	0.000	---	---	24.61802
GU2287	Z 212	36°58′31″	121°56′58″	.540	19.47200	19.35700	19.46874
GU4168	N 1456	36°58′59″	121°57′22″	1.631	---	---	10.90370
GU4169	32 WLS	36°59′26″	121°57′24″	2.473	12.55000	12.44000	12.58387
HS5194	P 1456	37°00′19″	121°57′08″	4.081	---	---	32.43278
HS5195	Q 1456	37°01′18″	121°57′01″	6.098	---	---	63.00953
HS5196	Chiseled square A	37°02′09″	121°56′35″	7.938	69.45100	69.35200	69.68787
HS5197	R 1456	37°02′44″	121°56′18″	9.183	---	---	70.75253
HS5198	S 1456	37°03′19″	121°56′21″	10.388	---	---	80.92999
HS5199	T 1456	37°04′09″	121°56′15″	12.079	---	---	141.75804
HS5200	U 1456	37°04′36″	121°56′21″	12.914	---	---	176.51875
HS5201	1940	37°05′10″	121°57′02″	14.197	---	---	253.93246
HS5202	28 WLS	37°05′41″	121°56′57″	15.556	338.66800	338.58500	339.14897
HS5203	Chiseled square B	37°06′08″	121°56′47″	16.474	393.53200	393.45100	394.06493
HS5210	Z 1456	37°06′39″	121°56′52″	17.769	---	---	437.11351
HS5204	Burdett	37°06′37″	121°56′43″	18.074	---	---	458.02049
HS5205	27 WLS	37°06′52″	121°56′20″	18.770	471.42400	471.34800	471.73675
HS5206	V 1456	37°07′06″	121°55′26″	20.234	---	---	477.26362
HS5207	W 1456	37°06′40″	121°54′40″	21.624	---	---	548.68660
HS5208	X 1456	37°06′22″	121°53′56″	22.910	---	---	572.60387
HS5209	Y 1456	37°06′19″	121°53′36″	23.577	---	---	609.21796
HS5211	A 1457	37°06′19″	121°53′20″	24.432	---	---	687.67126
HS5212	B 1457	37°06′17″	121°52′45″	25.372	---	---	762.65041
HS5213	C 1457	37°05′56″	121°52′02″	26.767	---	---	768.58749
HS5214	D 1457	37°06′01″	121°51′42″	27.478	---	---	844.04796
HS5215	E 1457	37°05′56″	121°51′13″	28.106	---	---	906.54151
HS5216	F 1457	37°05′49″	121°50′41″	29.151	---	---	939.09174
HS5217	G 1457	37°06′22″	121°50′49″	30.546	---	---	1,024.92195
HS5218	Loma Prieta reset 1958	37°06′40″	121°50′35″	30.796	---	---	1,154.12757
HS5219	LOMA	37°06′41″	121°50′35″	31.045	---	---	1,154.70909
HS5220	Loma Prieta 1	37°06′35″	121°50′37″	31.295	---	---	1,152.23547
HS5221	H 1457	37°06′25″	121°50′14″	31.544	---	---	906.77804
HS5222	J 1457	37°06′35″	121°50′06″	31.997	---	---	870.71964
HS5223	K 1457	37°06′18″	121°49′14″	33.535	---	---	788.32005
HS5224	HJH 55	37°06′09″	121°48′20″	34.950	728.26800	728.22600	728.13323
HS5225	L 1457	37°06′19″	121°48′18″	35.769	---	---	600.76979
HS5226	M 1457	37°06′41″	121°48′19″	36.585	---	---	480.67933
HS5227	N 1457	37°06′47″	121°48′25″	37.650	---	---	364.02224
HS5228	P 1457	37°07′11″	121°48′06″	38.787	---	---	300.72020
HS5230	Q 1457	37°07′25″	121°47′40″	39.885	---	---	279.08001
HS5229	TBM angle iron	37°07′25″	121°47′39″	39.892	276.80400	276.77200	276.70031
HS5231	HJH 53	37°07′56″	121°47′30″	40.985	246.37300	246.34400	246.26767
HS5232	R 1457	37°08′26″	121°46′58″	42.420	---	---	227.65294
HS5233	Chiseled square C	37°08′54″	121°46′15″	43.885	207.11700	207.09400	207.03122
HS5234	S 1457	37°09′07″	121°45′35″	45.050	---	---	203.26228
HS5235	TBM spike	37°09′07″	121°45′35″	45.073	201.97200	201.95100	201.86131
HS5236	T 1457	37°09′05″	121°44′49″	46.341	---	---	191.44521
HS5237	U 1457	37°09′37″	121°44′56″	47.370	---	---	230.54392
HS5238	TBM manhole	37°09′37″	121°44′56″	47.390	230.22200	230.20600	230.15221
HS5239	HJH 51	37°10′20″	121°45′30″	49.067	156.36400	156.35200	156.30456
HS5240	V 1457	37°11′03″	121°45′12″	50.963	---	---	145.71067
HS5241	W 1457	37°11′16″	121°45′19″	51.695	---	---	94.49410
HS5242	X 1457	37°11′47″	121°44′31″	53.190	---	---	76.86677
HS2775	L 174	37°12′22″	121°43′41″	54.849	79.81900	79.81900	79.78395
HS2776	P 19	37°13′00″	121°44′21″	56.388	---	---	77.63078

Table 15.—*Leveling observations along a line from 9.6 km south of Morgan Hill to Loma Prieta*

[See figure 1 for locations. Number in parentheses below year of survey indicates month when survey was conducted; month of 1953 survey is unknown. L-number is U.S. National Geodetic Survey designation; PV-number is U.S. Geological Survey (USGS) field-summary-book designation. Obs., original field observations, with previous USGS adjustments removed; adj., observations adjusted for consistent coseismic network (see text)]

ACRN	Designation	Latitude N.	Longitude W.	Leveled distance (km)	Orthometric height (m)		
					1953 (obs.)	1953 (adj.)	1990 (4) L25239.5
					PV220		
HS5243	Q 1458	37°01′50″	121°39′20″	0.000	---	---	103.30476
HS5244	P 1458	37°01′49″	121°39′49″	1.359	---	---	108.51847
HS5245	N 1458	37°01′58″	121°40′57″	3.171	---	---	134.40205
HS5246	M 1458	37°01′50″	121°41′39″	4.277	---	---	130.16365
HS5247	Chiseled square 1	37°02′04″	121°42′26″	5.612	148.60100	148.62000	148.45545
HS5248	L 1458	37°01′50″	121°42′34″	6.357	---	---	230.89985
HS5249	K 1458	37°01′36″	121°42′56″	7.649	---	---	350.51604
HS5250	J 1458	37°01′11″	121°43′05″	8.844	---	---	456.09991
HS5251	H 1458	37°00′48″	121°43′01″	9.694	---	---	520.93831
HS5252	114 JD	37°00′48″	121°43′02″	9.702	521.12900	521.14500	521.00357
HS5253	Y 1459	37°01′03″	121°43′24″	10.518	---	---	559.60387
HS5254	G 1458	37°01′22″	121°43′37″	11.149	---	---	571.23601
HS5255	X 1459	37°01′37″	121°44′15″	12.154	---	---	595.91950
HS5256	115 JD	37°01′57″	121°44′34″	13.004	634.32700	634.34200	634.21884
HS5257	W 1459	37°02′17″	121°44′49″	13.810	---	---	632.27002
HS5258	F 1458	37°02′32″	121°44′59″	14.328	---	---	639.93276
HS5259	P 1459	37°02′55″	121°45′14″	15.180	---	---	649.37932
HS5260	E 1458	37°02′52″	121°45′34″	15.880	---	---	701.83374
HS5261	Q 1459	37°02′55″	121°45′46″	16.254	---	---	732.00264
HS5262	116 JD	37°03′03″	121°45′43″	16.598	756.42800	756.44000	756.34069
HS5263	V 1459	37°03′10″	121°46′15″	17.554	---	---	738.38598
HS5264	D 1458	37°03′22″	121°46′39″	18.393	---	---	771.94006
HS5265	R 1459	37°03′38″	121°47′02″	19.198	---	---	763.99801
HS5266	C 1458	37°03′46″	121°47′16″	19.659	---	---	792.56946
HS5267	B 1458	37°03′50″	121°47′36″	20.393	---	---	834.10806
HS5268	N 1459	37°04′04″	121°48′08″	21.320	---	---	855.10936
HS5269	END	37°04′25″	121°48′46″	22.565	---	---	848.20998
HS5271	A 1458	37°04′40″	121°48′59″	23.245	---	---	908.00462
HS5272	S 1459	37°04′49″	121°48′57″	23.527	---	---	914.07271
HS5273	Z 1457	37°05′07″	121°49′16″	24.254	---	---	874.75632
HS5274	T 1459	37°05′18″	121°49′43″	25.190	---	---	894.27193
HS5275	Y 1457	37°05′24″	121°49′54″	25.613	---	---	905.70397
HS5276	M 1459	37°05′31″	121°50′15″	26.288	---	---	914.85099
HS5216	F 1457	37°05′49″	121°50′41″	27.443	---	---	939.12012
HS5215	E 1457	37°05′56″	121°51′13″	28.502	---	---	906.57015

Table 16.—*Leveling observations along a line from Morgan Hill to Watsonville*

[See figure 1 for locations. Number in parentheses below year of survey indicates month when survey was conducted; month of 1953 survey is unknown. L-number is U.S. National Geodetic Survey designation; PV-numbers are U.S. Geological Survey (USGS) field-summary-book designations. Obs., original field observations, with previous USGS adjustments removed; adj., observations adjusted for consistent coseismic network (see text)]

ACRN	Designation	Latitude N.	Longitude W.	Leveled distance (km)	Orthometric height (m)		
					1953 (obs.) PV208, PV220	1953 (adj.) PV208, PV220	1990 (4) L25239.6
HS5168	N 1448	37°07′22″	121°38′34″	0.000	---	---	103.40712
HS5169	P 1448	37°06′56″	121°38′07″	1.020	---	---	99.90679
HS5277	Chiseled square 3	37°06′26″	121°38′05″	2.569	96.51000	96.48300	96.48369
HS5278	R 1458	37°05′39″	121°38′42″	4.297	---	---	102.69264
HS5279	S 1458	37°05′06″	121°39′10″	5.579	---	---	111.92432
HS5280	Chiseled square B	37°05′05″	121°39′12″	5.647	112.89600	112.87000	110.35487
HS5279	S 1458	37°05′06″	121°39′10″	5.579	---	---	111.92432
HS5281	109 JD	37°04′05″	121°39′32″	7.545	130.46300	130.43800	130.33963
HS5282	T 1458	37°03′25″	121°39′40″	8.857	---	---	116.77682
HS5283	110 JD	37°02′43″	121°39′07″	10.331	102.58700	102.56400	102.47966
HS5243	Q 1458	37°01′50″	121°39′20″	12.028	---	---	103.30476
HS5284	U 1458	37°00′57″	121°38′57″	14.040	---	---	98.28815
HS5285	38 WLS	37°00′39″	121°39′43″	15.526	109.07800	109.05800	108.98607
HS5288	L 1459	37°00′13″	121°40′16″	16.882	---	---	143.68643
HS5286	V 1458	37°00′16″	121°40′49″	17.563	---	---	149.51767
HS5287	W 1458	37°00′02″	121°41′06″	18.286	---	---	184.20379
GU4170	X 1458	36°59′32″	121°41′14″	19.203	---	---	220.40284
GU4171	Y 1458	36°59′25″	121°41′58″	20.326	---	---	278.43834
GU4172	Z 1458	36°59′40″	121°42′20″	21.175	---	---	327.78833
GU4173	Chiseled triangle A	36°59′50″	121°42′47″	22.214	---	---	389.73900
GU4175	36 WLS	36°59′50″	121°43′00″	22.611	406.73500	406.71800	406.67640
GU4176	B 1459	36°59′24″	121°42′54″	23.275	---	---	371.84734
GU4177	Chiseled square 2	36°59′10″	121°43′01″	24.304	315.72500	315.70900	315.71218
GU4178	C 1459	36°59′06″	121°42′47″	24.847	---	---	288.18594
GU4179	D 1459	36°58′49″	121°43′00″	25.650	---	---	249.36555
GU4180	E 1459	36°58′45″	121°42′36″	26.278	---	---	214.85295
GU4181	F 1459	36°58′30″	121°43′07″	27.546	---	---	159.18544
GU4182	G 1459	36°58′06″	121°43′06″	28.427	---	---	109.08097
GU4183	H 1459	36°57′34″	121°43′20″	29.569	---	---	59.13198
GU4184	J 1459	36°56′54″	121°44′01″	31.158	---	---	35.16116
GU4185	33 WLS reset 1965	36°56′07″	121°44′32″	32.808	21.07700	21.06500	20.96856
GU4186	W 17	36°55′31″	121°44′42″	33.953	---	---	17.04438
GU4187	W 16	36°55′10″	121°44′49″	34.600	---	---	12.49995
GU4188	K 1459	36°55′01″	121°45′09″	35.319	---	---	12.50816
GU4189	W 9	36°54′37″	121°45′32″	36.326	---	---	8.56993
GU4162	H 249 reset 1979	36°54′28″	121°45′37″	36.778	---	---	8.14009
GU2246	W 1236	36°54′19″	121°45′23″	37.215	---	---	7.40400
GU2245	V 1236	36°54′12″	121°45′13″	37.586	---	---	10.10877

Table 17.—*Leveling observations along a line from Watsonville, through Freedom, Browns Valley Road, and Casserly Road, to 6.1 km northwest of Watsonville*

[See figure 1 for locations. Numbers in parentheses below year of survey indicate months when survey was conducted; month of 1970 survey is unknown. L-number is U.S. National Geodetic Survey designation]

ACRN	Designation	Latitude N.	Longitude W.	Leveled distance (km)	Orthometric height (m)	
					1970	1990 (4–5) L25251.1
GU4183	H 1459	36°57′34″	121°43′20″	0.000	- - -	59.13198
GU4203	157.24=118	36°57′23″	121°43′35″	.506	47.92800	47.91718
GU4204	150.42=119	36°57′38″	121°43′47″	1.127	45.84800	45.87621
GU4205	A 1460	36°57′54″	121°44′14″	2.032	- - -	39.47554
GU4206	133.06=121	36°58′14″	121°44′15″	3.150	40.56000	40.62783
GU4207	138.62=122	36°58′34″	121°44′29″	3.900	42.25000	42.37796
GU4208	271.10=319	36°59′21″	121°44′19″	5.492	82.63000	82.76526
GU4209	423.34=318	36°59′35″	121°44′03″	6.165	129.03300	129.12294
HS5289	412.23=317	37°00′06″	121°44′20″	7.231	125.64600	125.96969
HS5290	B 1460	37°00′23″	121°44′45″	8.069	- - -	174.79177
HS5291	737.58=316	37°00′48″	121°45′04″	8.970	224.81500	225.12059
HS5292	C 1460	37°01′09″	121°45′46″	9.896	- - -	244.48891
HS5293	739.34=315	37°01′16″	121°45′27″	10.449	225.35000	225.36587
HS5294	D 1460	37°01′24″	121°46′07″	11.229	- - -	192.87509
HS5295	529.07=314	37°01′34″	121°46′43″	12.050	161.26000	161.39395
HS5296	411.31=313	37°00′59″	121°47′15″	13.544	125.36700	125.60414
HS5297	361.00=312	37°00′29″	121°47′36″	14.729	110.03400	110.29602
HS5298	323.74=311	37°00′03″	121°47′47″	15.558	98.67500	98.93378
GU4210	270.33=310	36°59′19″	121°47′59″	16.985	82.39500	82.63666
GU4211	236.78=309	36°58′50″	121°48′00″	17.875	72.17200	72.38569
GU4212	295.16=308	36°58′17″	121°47′39″	19.074	89.96600	90.12004
GU4213	257.94=307	36°57′54″	121°47′32″	19.783	78.62000	78.75199
GU4214	223.07=306	36°57′36″	121°47′11″	20.511	67.99000	68.09088
GU4215	149.99=304	36°56′59″	121°46′17″	22.303	45.71700	45.71554
GU4216	Gaging station	36°56′21″	121°46′10″	23.739	- - -	32.74371
GU4217	Z 1459	36°56′04″	121°46′18″	24.324	- - -	35.32309
GU2250	T 738 reset 1963	36°55′32″	121°45′44″	25.605	27.50600	27.47638
GU4188	K 1459	36°55′01″	121°45′09″	27.021	- - -	12.49315

Table 18.—*Leveling observations along a line from 0.5 km west of Corralitos through Freedom Boulevard to Aptos*

[See figure 1 for locations. Number in parentheses below year of survey indicates month when survey was conducted; month of 1970 survey is unknown. L-number is U.S. National Geodetic Survey designation]

ACRN	Designation	Latitude N.	Longitude W.	Leveled distance (km)	Orthometric height (m)	
					1970	1990 (4) L25251.2
GU4210	270.33=310	36°59′19″	121°47′59″	0.000	82.39500	82.63666
GU4218	E 1460	36°59′20″	121°48′05″	.168	- - -	77.26547
GU4219	271.52=301	36°59′18″	121°48′20″	.553	82.75900	82.99344
GU4220	469.60=300	36°59′40″	121°48′54″	1.722	143.13500	143.41648
GU4221	K 1460	36°59′29″	121°49′17″	2.441	- - -	126.06179
GU4222	48	36°59′25″	121°49′38″	2.985	113.76000	113.52423
GU4223	J 1460	36°59′15″	121°50′09″	4.013	- - -	110.88108
GU4224	H 1460	36°59′12″	121°50′46″	4.966	- - -	111.28063
GU4225	G 1460	36°59′04″	121°51′43″	6.422	- - -	69.80046
GU4226	R 125	36°58′12″	121°52′21″	8.241	- - -	54.80430
GU4227	F 1460	36°58′31″	121°53′07″	9.992	- - -	46.45767
GU2278	RV 5	36°58′33″	121°53′51″	11.336	29.80000	29.91452

Table 19.—*Leveling observations along a line from 0.8 km northwest of Freedom, through Valley Road and Buena Vista Drive, to 0.6 km south of La Selva Beach*

[See figure 1 for locations. Numbers in parentheses below year of survey indicate months when survey was conducted; month of 1970 survey is unknown. L-number is U.S. National Geodetic Survey designation]

ACRN	Designation	Latitude N.	Longitude W.	Leveled distance (km)	Orthometric height (m)	
					1970	1990 (4–5) L25251.3
GU4217	Z 1459	36°56′04″	121°46′18″	0.000	- - -	35.32309
GU4228	1	36°56′26″	121°46′51″	1.086	43.29800	43.30354
GU4229	158.34=96	36°56′22″	121°47′17″	1.827	48.26000	48.29119
GU4230	97	36°56′25″	121°47′49″	2.666	51.08000	51.11660
GU4231	35.89=98	36°56′16″	121°48′21″	3.689	10.94000	10.96152
GU4232	67.40=219	36°56′36″	121°48′52″	4.672	20.54300	20.60159
GU4233	93.74=220	36°56′49″	121°49′19″	5.473	28.57300	28.62398
GU4234	130.54=221	36°57′03″	121°49′45″	6.290	39.78800	39.86020
GU4235	277.62=223	36°57′13″	121°50′45″	7.945	84.61700	84.71139
GU4236	R 121	36°56′56″	121°51′00″	8.594	- - -	86.33585
GU4237	227 reset	36°56′32″	121°51′23″	9.798	51.56600	51.60000
GU2269	RV 6=4	36°56′10″	121°51′50″	10.955	23.46000	23.43919

Table 20.—*Leveling observations along a line from 5.3 km north of Soquel, through Laurel Glen Road and Granite Creek Road, to 2.7 km north of Scotts Valley*

[See figure 1 for locations. Number in parentheses below year of survey indicates month when survey was conducted; month of 1970 survey is unknown. L-number is U.S. National Geodetic Survey designation]

ACRN	Designation	Latitude N.	Longitude W.	Leveled distance (km)	Orthometric height (m)	
					1970	1990 (5) L25251.4
HS5195	Q 1456	37°01′18″	121°57′01″	0.000	- - -	63.00953
HS5300	225.29=273	37°02′06″	121°56′47″	1.601	68.66800	68.91768
HS5301	L 1460	37°02′43″	121°57′05″	2.868	- - -	83.43431
HS5302	326.21=275	37°03′12″	121°57′16″	3.891	99.42700	99.75107
HS5303	M 1490	37°03′24″	121°57′30″	4.463	- - -	140.12288
HS5304	616.48=276	37°03′20″	121°57′43″	5.024	187.90200	188.58406
HS5305	N 1460	37°03′22″	121°58′12″	5.870	- - -	114.50819
HS5306	329.11=277	37°03′15″	121°58′36″	6.445	100.31200	100.60661
HS5307	P 1460	37°02′55″	121°58′51″	7.177	- - -	95.08478
HS5308	273.96=278	37°02′27″	121°59′01″	8.106	83.50400	83.73823
HS5309	Q 1460	37°02′02″	121°59′08″	9.005	- - -	80.62321
HS5310	179.72=279	37°01′40″	121°59′11″	9.674	54.77900	54.96567
HS5311	164.37=280	37°01′25″	121°59′19″	10.271	50.10100	50.26312
HS5312	145.36=281	37°01′05″	121°59′46″	11.320	44.30600	44.41088
HS5313	224.23=282	37°01′37″	121°59′42″	12.181	68.34400	68.50599
HS5314	R 1460	37°02′21″	121°59′45″	13.702	- - -	135.22959
HS5315	490.32=284	37°02′49″	121°59′51″	14.666	149.44900	149.67292
HS5316	S 1460	37°03′04″	121°59′48″	15.215	- - -	177.79975
HS5317	723.10=285	37°03′21″	121°59′47″	15.748	220.40200	220.66285
HS5299	S 1455	37°03′38″	121°59′47″	16.609	- - -	192.80965

Table 21.—*Leveling observations along a line from the junction of Mount Hermon Road and Zayante Road 1 km east of Felton through Olympia to 4.3 km northeast of Zayante*

[See figure 1 for locations. Number in parentheses below year of survey indicates month when survey was conducted; month of 1970 survey is unknown. L-number is U.S. National Geodetic Survey designation]

ACRN	Designation	Latitude N.	Longitude W.	Leveled distance (km)	Orthometric height (m)	
					1970	1990 (5) L25251.5
HT3570	P 1455	37°03′19″	122°03′36″	0.000	---	106.74056
HT3569	N 1455	37°03′20″	122°03′31″	.140	---	109.07589
HT3574	312.55=65	37°03′36″	122°03′26″	.525	95.26700	95.35649
HT3575	T 1460	37°04′18″	122°03′19″	1.898	---	106.51974
HT3576	373.95=399	37°04′55″	122°02′58″	3.211	113.98000	114.15402
HT3577	379	37°05′00″	122°02′59″	3.374	122.92900	123.09959
HT3578	Gaging station	37°05′09″	122°02′45″	3.908	115.67000	116.47835
HT3579	415.66=381	37°05′22″	122°02′37″	4.541	126.69400	127.52141
HT3580	V 1460	37°05′37″	122°02′27″	5.108	---	163.04166
HT3581	U 1460	37°06′01″	122°02′00″	6.331	---	147.60536
HT3582	495.98=383	37°06′18″	122°01′33″	7.148	151.17500	152.13281
HT3583	539.94=384	37°06′35″	122°01′11″	8.353	164.57300	165.56408

Table 22.—*Leveling observations along a line from Felton, through Boulder Creek and China Grade Road, to the Santa Cruz-San Mateo County line*

[See figure 1 for locations. Numbers in parentheses below year of survey indicate months when survey was conducted; months of 1953 and 1970 surveys are unknown. PV-numbers are U.S. Geological Survey (USGS) field-summary-book designations. Obs., original field observations, with previous USGS adjustments removed]

ACRN	Designation	Latitude N.	Longitude W.	Leveled distance (km)	Orthometric height (m)		
					1953 (obs.) PV218	1970	1990 (5–6) L25251.6
HT3570	P 1455	37°03′19″	122°03′36″	0.000	---	---	106.74056
HT3584	W 1460	37°03′11″	122°04′07″	.960	---	---	85.42397
HT3585	X 1460	37°03′33″	122°04′40″	2.181	---	---	91.51486
HT3586	296.80=74	37°04′06″	122°04′54″	3.344	---	90.46500	90.54245
HT3587	324.23=72	37°04′27″	122°04′53″	4.214	---	98.82400	98.90366
HT3588	Y 1460	37°04′59″	122°04′40″	5.506	---	---	94.53565
HT3589	177 reset	37°05′20″	122°05′14″	6.743	---	96.42000	96.47190
HT3590	390.58=179	37°05′43″	122°05′45″	7.980	---	119.05000	119.13706
HT3591	446.86=181	37°06′22″	122°06′19″	9.617	---	136.20000	136.27642
HT3592	457.31=182	37°06′28″	122°06′44″	10.395	---	139.39000	139.46544
HT3593	Z 1460	37°06′46″	122°06′52″	11.017	---	---	141.07272
HT3594	501.74=184	37°07′09″	122°07′11″	12.026	---	152.93000	153.00554
HT3595	BEN 8	37°07′43″	122°07′18″	13.053	150.20200	150.20000	150.31979
HT3596	A 1461	37°07′40″	122°07′53″	14.339	---	---	166.63621
HT3597	566.17=187	37°07′55″	122°08′11″	15.064	---	172.57000	172.68552
HT3598	640.87=188	37°08′18″	122°08′33″	15.997	---	195.34000	195.39077
HT3599	799.37=190	37°08′41″	122°09′21″	17.578	---	243.65000	243.70177
HT3600	46 WLS	37°09′00″	122°09′49″	18.508	276.42500	276.43000	276.47643
HT3601	B 1461	37°09′22″	122°09′39″	19.019	---	---	247.76378
HT3602	C 1461	37°09′55″	122°09′43″	20.095	---	---	259.91990
HT3603	916 SF	37°10′26″	122°10′10″	21.484	279.17300	279.18100	279.22082
HT3604	D 1461	37°11′04″	122°10′46″	23.116	---	---	305.98060
HT3605	E 1461	37°11′06″	122°11′00″	23.487	---	---	346.52185
HT3606	F 1461	37°11′10″	122°11′14″	23.917	---	---	394.54974
HT3607	48 WLS	37°11′29″	122°11′27″	24.768	484.99500	485.00400	484.99741
HT3608	G 1461	37°11′36″	122°11′36″	25.321	---	---	540.41797
HT3609	H 1461	37°11′49″	122°11′40″	25.810	---	---	572.08818
HT3610	J 1461	37°11′56″	122°11′58″	26.278	---	---	606.54402
HT3611	K 1461	37°12′09″	122°12′08″	26.874	---	---	651.69761
HT3612	49 WLS	37°12′25″	122°12′19″	27.537	671.43100	671.44100	671.42870
HT3613	L 1461	37°12′33″	122°12′03″	27.947	---	---	686.34978
HT3614	M 1461	37°12′48″	122°12′20″	28.719	---	---	706.35417

Table 23.—*Leveling observations along a line from 1 km east of Felton, through Felton Empire Road and Bonny Doon Road, to 1.4 km southeast of Davenport*

[See figure 1 for locations. Number in parentheses below year of survey indicates month when survey was conducted; months of 1953 and 1970 surveys are unknown. L-number is U.S. National Geodetic Survey designation; PV-number is U.S. Geological Survey (USGS) field-summary-book designation. Obs., original field observations, with previous USGS adjustments removed]

ACRN	Designation	Latitude N.	Longitude W.	Leveled distance (km)	Orthometric height (m)		
					1953 (obs.) PV218	1970	1990 (6) L25251.7
HT3570	P 1455	37°03′19″	122°03′36″	0.000	---	---	106.74056
HT3584	W 1460	37°03′11″	122°04′07″	.961	---	---	85.42219
HT3615	N 1461	37°03′04″	122°04′40″	1.897	---	---	132.66295
HT3616	P 1461	37°02′56″	122°04′58″	2.402	---	---	160.46799
HT3617	Q 1461	37°02′59″	122°05′27″	3.192	---	---	225.17783
HT3618	R 1461	37°03′07″	122°05′40″	3.673	---	---	270.27996
HT3619	S 1461	37°03′14″	122°05′44″	4.225	---	---	304.49007
HT3620	170	37°03′21″	122°06′02″	4.896	---	363.45000	363.46421
HT3621	T 1461	37°03′28″	122°06′20″	5.341	---	---	404.93420
HT3622	168	37°03′36″	122°06′28″	5.838	---	443.64000	443.64950
HT3623	167	37°03′41″	122°06′45″	6.285	---	476.87000	476.86497
HT3624	U 1461	37°03′32″	122°06′54″	6.844	---	---	512.70295
HT3625	1822.20=360	37°03′29″	122°07′21″	7.540	---	555.41000	555.42330
HT3626	V 1461	37°04′00″	122°07′17″	8.748	---	---	601.72882
HT3627	163	37°04′20″	122°07′40″	9.672	---	614.27000	614.30540
HT3628	W 1461	37°04′40″	122°07′57″	10.534	---	---	663.20385
HT3629	X 1461	37°05′26″	122°08′18″	10.994	---	---	759.81158
HT3631	43 WLS	37°06′30″	122°08′39″	11.223	754.26300	754.27400	754.28303
HT3632	Z 1461	37°04′52″	122°08′21″	11.453	---	---	638.85854
HT3633	41 WLS	37°04′02″	122°08′24″	13.186	576.08000	576.09500	576.11380
HT3634	1707.48=202	37°03′45″	122°08′49″	14.018	---	520.44100	520.45432
HT3635	A 1462	37°03′11″	122°09′11″	15.164	---	---	450.14035
HT3636	40 WLS	37°02′40″	122°08′56″	16.312	404.66300	404.67900	404.68017
HT3637	REF WLS	37°02′40″	122°08′58″	16.331	404.01000	404.03000	404.02556
HT3638	122°0.26=366	37°02′12″	122°09′04″	17.243	---	371.93700	371.92109
HT3639	B 1462	37°01′51″	122°09′17″	18.108	---	---	301.01995
HT3640	C 1462	37°01′39″	122°09′27″	18.732	---	---	237.56842
HT3641	D 1462	37°01′22″	122°09′55″	19.645	---	---	173.17029
HT3642	E 1462	37°01′02″	122°10′02″	20.135	---	---	123.63265
HT3643	86.24=199	37°00′42″	122°10′32″	21.331	---	26.28600	26.23643
HT1572	H 1238	37°00′04″	122°10′45″	22.456	---	---	17.38950

Table 24.—*Leveling observations along a line from Santa Cruz through Davenport to 1 km northwest of the Santa Cruz-San Mateo County line*

[See figure 1 for locations. Number(s) in parentheses below year of survey indicates month(s) when survey was conducted; months of 1953 and 1970 surveys are unknown. L-number is U.S. National Geodetic Survey designation; PV-number is U.S. Geological Survey (USGS) field-summary-book designation. Obs., original field observations, with previous USGS adjustments removed. Subsidence correction applies to 1978–90 height difference]

ACRN	Designation	Latitude N.	Longitude W.	Leveled distance (km)	Orthometric height (m)					Subsidence correction (mm)
					1953 (obs.) PV218	1970	1972 (9–10) L22869	1978 (5) L24298	1990 (2) L25251.8	
GU4167	B 1455	36°58′15″	122°01′50″	0.000	---	---	---	---	4.41596	---
GU4240	M 1462	36°57′49″	122°02′04″	1.248	---	---	---	---	16.43267	---
GU1954	V 1237	36°57′41″	122°02′28″	1.935	---	---	16.66813	16.65667	16.66569	−8.09
GU1959	W 1237	36°57′32″	122°03′04″	2.913	---	---	20.90586	20.89493	20.89860	−2.00
GU1960	X 1237	36°57′40″	122°03′20″	3.708	---	---	27.23047	27.22063	27.22301	−.92
GU1964	Y 1237	36°57′44″	122°04′22″	5.215	---	---	28.97503	28.96455	28.96023	1.31
GU4239	L 1462	36°57′42″	122°05′15″	6.559	---	---	---	---	17.55808	---
GU1970	A 1238	36°57′52″	122°06′12″	8.067	---	---	37.42997	37.42533	37.41212	.00
GU1971	B 1238	36°58′10″	122°06′58″	9.253	---	---	22.21088	22.19706	22.15864	.00
GU4238	83.13=196	36°58′21″	122°07′37″	10.329	---	25.33800	---	---	25.29608	---
GU1972	C 1238	36°58′29″	122°07′48″	10.661	---	---	30.61819	30.59394	30.57968	.00
GU1974	W 1241	36°58′52″	122°08′23″	11.711	---	---	25.86363	25.85264	25.84810	.00
GU1975	D 1238	36°59′00″	122°08′37″	12.211	---	---	39.76853	39.75735	39.74951	.00
GU1976	E 1238	36°59′16″	122°09′18″	13.351	---	---	22.43417	22.41807	22.40278	.00
GU1978	F 1238	36°59′25″	122°09′42″	13.996	---	---	31.25946	31.24745	31.23566	.00
GU1979	G 1238	36°59′55″	122°10′35″	15.796	---	---	21.60505	21.59166	21.58221	.00
HT1572	H 1238	37°00′04″	122°10′45″	16.182	---	---	17.42189	17.40993	17.40127	.00
HT3654	K 1462	37°00′24″	122°11′09″	16.985	---	---	---	---	33.64295	---
HT1568	N 212	37°00′55″	122°12′00″	19.227	30.35400	30.35400	30.35193	30.33650	30.31804	.00
HT1567	62.66=255	37°01′29″	122°12′39″	20.487	---	19.09800	19.08944	19.07194	19.05309	.00
HT1566	L 1238	37°01′43″	122°12′52″	21.036	---	---	25.62267	25.60467	25.58826	.00
HT1565	X 1241	37°01′45″	122°12′56″	21.155	---	---	31.58854	31.57324	31.55260	.00
HT3653	93.17=270	37°01′48″	122°13′02″	21.351	---	28.56300	---	---	28.51359	---
HT1564	76.85=256	37°02′14″	122°13′10″	22.220	---	23.42200	23.41831	23.40107	23.38483	.00
HT3652	24.85=269	37°02′25″	122°13′40″	22.860	---	7.57300	---	---	7.47924	---
HT1563	43.94=257	37°02′35″	122°13′15″	23.228	---	13.39300	13.37642	13.35670	13.33919	.00
HT1562	M 1238	37°03′06″	122°13′28″	24.212	---	---	7.12583	7.10686	7.08926	.00
HT3651	188.54=267	37°03′12″	122°14′30″	24.722	---	57.46000	---	---	57.40858	---
HT1559	L 212	37°03′35″	122°13′27″	25.232	---	33.94700	33.93433	33.91710	33.90047	.00
HT1558	N 1238	37°03′49″	122°13′31″	25.694	---	---	21.80674	21.78391	21.77368	.00
HT3650	187.39=266	37°03′44″	122°15′04″	26.107	---	57.11600	---	---	57.07146	---
HT1557	60.71=259	37°04′01″	122°13′41″	26.109	---	18.50000	18.48609	18.46317	18.44942	.00
HT3649	J 1462	37°04′21″	122°15′29″	27.371	---	---	---	---	63.89437	---
HT1556	P 1238	37°04′40″	122°14′34″	28.069	---	---	28.43204	28.40855	28.39844	.00
HT3648	116.40=264	37°04′48″	122°15′50″	28.384	---	50.71900	---	---	50.65059	---
HT1555	K 212	37°04′48″	122°14′43″	28.399	---	30.84800	30.81644	30.79572	30.77721	.00
HT1554	321.22=261	37°05′07″	122°15′00″	29.343	---	97.90900	97.90094	97.89572	97.90777	.00
HT1552	Y 1241	37°05′00″	122°15′21″	30.107	---	---	148.16900	148.15189	148.13270	.00
HT1549	R 1238	37°05′48″	122°16′36″	30.615	---	---	5.73782	5.71298	5.66232	.00
HT3644	19.13=272	37°05′48″	122°16′38″	30.676	---	5.83000	---	---	5.73119	---
HT3647	H 1462	37°05′03″	122°15′43″	30.770	---	---	---	---	116.02240	---
HT3646	G 1462	37°04′54″	122°15′43″	31.184	---	---	---	---	103.58959	---
HT1547	S 1238	37°06′16″	122°17′14″	31.905	---	---	9.91889	9.89843	9.88313	.00
HT3645	F 1462	37°05′04″	122°16′03″	32.092	---	---	---	---	45.96247	---
HT1545	Z 1241	37°06′51″	122°18′02″	33.558	---	---	30.12716	30.10597	30.08577	.00

Figure 15.—Schematic map of Loma Prieta region, Calif., showing locations of leveling network of bench marks used in this study (dots) and additional bench marks for which coseismic elevation changes were measured (triangles). Unused bench marks were surveyed by Santa Cruz County at low precision; unassessed elevation-dependent error evident in Santa Cruz County observations limits their utility for geodetic modeling. Quaternary faults (dashed where inferred) from Jennings (1975). LP, Loma Prieta (solid triangle).